1968

Absolute specification of x-ray spectra by Laplace transform analysis of attenuation data

Gerald Robert Lusk

ABSOLUTE SPECIFICATION OF X-RAY SPECTRA BY LAPLACE TRANSFORM ANALYSIS OF ATTENUATION DATA

BY

GERALD ROBERT LUSK

A

THESIS

submitted to the faculty of

THE UNIVERSITY OF MISSOURI - ROLLA

in partial fulfillment of the requirements for the

Degree of

MASTER OF SCIENCE IN PHYSICS

Rolla, Missouri

1968

Approved by

Otto H. Hill (advisor) H. P. Hotz

D R Edwards

ABSTRACT

A well characterized, variable plate separation ion chamber was utilized as a detector to collect x-ray attenuation data for generating information on the Laplace transform predicted spectrum of a 50 KvCP conventional x-ray tube. The variable plate separation feature allows one to include a wavelength dependent correction to the detector response which is associated with the hardening of the x-ray spectrum as it traverses the attenuating material. With this correction, the conventional two-term Laplace transform was shown to approximate independently the bremsstrahlung and characteristic L radiation from the tungsten target. The detector provides an absolute statement of the target-referenced x-ray spectrum which can be employed to specify the energy deposition in any arbitrary material system for which adequate data on the mass energy transfer coefficients are available. The aluminum attenuated derived spectrum was applied to polyethylene, and experimental and predicted data agreed to within 1% for thickness of polyethylene extending to one centimeter and exhibited a maximum average error of less than 3% for thickness up to 2.5 centimeters. The results of this study are critically compared with the literature available to-date and sources of error inherent in the published information generated with window type, fixed plate separation ion chambers are analyzed.

ACKNOWLEDGEMENT

I wish to thank Dr. Otto H. Hill for his suggestion of the problem and his many helpful discussions about x-ray dosimetry. I also wish to thank Mr. Christopher K. Wu for his assistance with the generation of a non-linear regression analysis, and the Consolidated Aluminum Corp., Jackson, Tenn., for providing the aluminum stock and its composition analysis. In addition, I wish to express my appreciation to the Graduate Center for Materials Research of the Space Sciences Research Center of the University of Missouri for the availability of facilities and financial support. Finally, I want to thank my wife, Sharon, for her assistance and encouragement.

May, 1968 G.R.L.

TABLE OF CONTENTS

LIST OF FIGURES

LIST OF TABLES

I. INTRODUCTION

Precision fundamental radiation chemistry studies require a radiation source which can be integrally mated to analytical equipment providing continuous data on the rates at which radiation induced processes occur in a material. Because of its accessibility, ease of shielding, its satisfaction of conditions of "charged particle equilibrium"[1] in thin (<0.010 inch) samples required in some analytical systems, and variable dose rates extending to relatively high intensities ($\geq 10^{16} ev \cdot g^{-1} \cdot s^{-1}$), soft x-rays (<75 Kv) generated by conventional commercial tubes represent a desirable source of radiation. Reservations concerning the precise specification of the absolute energy deposition in materials irradiated with such broad spectrum sources have been the principal reason for their limited service to date. However, "homogeneous", variable plate separation ionization chambers composed of polyethylene bodies and utilizing flowing ethylene gas as the cavity gas have been designed and built recently which specify the absolute energy deposition in typical hydrocarbons with demonstrated accuracies of ±3% (JOYNER, 1967).

---

[1] To be in charged particle equilibrium at a point, the International Commission on Radiological Units and Measurements (ICRU, 1964) has set forth the following criteria:

> Charged particle equilibrium would exist at a point within a medium under irradiation if (a) the intensity and energy spectrum of the primary radiation were constant throughout a region extending in all directions from the point, to a distance at least as great as the maximum range of the secondary charged particles generated by the primary radiation, and (b) the energy absorption coefficient for the primary radiation and the stopping power for the secondary charged particles were constant in the medium throughout the same region as in (a).

The extension of the use of these x-ray sources to studies of materials for which the development of such homogeneous ion chambers is not feasible requires some form of extrapolative or predictive dosimetry technique. For example, if one knew the relative spectral intensity of such a broad spectrum source and the precise wavelength dependence of the energy transfer coefficients for some standard system, say ethylene, and any other material of interest, one could compute relative absorbances in the two systems by square counting if necessary and then use this ratio to deduce the energy deposition in the sample material from a primary measurement made with the standard. Of course, if one has an absolute rather than a relative spectral energy distribution, one could compute the energy deposition in the sample directly from a knowledge of its wavelength dependent energy transfer coefficients.

There exists a wealth of literature on experimental attempts[1] to establish either the relative or absolute spectral distributions from commercial x-ray tube sources. Prior to the recent advent of scintillation and solid state detector spectrometry, most of the early workers used Laplace transform techniques to convert attenuation data monitored by various types of ionization chambers into some accessible equivalent spectral description. A discussion of the errors inherent in the use of these methods will constitute one of the features of this paper. However, even adequate quality data on the relative spectral distribution of such

---

[1] Refer to references: Ulrey (1918), Kramers (1923), Silberstein (1933), Bell (1936), Jones (1936), Greening (1947, 1950, 1951), Greenfield, et al (1952), Jennings (1953), Emigh & Megill (1953), Norman & Greenfield (1955), Ehrlich (1955), Wang, Raridon & Crawford (1957), Loevinger & Yaniv (1965), Epp & Weiss (1966), Ray, et al (1967).

sources is difficult to find, and dependable information on the <u>absolute</u> spectral distribution is essentially non-existent.

The closest approximation to primary spectral data is provided by the previously mentioned scintillation and solid state detector spectrometers. However, the former exhibit poor resolution (≈30%) in the lower energy (∿10 kev) region and the latter are at present prohibitive in price for detectors of sufficient thickness to absorb <u>all</u> of the impinging radiation although their resolution is much better. Even these methods require some "unfolding" of the monitored spectrum to generate the primary spectrum responsible for the observation.

The bremsstrahlung spectrum of x-rays generated by thick target sources has been treated theoretically most prominently by KRAMERS (1923). EHRLICH (1955) has modified Kramers' theory to include consideration of electron backscatter and target self-absorption. Ehrlich's experimental data, which was obtained by scintillation spectrometry techniques, does not agree with theory sufficiently well to allow one to use the theoretical spectrum with confidence to predict precision energy deposition in material systems.

The purpose of the present study is to examine in detail the feasibility of employing a precision ionization chamber detector and the attenuation method to deduce a useful empirical absolute spectral distribution which can be employed to predict the energy deposition in any arbitrary material system for which the energy transfer coefficients are known. In the course of this study some of the subtle errors in previous experimental work will be discussed and some additional information ordinarily hidden in the Laplace transformation techniques will be elaborated.

II. THEORY

Conventional, commercial x-ray tubes produce radiation by an inverse photoelectric effect which involves bombarding a target material with approximately monoenergetic electrons. The deceleration of these electrons within the target produces a continuously distributed bremsstrahlung or "braking radiation" extending up to a frequency corresponding to the quantum energy equivalent to the kinetic energy of the impinging electrons, and, depending upon the magnitude of the exciting potential, a certain amount of characteristic radiation arising from interactions of the impinging electrons and orbital electrons of the target material.

We shall be concerned with describing a technique for deducing the spectral energy distribution of such radiation incident upon a material system of known wavelength dependent attenuation coefficients from measurements of <u>either</u> the attenuation of the total intensity of the radiation <u>or</u> the attenuation of a detector monitored spectral absorbance as the radiation traverses different thicknesses of the material. We shall discuss the latter case first since it is the most general and then consider the simple modification of these results which corresponds to the monitoring of the total attenuated intensity.

In actual practice one never monitors directly the spectral distribution, say $f_0(\lambda)$, referenced to the target position within the x-ray tube, but always deals with a modification of this spectrum, say $f_y(\lambda)$, resulting from inherent or imposed filtration. We shall maintain a distinction between these terms. Let us first define

$$f_y(\lambda)d\lambda = A_y f_y^*(\lambda)d\lambda \tag{1}$$

which represents an appropriately normalized absolute intensity contribution in the wavelength range between λ and $\lambda+d\lambda$. We shall choose for A_Y the units of energy per steradian per unit time per unit of x-ray tube current. The $f_Y^*(\lambda)d\lambda$ quantity represents the fraction of the total absolute intensity in the wavelength region between λ and $\lambda+d\lambda$ and has the property

$$\int_{\lambda_0}^{\infty} f_Y^*(\lambda)\,d\lambda \equiv 1 \qquad (2)$$

so that

$$\int_{\lambda_0}^{\infty} f_Y(\lambda)\,d\lambda = A_Y \quad . \qquad (3)$$

After passage through a material of thickness x with attenuation coefficient $\mu_x(\lambda)$ the incident spectrum $f_Y(\lambda)$ will be modified and the emerging spectrum will be $f_Y(\lambda)\cdot\exp[-\mu_x(\lambda)x]$. If this emerging spectrum interacts with a detector of thickness or path length L and absorption or energy transfer coefficient $\mu_D(\lambda)$, then the intensity of the radiant energy deposition in the detector $(\dot{D}_x)$ is given by

$$\dot{D}_x = \int_{\lambda_0}^{\infty} f_Y(\lambda)\cdot\exp[-\mu_x(\lambda)x]\cdot\{1-\exp[-\mu_D(\lambda)L\}d\lambda \quad . \qquad (4)$$

If $\mu_D(\lambda)L<<1$ as it is for most cavity ionization chambers, then $\{1-\exp[-\mu_D(\lambda)L]\} \simeq \mu_D(\lambda)L$ and one may rewrite Eq. (4) from this observation and Eq. (1) to obtain

$$\dot{D}_x = A_Y\int_{\lambda_0}^{\infty} f_Y^*(\lambda)\cdot\mu_D(\lambda)L\cdot\exp[-\mu_x(\lambda)x]\,d\lambda \quad . \qquad (5)$$

We may now define an effective detector spectral absorbance $F_Y(\lambda)$ given by

$$F_Y(\lambda) = \{1-\exp[-\mu_D(\lambda)L]\}f_Y^*(\lambda) \simeq \mu_D(\lambda)L\cdot f_Y^*(\lambda) \qquad (6)$$

where $F_y(\lambda)d\lambda$ represents that portion of the fraction of the total spectral intensity in the wavelength region between λ and $\lambda+d\lambda$ which is absorbed by the detector.

Substituting Eq. (6) into Eq. (5) yields

$$\dot{D}_x = A_y \int_{\lambda_0}^{\infty} F_y(\lambda) \cdot \exp[-\mu_x(\lambda)x]d\lambda \quad . \tag{7}$$

However, this form is not convenient for the application of the transform techniques which will be required in our search for $F_y(\lambda)$ and $f_y(\lambda)$. We may rephrase our description by noting that there exists a one-to-one correspondence between λ and μ_x for the attenuation material. Let us therefore define

$$t \equiv \mu_x - \mu_0 \tag{8}$$

and

$$\Phi_y(t)dt = F_y(\lambda)d\lambda \tag{9}$$

where $\mu_0 \equiv \mu_x(\lambda_0)$ and λ_0 is the Duane-Hunt limiting wavelength associated with the maximum kinetic energy of the impinging electrons. Substituting Eq. (9) into Eq. (7) yields

$$\dot{D}_x = A_y \int_0^{\infty} \Phi_y(t) \cdot \exp[-tx-\mu_0 x]dt \quad ,$$

and noting that $\exp[-\mu_0 x]$ is independent of the integration involved

$$\dot{D}_x \cdot \exp[\mu_0 x] = A_y \int_0^{\infty} \Phi_y(t) \cdot \exp[-tx]dt \quad . \tag{10}$$

We are now in a position to address ourselves to the question of the method of experimentally measuring $\dot{D}_x$ and interpreting the physical significance of the measurement. We do not measure it directly, but rather deduce its value in a majority of dosimetry devices.

If we employ an ionization chamber, as in the present study, then we will detect an electric current resulting from the radiation induced ionization of a cavity gas of known chemical composition and occupying a known volume. If we note that $\dot{D}_x$ has the units of A_y, then we may relate it to the ion chamber current i_x by

$$\dot{D}_x = i_x \left[\frac{W}{eI \cdot d\Omega} \right] \tag{11}$$

where W is the energy required to form an ion pair in the cavity gas employed, e is the charge of the electron in units compatible with i_x, I is the x-ray tube electron current in milliamperes in our case, and $d\Omega$ is the solid angle subtended by the collector volume of the dosimeter referenced to the x-ray tube target.

It is important to note that i_x references events which originate in the cavity gas of the detector. It assumes that charged particle equilibrium exists in the dosimeter and that the ionization current associated with this equilibrium is i_x. If chamber inhomogeneities are present (as they always are because of the conducting electrodes required and the thinness of the detector windows, among other things), then the experimentally detected ionization current (i_{Ex}) will be the sum of i_x and a current associated with chamber inhomogeneities (i_{cx}) so that

$$i_{Ex} \equiv i_x + i_{cx} \quad . \tag{12}$$

The variable plate separation ion chamber employed in these studies allows one to relate i_x to i_{Ex} by the definition of a parameter β_x which is equivalent to

$$\beta_x \equiv i_x / i_{Ex} \tag{13}$$

and is discussed in detail in the subsequent chapter on Experimental Procedure. Substituting from Eqs. (11) and (13) into Eq. (10) yields

$$\left[\frac{W}{eI \cdot d}\right] \cdot \beta_x i_{Ex} \cdot \exp[\mu_0 x] = A_y \int_0^{\infty} \Phi_y(t) \cdot \exp[-tx]\,dt \quad . \tag{14}$$

The quantity in brackets [ ] on the left in Eq. (14) and A_y are constants. One may generate an expression for the case corresponding to x = 0 and divide Eq. (14) by this result to obtain

$$\exp[\mu_0 x]\left[\frac{\beta_x i_{Ex}}{\beta_0 i_{Eo}}\right] = \frac{\int_0^{\infty} \Phi_y(t) \cdot \exp[-tx]\,dt}{\int_0^{\infty} \Phi_y(t)\,dt} = \int_0^{\infty} \Psi_y(t) \cdot \exp[-tx]\,dt \tag{15}$$

and

$$\Psi_y(t) = \frac{\Phi_y(t)}{\int_0^{\infty} \Phi_y(t)\,dt} = \left[\frac{A_y eI \cdot d\Omega}{W\beta_0 i_{Eo}}\right] \cdot \Phi_y(t) \quad . \tag{16}$$

For the purposes of subsequent discussion it is convenient to define

$$j(x) = \left[\frac{\beta_x i_{Ex}}{\beta_0 i_{Eo}}\right] \cdot \exp[\mu_0 x] \quad . \tag{17}$$

The problem is now one of finding a convenient and useful multiparameter function which can be curve-fitted to the experimental data represented by the left hand side of Eq. (15) and whose transform $\Psi(t)$ is known.

GREENING (1950) has shown that there are no unique choices for the function-transform combination. EMIGH and MEGILL (1953) have proposed a five parameter function defined in our nomenclature by

$$j(x) \equiv a \cdot \exp[-b(\sqrt{x+c} - \sqrt{c})] + (1-a) \cdot \left[\frac{\alpha}{x+\alpha}\right]^{\gamma} \tag{18}$$

where the constants a,b,c,α,γ may be adjusted for best fit of the experimental data. The Laplace transform of this function is given by

$$\Psi_y(t) = \left[\frac{a \cdot b}{2\sqrt{\pi}\ t^{3/2}}\right] \cdot \exp[b\sqrt{c} - ct - b^2/(4t)] + \left[\frac{(1-a)}{\Gamma(\gamma)}\right] \cdot t^{\gamma-1} \cdot \exp[-\alpha t] \ . \tag{19}$$

We may now reconstruct our desired absolute spectrum $f_y(\lambda)$ on the basis of the values of a,b,c,α,γ which are used to describe $\Psi_y(t)$ in Eq. (19). It is important to note at this point that Eq. (18) contains two separate terms which generate the transform in Eq. (19) containing two terms. Each of these terms will experience a maximum value at some particular value of wavelength. In the experimental process of curve fitting, a useful procedure is to fit the second term in Eq. (18) to the attenuation data at large attenuator thicknesses and, holding the resulting values of a,α,γ fixed, to use the complete model in fitting all of the thickness data, adjusting only b and c. It will be convenient for us to consider the two terms separately when we discuss the physical significance of the fitted function. In anticipation of this we will define

$$\Psi_y(t) \equiv \Psi_y^C(t) + \Psi_y^B(t) \tag{20}$$

where

$$\Psi_y^C(t) \equiv \left[\frac{a \cdot b}{2\sqrt{\pi} \cdot t^{3/2}}\right] \cdot \exp[b\sqrt{c} - ct - b^2/(4t)] \tag{21}$$

and

$$\Psi_y^B(t) \equiv \left[\frac{(1-a)}{\Gamma(\gamma)}\right] \cdot t^{\gamma-1} \cdot \exp[-\alpha t] \quad . \tag{22}$$

The superscripts C and B are employed in anticipation of the observation that $\Psi_y^C(t)$ attempts to fit the characteristic radiation contribution in our studies of the 50 KvCP excited spectrum and the $\Psi_y^B(t)$ is associated with the continuous or bremsstrahlung spectrum. Substituting from Eqs. (6), (9), (16), (19), (21), and (22) into Eq. (1) and solving for $f_y(\lambda)$ yields

$$\begin{aligned} f_y(\lambda) = &\left[\frac{W\beta_0 i_{Eo}}{eI \cdot d\Omega}\right] \cdot \Psi_y^C(t) \cdot \left[\frac{dt/d\lambda}{\mu_D(\lambda)L}\right] \\ &+ \left[\frac{W\beta_0 i_{Eo}}{eI \cdot d\Omega}\right] \cdot \Psi_y^B(t) \cdot \left[\frac{dt/d\lambda}{\mu_D(\lambda)L}\right] \quad . \end{aligned} \tag{23}$$

For convenience, we shall again define $f_y(\lambda)$ as the sum of two terms

$$f_y^C(\lambda) \equiv \left[\frac{W\beta_0 i_{Eo}}{eI \cdot d\Omega}\right] \cdot \Psi_y^C(t) \cdot \left[\frac{dt/d\lambda}{\mu_D(\lambda)L}\right] \tag{24}$$

and

$$f_y^B(\lambda) \equiv \left[\frac{W\beta_0 i_{Eo}}{eI \cdot d\Omega}\right] \cdot \Psi_y^B(t) \cdot \left[\frac{dt/d\lambda}{\mu_D(\lambda)L}\right] \quad . \tag{25}$$

The resulting expression for $f_y(\lambda)$ describes an <u>absolute</u> spectral distribution normalized to the x-ray tube current (I) employed and the unit solid angle ($d\Omega$) into which the radiation is emitted. The experimentally derived spectrum depends sensitively upon the quality of the curve fit of the attenuation data and the quality of the attenuation coefficient data for the attenuating material used to characterize the spectrum, as well as the true absorption or energy transfer coefficient (μ_D) for the detector.

The treatment of predicting the spectrum by monitoring the total intensity of the radiation emerging from an attenuating material as a function of the thickness of the material is much simpler, but experimental data seldom satisfy the constraints imposed by the analytical method. If one assumes that (a) the detector is wavelength independent in that it absorbs all of the radiation impinging upon it or the same fraction of the spectral intensity at all wavelengths and (b) a known one-to-one correspondence exists between the energy absorbed in such a detector and the physical property it monitors, then we may modify our earlier development accordingly. Under these conditions the spectral absorbance of the detector $f_y(\lambda)\cdot\exp[-\mu_x(\lambda)]\cdot\{1-\exp[-\mu_D(\lambda)L]\}$ in Eq. (4) is either some constant fraction of, or exactly equal to, the spectral intensity $f_y(\lambda)\cdot\exp[-\mu_x(\lambda)x]$; i.e., either $\mu_D(\lambda)$ is wavelength independent or $\exp[-\mu_D(\lambda)L] = 0$. Therefore, one may write for the intensity monitored after the incident spectrum has been modified by passing through a thickness x of attenuator

$$I_x = I_o\int_{\lambda_0}^{\infty} f_y^*(\lambda)\cdot\exp[-\mu_x(\lambda)]d\lambda \quad . \tag{26}$$

The remaining development is simpler since the detector is wavelength independent. Thus, again defining as in Eq. (8)

$$t \equiv \mu_x - \mu_0 \quad , \tag{27}$$

we obtain

$$f_y^*(\lambda)d\lambda = \Phi_y(t)dt \tag{28}$$

rather than $F_y(\lambda)d\lambda$ as in Eq. (9), which was forced by consideration of the spectral response of the detector. $\Phi_y(t)$ is therefore self-normal in this case and the analog of Eq. (15) becomes

$$\left[\frac{I_x}{I_0}\right]\cdot\exp[\mu_0 x] = \int_0^{\infty}\Phi_y(t)\cdot\exp[-tx]\,dt \quad . \tag{29}$$

The transform $\Phi_y(t)$ is identical to that of $\Psi_y(t)$ in Eq. (19) provided that a,b,c,α,γ are fitted to the data represented by the left hand side of Eq. (29).

It is important to note here that if one assumes a particular detector is wavelength independent when this condition is not truly met, then an analysis of the type resulting in Eqs. (27) - (29) will generate not the true spectral intensity, but the detector spectral absorbance. Furthermore, absolute spectral intensities in this case can only be deduced when the detector response can be absolutely calibrated against energy and it is not sufficient to know simply the ratio I_x/I_0 with precision.

III. EXPERIMENTAL PROCEDURE

A. Radiation Source

The x-radiation source for this study was a G.E. type EA-75 tungsten target x-ray tube. The x-ray tube was driven by a Universal Voltronics, Inc., model BAL-75-50-UM constant voltage power supply with a ripple specification of less than 0.1% rms. The present studies are concerned with the 50 KvCP spectrum only and nominal tube currents of 10-20 milliamperes were employed.

B. Radiation Detector

The detector employed here consisted of a "homogeneous", variable plate separation ion chamber incorporating a polyethylene body and utilizing research-grade ethylene as the cavity gas. With suitable corrections of the readout data, which will be discussed, it yielded information on the absolute rate of energy deposition in the cavity gas by the x-radiation employed. Figure (1) shows a cross sectional view of the dosimeter. The cavity volume is cylindrical in geometry with the stainless steel sliding barrel measuring 1.50 inches in diameter, and includes a co-axially inscribed circular collector area with a diameter of 0.374 ±0.001 inches. The ethylene gas was maintained at approximately atmospheric pressure (P_o + <1 torr) while flowing continually through the chamber at a moderate rate of 180 cc/min. The flowing cavity gas is required to minimize the effects of the radiation induced alteration of its composition. Charge leakage between the beryllium window (A) and Aquadaged collector plate (B) of the chamber was minimized by making the sliding stainless steel barrel (G) part of the guard ring element.

FIGURE 1

CROSS SECTIONAL VIEW OF DOSIMETER. (A) Beryllium front window, (B) Collector, (C) Gas inlet port, (D) Anti-rotation fin, (E) Ball-bearing coupler, (F) Micrometer barrel, (G) Sliding barrel, (H) Picoammeter, (I) Power supply, (J) Gas outlet port, (K) Electrical connection to front window, (d) Target t detector window distance (or FSD), (†) Projected focal spot of 5mm.

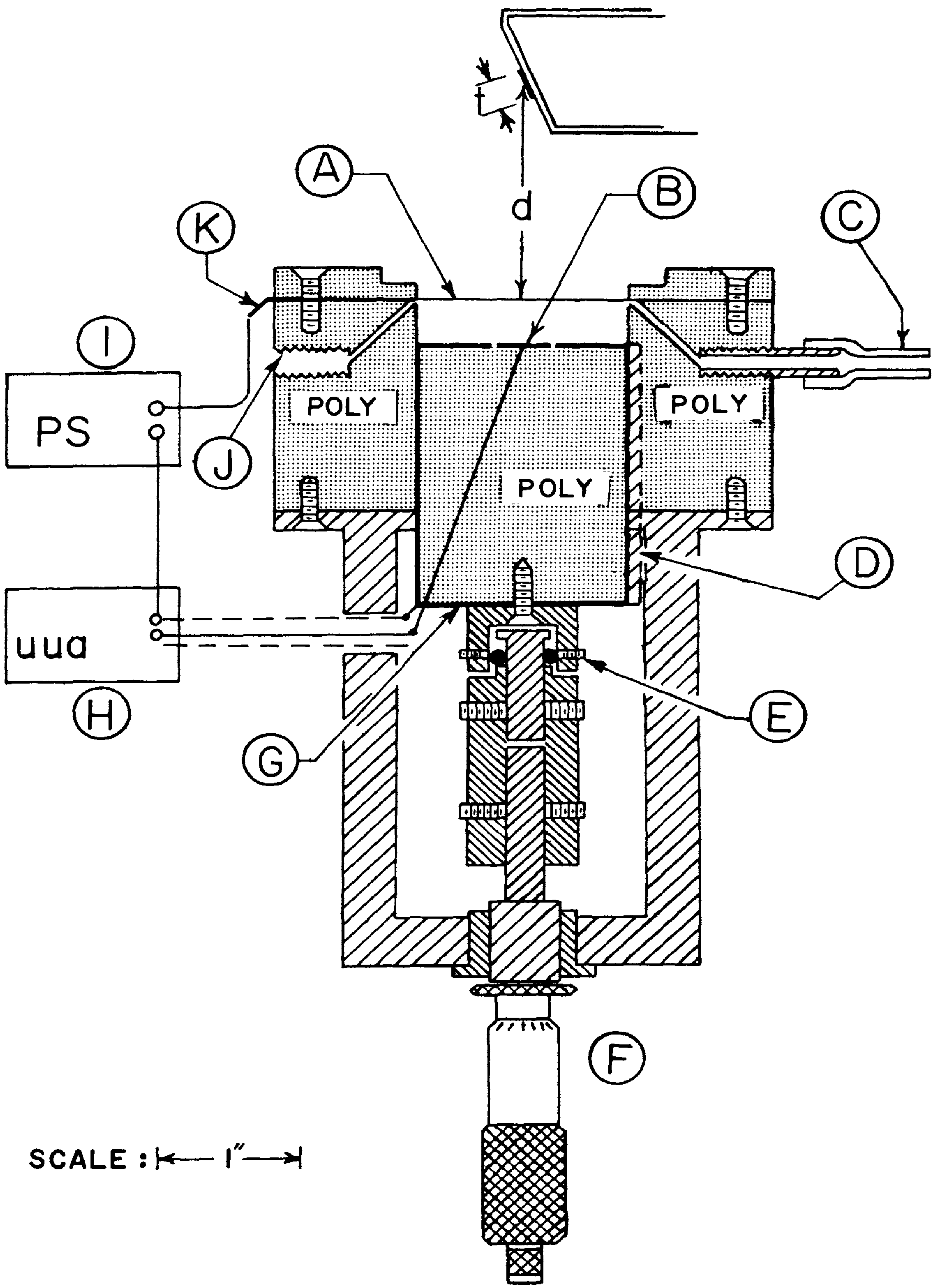
t
d
A
B
C
K
I
PS
J
POLY
POLY
POLY
D
uua
H
G
E
F
SCALE : 1"

The collection efficiency (f) of a parallel plate ion chamber, which was formulated by BOAG & WILSON (1952) and discussed in HEINE & BROWNELL (1956), is given by

$$f = \frac{1}{1+\eta} \tag{30}$$

where

$$\eta = Ai\cdot[L^3/v^2] \tag{31}$$

and where A is a system constant, i is the ionization current, L is the plate separation, and v is the collecting voltage. To insure constant and approximately 100% collection efficiency for the ion chamber during collection of variable plate separation data, a value of $L^3/v^2 = 1.372\cdot 10^{-8}$ $in^3/volt^2$ was employed which lay on the plateau portion of the saturation curve for the entire range of current values. A better approximation to constant collection efficiency (f) would have been provided with constant L^2/v since i is approximately proportional to L over the range of interest. However, the saturation plateau was sufficiently broad that no variation in collector current was observed over the range studied as the collector voltage was varied.

C. Deduction of X-Radiation Energy Deposition Rates

Ion chamber current was monitored with a Keithley model 417 picoammeter and recorded on a Moseley model 7100B dual channel strip chart recorder. The current suppression feature of the picoammeter was employed to maximize the resolution of the small changes in current associated with the small changes in plate separation which occurred in the presence of large absolute values of current and plate separation. Absolute current data were obtained by summing the differential data and incorporating correction factors arising from the differences in the scale ranges employed. Thus, the magnification of current variations was effected by partially suppressing the recorded initial absolute current value with the suppression feature of the Keithley 417 and observing the variation of the small residual current on a more sensitive scale.

Two corrections to the recorded ion current (i_{Ex}) are required to obtain the effective ionization current associated with events originating in the cavity gas (i_x) from which the rate of energy deposition in the gas may be deduced. These are associated with the fact that (a) the x-rays emanate from essentially a point source and represent a diverging beam, and (b) the Aquadag film of the collector plate-guard ring assembly and the beryllium window represent inherent inhomogeneities with respect to charged particle equilibrium in the chamber.

The ion chamber effectively measures the average rate of ionization at a position on its axis midway between the plates. As the plate separation increases, the midpoint moves further away from the radiation source; hence, it appears as if the ion chamber were moving away from the source of radiation. Since one wishes to deduce the equivalent rate of energy deposition at a fixed and known solid angle subtended by the collector area referenced to the target source, it is necessary to generate a means of normalizing the ion chamber data with respect to some fixed plane, which in this case was chosen to be the front face of the chamber window since it remains stationary. Hence, each ion chamber current reading is multiplied by a divergence correction factor (α) defined by

$$\alpha = \left[\frac{[d + (1/2)\ L]}{d} \right]^{1.980} \qquad (32)$$

where d is the distance from the x-ray target to the front face of the ion chamber window and L is the ion chamber plate separation read from the micrometer (F) in Fig. (1). The exponent value of 1.980 rather than the anticipated value of 2.000 best fit the data of JOYNER (1966), upon whose work the present dosimetry methods are based. However, at the values of $10 \leqq d \leqq 15$ inches used in the present study, the choice of the exponent is not critical.

In a truly homogeneous ion chamber, the ratio of ionization current to chamber volume should be a constant value independent of chamber volume, but if charged particle equilibrium does not exist, then a systematic variation of the ratio with volume should be anticipated. The variable plate separation ion chamber allows one to extract information on the number of ionization events per unit time which are characteristic of events originating within the cavity gas and which satisfy the conditions of charged particle equilibrium. As the plate separation increases, the change in the number of ionizing events per unit change in volume approaches a constant value. Mathematically, this suggests a correction statement of the form

$$\beta_x = \frac{\lim\limits_{V \to \infty} (\Delta \alpha i_{Ex} / \Delta V)}{\alpha i_{Ex} / V} \quad . \tag{33}$$

The significant difference between the variable plate separation ion chamber and the fixed plate separation chamber is demonstrated in Fig.(2) which depicts representative data used to correct for the chamber inhomogeneities and to provide an energy deposition rate which is characteristic of the ethylene gas only. The limiting value of $\Delta \alpha i_{Ex}/\Delta V$ as chamber volume (V) increases without limit represents ionization events originating in the cavity gas while the ratio of $\alpha i_{Ex}/V$ includes the

FIGURE 2

BETA CALIBRATION DATA: ZERO THICKNESS OF ATTENUATOR. □ -- Divergence (α) corrected ionization current density ($\alpha i_{Ex}/V$) vs. absolute plate separation (L). ◐ , ○ -- Differential divergence (α) corrected ionization current density ($\Delta\alpha i_{Ex}/\Delta V$) vs. average plate separation ($\bar{L}$): ◐ → ΔL = 0.100 inches, ○ → ΔL = 0.040 inches. $L^3/V^2 = 1.372 \cdot 10^{-8}$ in^3/v^2. Ethylene flow rate = 180 cc/min.

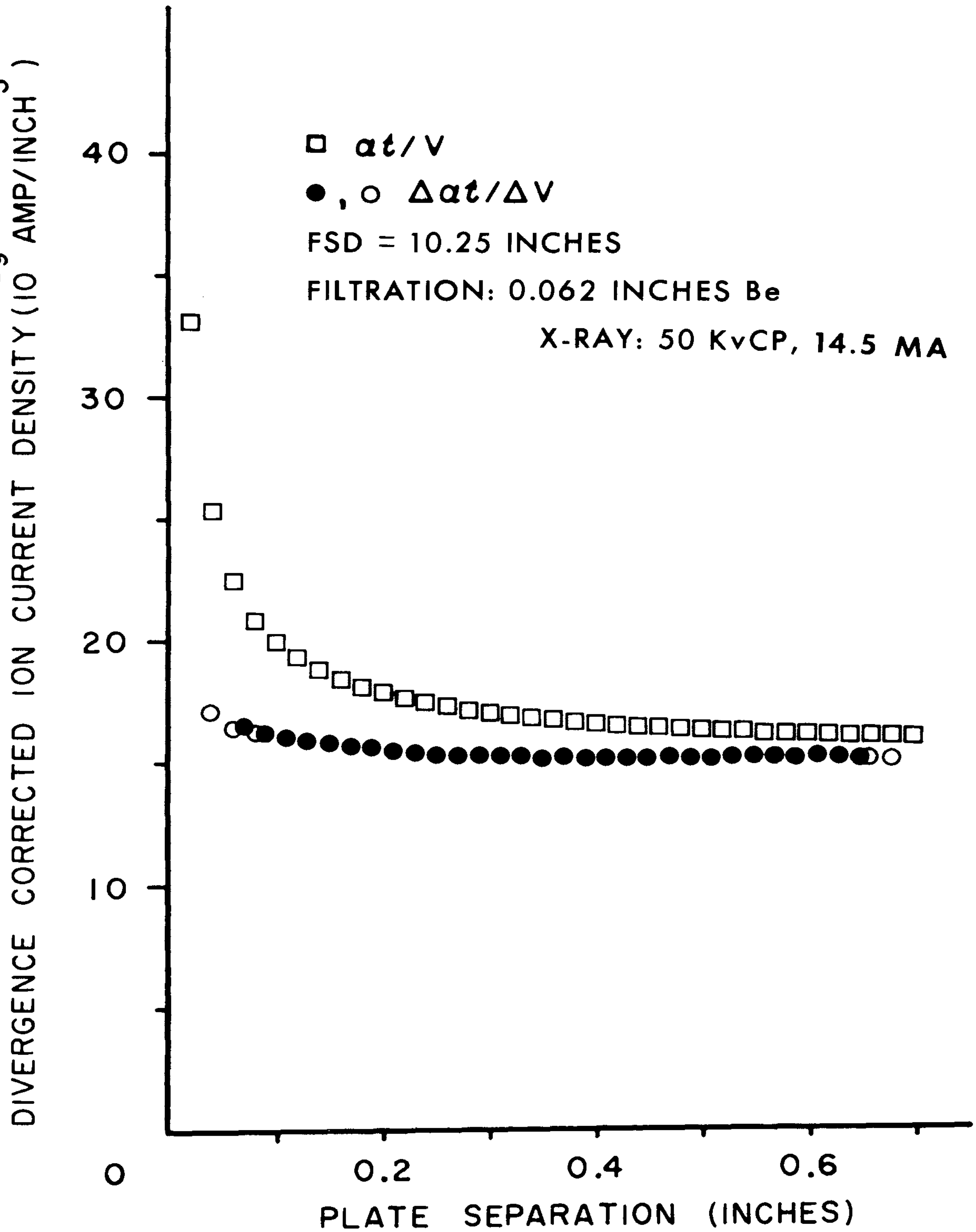

□ $a t/V$
●, ○ $\Delta a t/\Delta V$
FSD = 10.25 INCHES
FILTRATION: 0.062 INCHES Be
X-RAY: 50 KvCP, 14.5 MA
DIVERGENCE CORRECTED ION CURRENT DENSITY (10^{-9} AMP/INCH^3)
40
30
20
10
0
0.2
0.4
0.6
PLATE SEPARATION (INCHES)

contributions associated with the chamber inhomogeneities. Operating in a constant volume mode, Eq. (33) is equivalent to the previous Eq. (13) and serves to define how i_x is measured. It should be noted that β_x is a function of the plate separation L in the fixed plate separation mode.

The β_x correction is a function of the thickness of attenuator (x) through which the x-ray beam has passed before being intercepted by the detector. As the spectrum hardens, β_x decreases. In order to correctly interpret events originating in the cavity gas, it was necessary to measure β_x for various attenuator thicknesses in order to correctly specify

$$i_x = \alpha\beta_x i_{Ex} \tag{34}$$

which is the fraction of the measured ionization current (i_{Ex}) associated with events originating within the cavity gas and referenced to the front face of the dosimeter.

Data equivalent to that presented in Fig. (2) were generated to evaluate β_x as a function of attenuator thickness for both aluminum and polyethylene. These are collected in Appendices II and III. The results of these measurements for aluminum are tabulated in Table I and plotted in Fig. (3). Similar results for polyethylene are presented in Table II and Fig. (4).

This β_x correction is essentially a dosimeter wavelength dependence correction in addition to an ion chamber inhomogeneity correction. It can only be obtained with a variable plate separation chamber. Any fixed plate separation chamber would automatically incorporate the error which this β_x data removes from the experiment.

TABLE I

CHAMBER INHOMOGENEITY CORRECTION (β_x)
AS A FUNCTION OF ALUMINUM ATTENUATOR THICKNESS (x)
FOR PLATE SEPARATION (L) = 0.360 INCHES

x (g/cm^2)	$\left(\frac{\Delta\alpha i}{\Delta V}\right)$ Avg. (10^{9} amp/in^3)	$\frac{\alpha i}{V}$ (10^{9} amp/in^3)	β_x	$\sigma(\beta)$
0.0	1.519	1.674	0.9076	±0.0016
0.1315	1.782	2.388	0.7463	±0.0103
0.2632	0.9314	1.414	0.6586	±0.0023
0.5246	0.4791	0.8142	0.5884	±0.0019
1.002	0.2312	0.4287	0.5392	±0.0007
1.539	0.1193	0.2431	0.4909	±0.0008
2.469	0.0565	0.1173	0.4820	±0.0008

FIGURE 3

ION CHAMBER INHOMOGENEITY CORRECTION (β_x) FOR A PLATE SEPARATION (L) OF 0.360 INCHES AS A FUNCTION OF ALUMINUM ATTENUATOR THICKNESS (x). 50 KvCP x-ray beam with inherent filtration of 0.062 inches beryllium and 9.17 inches air. FSD = 10.25 inches.

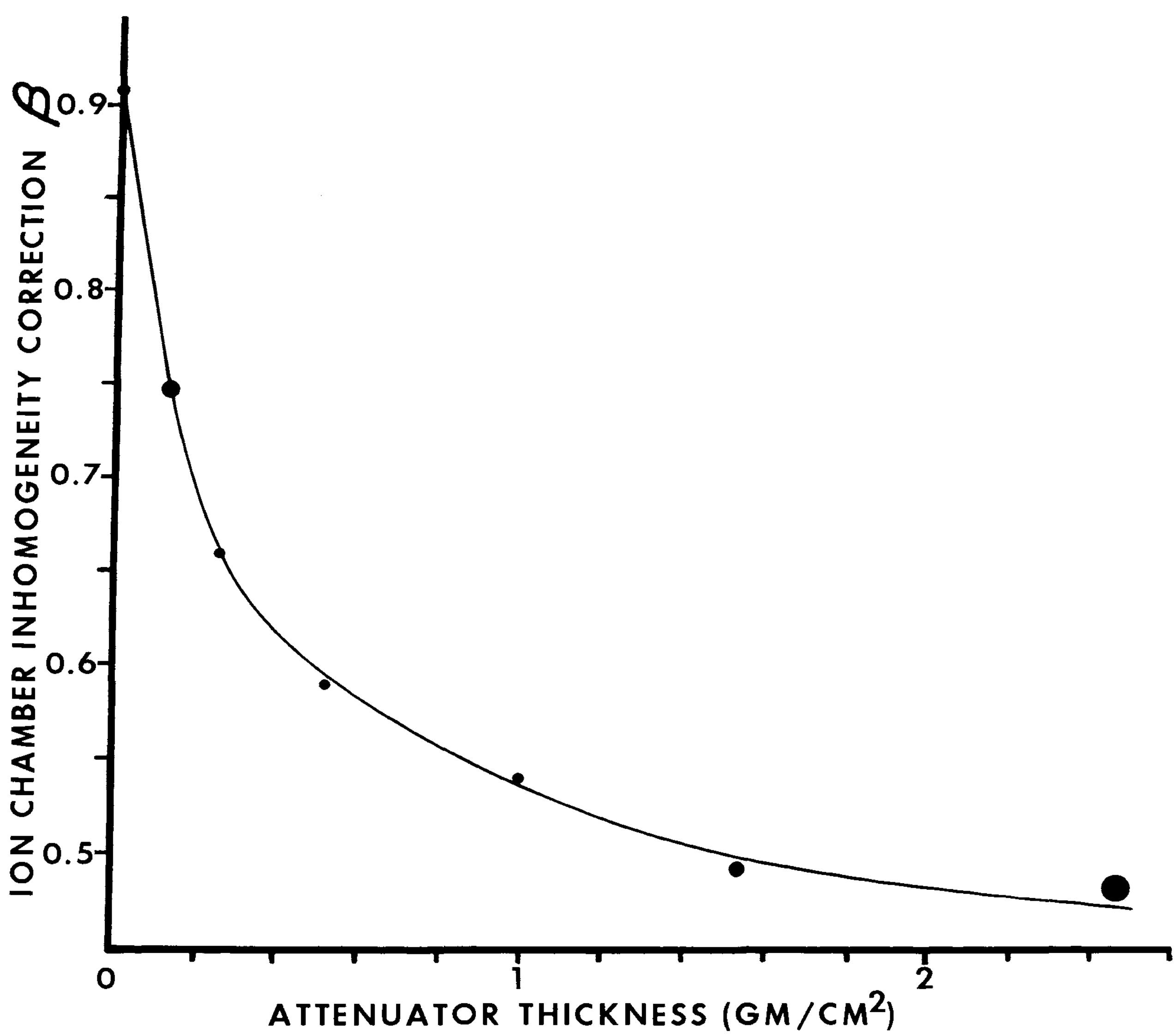
ION CHAMBER INHOMOGENEITY CORRECTION β
0.9
0.8
0.7
0.6
0.5
0
1
2
ATTENUATOR THICKNESS (GM/CM2)

TABLE II

CHAMBER INHOMOGENEITY CORRECTION (β_x)
AS FUNCTION OF ALUMINUM FILTERED (0.1315 g/cm^2) POLYETHYLENE
ATTENUATOR THICKNESS (x) FOR PLATE SEPARATION (L) = 0.360 INCHES

x (g/cm^2)	$\left(\frac{\Delta\alpha i}{\Delta V}\right)$ Avg. (10^{-9}amp/in^3)	$\frac{\alpha i}{V}$ (10^{-9}amp/in^3)	β_x	$\sigma(\beta)$
0.0	1.782	2.388	0.7463	±0.0103
0.1637	1.528	2.098	0.7301	±0.0073
0.3337	1.373	1.904	0.7213	±0.0040
0.6279	1.148	1.616	0.7107	±0.0037
1.317	0.8353	1.209	0.6910	±0.0049
2.594	0.5007	7.597	0.6591	±0.0017

FIGURE 4

ION CHAMBER INHOMOGENEITY CORRECTION (β_x) FOR A PLATE SEPARATION (L) OF 0.360 INCHES AS A FUNCTION OF POLYETHYLENE ATTENUATOR THICKNESS (x). 50 KvCP x-ray beam with inherent filtration of 0.062 inches beryllium, 9.17 inches air, and 0.1315 g/cm^2 aluminum. FSD = 10.25 inches.

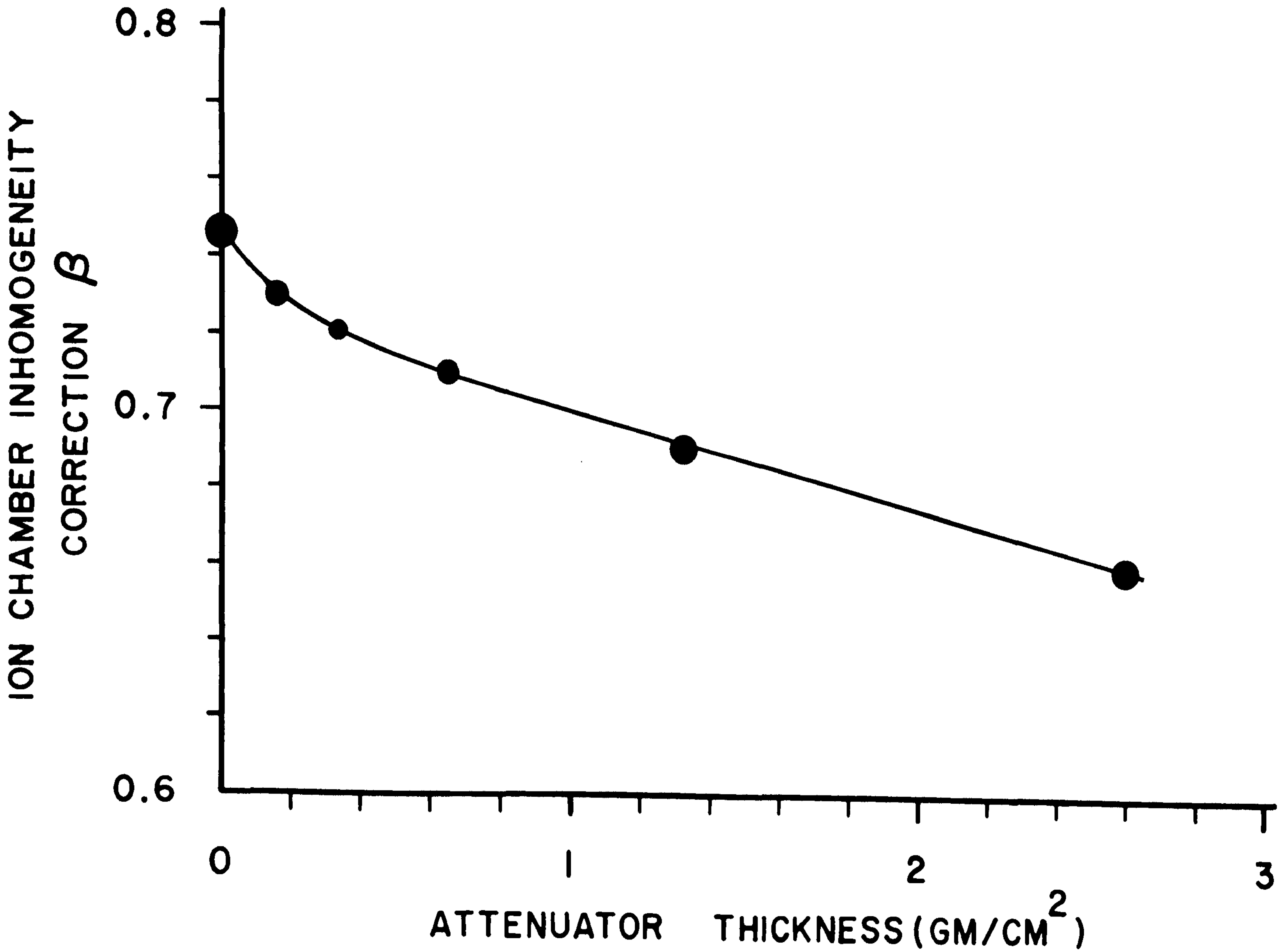
ION CHAMBER INHOMOGENEITY
CORRECTION β
0.8
0.7
0.6
0
1
2
3
ATTENUATOR THICKNESS (GM/CM²)

D. Selection of X-Ray Mass Attenuation and Absorption Coefficients

If we consider the basic interaction processes of photons with matter which can occur as the radiation traverses the distance between the radiation source and the detector, some insight can be gained with respect to the selection of attenuation coefficients. For the energy range employed here, only photoelectric absorption and atomic scattering events need be given consideration. These coefficients play a sensitive role in the deduction of the x-ray spectrum and the specification of the detector spectral absorbance. One notes in Eq. (23) that the derivative $dt/d\lambda$ is a factor in specifying $f_Y(\lambda)$, and $\mu_D(\lambda)L$ appears in the description of the detector response which is pertinent in the deduction of the spectrum. We shall be concerned with both mass attenuation coefficients and mass energy transfer coefficients in our analysis. Geometrical considerations will dictate in part the selection of the contributions to the attenuation coefficient that will be employed.

Since the attenuation coefficient of the standard aluminum attenuator does play such an important role in deducing the spectrum, it was necessary to perform an experiment to assess the amount of coherent and Compton scattering intercepted by the detector in order to justify their contribution to this term. The geometry employed was an extended version of the final configuration illustrated in Fig. (5) which allowed the dosimeter (window) to be placed at a position of 15.3 inches from the x-ray target. A 0.6 inch thick sample of polyethylene, 2.00 inches in diameter, was positioned at various points along the axis between the ion chamber window and the x-ray target; the ionization current as a function of position was then recorded with the results shown in Fig. (6). Examination of these results reveals scattering contributions to be

FIGURE 5

TOP VIEW OF EXPERIMENTAL GEOMETRY. (A) Tungsten target with 5 mm projected focal spot, (B) X-Ray tube window of 0.030 inches beryllium, (C) Attenuator chamber, (D) Lead baffles of $\sim$1/16 inch thickness with diameters specified by indicated solid angle, (E) Baffle housing and alignment jig, (F) Variable plate separation ion chamber window of 0.032 inches beryllium.

GE EA-75
X-RAY TUBE

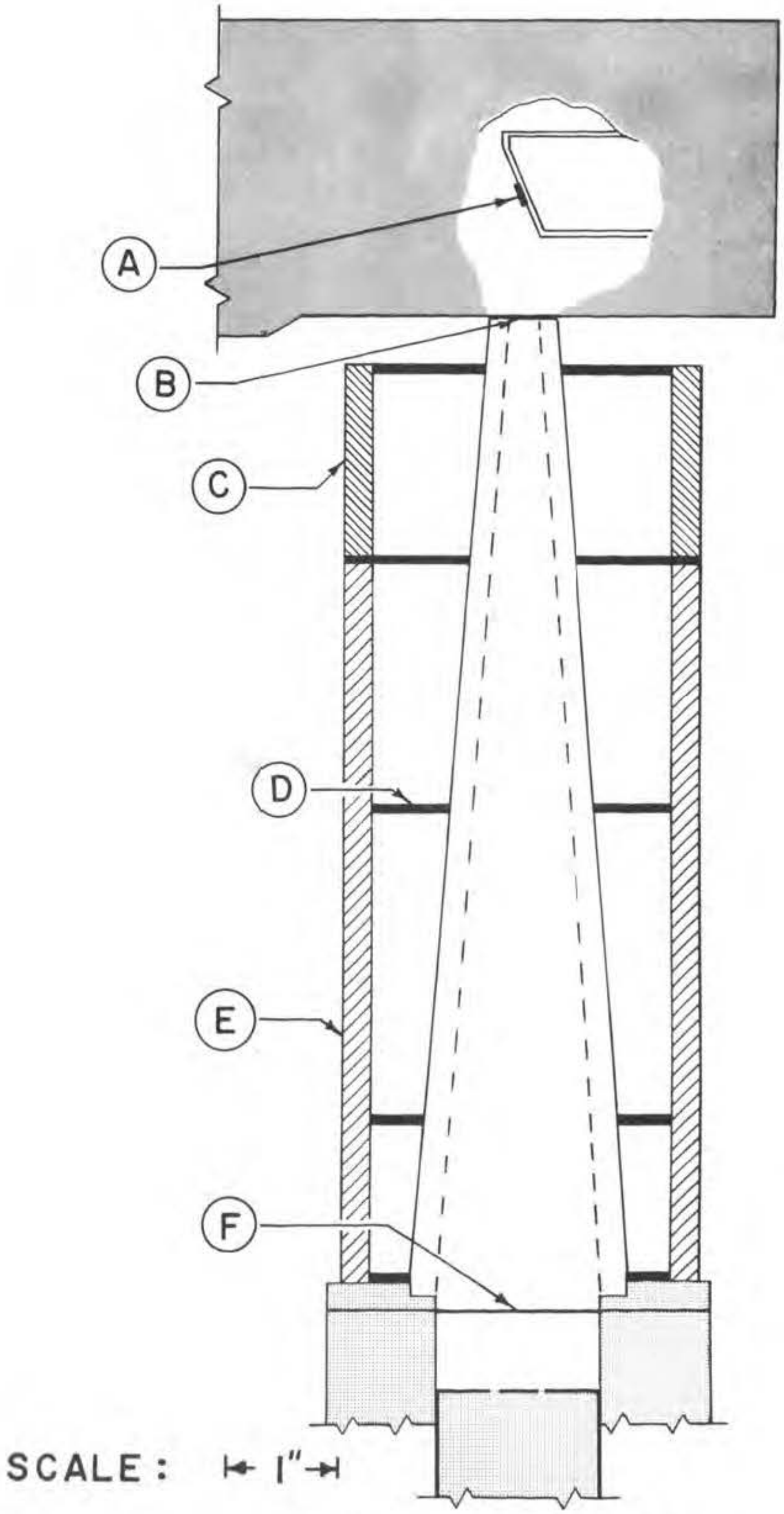

VARIABLE-PLATE
IONIZATION CHAMBER

FIGURE 6

ION CURRENT (i_{Ex}) AS A FUNCTION OF ATTENUATOR DISTANCE FROM DETECTOR WINDOW. 50 KvCP x-ray beam with inherent filtration of 0.062 inches beryllium, 14.22 inches air, and 1.353 g/cm^2 polyethylene. FSD = 15.30 inches.

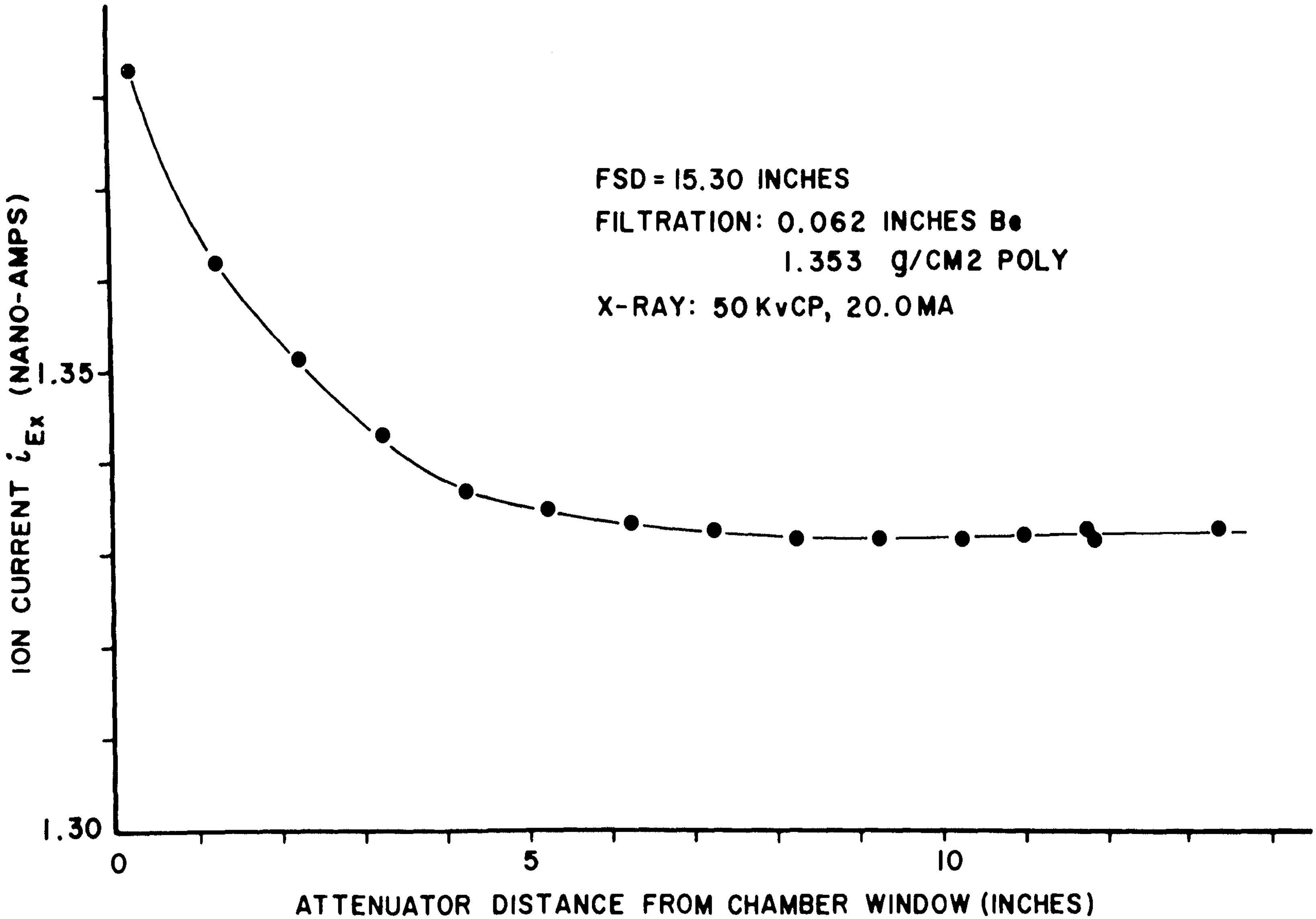

FSD = 15.30 INCHES
FILTRATION: 0.062 INCHES Be
1.353 g/CM2 POLY
X-RAY: 50 KvCP, 20.0 MA
ION CURRENT i_{Ex} (NANO-AMPS)
1.35
1.30
0
5
10
ATTENUATOR DISTANCE FROM CHAMBER WINDOW (INCHES)

negligible (or constant) for sample positions exceeding eight inches from the dosimeter window. To improve signal/noise ratios in data acquisition, the dosimeter and associated baffling were arranged as shown in Fig. (5) with a focus-surface distance (FSD) of 10.25 inches for all subsequent measurements involving the aluminum and polyethylene attenuators.

On the basis of this data it appeared justified to employ a $\mu_{tot}(\lambda)$ containing contributions from both scattering processes (since this energy was removed from the beam as far as the detector was concerned) and the photoelectric absorption for any attenuator being imposed in the beam in this geometry; thus,

$$\mu_{tot}(\lambda) = \mu_{inc}(\lambda) + \mu_{coh}(\lambda) + \mu_{\tau}(\lambda) \tag{35}$$

where $\mu_{inc}(\lambda) \equiv$ total Compton mass attenuation coefficient, $\mu_{coh}(\lambda) \equiv$ coherent scattering mass attenuation coefficient, $\mu_{\tau}(\lambda) \equiv$ photoelectric mass absorption coefficient.

In the case of the dosimeter one is only concerned with processes which relate to energy deposition in the cavity gas. Only two events impart energy to the medium, and these are photoelectric absorption and that fraction of the Compton process which is associated with the ejected electron.

Any attempt to reconstruct the spectrum of the x-ray tube target requires careful consideration of the position of the filtration material relative to the dosimeter in order to assess the various contributions to its attenuation coefficients.

A survey of the x-ray mass attenuation coefficients compiled by VICTOREEN (1943), GRODSTEIN (1957), McGINNIES (1959), and BERGER (1961) led to the conclusion that the most accurate information to-date was that of Berger, McGinnies, and Grodstein. This conclusion was based upon the reported percentages of accuracy of each reference; however, both Grodstein and McGinnies state that inaccuracies or estimated errors in earlier tabular information could easily approach 10% for coefficients corresponding to energies below 50 Kev, especially for light elements. However, due to considerable new experimental data, McGinnies states that her tabulation exhibits accuracies to 2% in the energy regime with which we are involved. Berger's paper was based upon and was intended to be utilized with the NBS Circular 583 and its supplement. After completion of the present study, the author noted a new and much more detailed summary report of x-ray attenuation coefficient data published by the Los Alamos Scientific Laboratory which is recommended for any further studies of this type [Ellery Storm and Harvey I. Israel, "Photon Cross Sections from 0.001 to 100 MeV for Elements 1 through 100" LA-3753, TID-4500 LASL, Nov. 15, 1967].

The various attenuation coefficient data required in this study were subjected to a least squares analysis to generate a polynomial describing their wavelength dependence. The FORTRAN logic for this analysis is listed in Appendix IV.

Table III shows the literature values and resulting 5th order predicted values of the mass energy transfer coefficients for the ethylene cavity gas. These values are the ones employed to specify $\mu_D(\lambda)$ in the analysis.

Table IV shows the literature and resulting 5th order polynomial predicted values for the total mass attenuation coefficients for (poly)-ethylene. These values were employed in the studies of the attenuation

TABLE III

MASS ENERGY TRANSFER OR ABSORPTION COEFFICIENTS FOR C, H, C_2H_4
(cm^2/g)

Source: Berger, 1961

Energy (kv)	(A)	C	H	Ethylene C_2H_4 (Literature)	C_2H_4 (Fitted)
100	0.12396	0.0214	0.0406	0.0242	0.02393
80	0.15496	0.0200	0.0362	0.0223	0.02248
60	0.20661	0.0201	0.0306	0.0216	0.02170
50	0.24793	0.0221	0.0271	0.0228	0.02302
40	0.30991	0.0302	0.0231	0.0291	0.02911
30	0.47321	0.0595	0.0186	0.0536	0.05319
20	0.61982	0.199	0.0133	0.1722	0.17244
15	0.82643	0.494	0.0111	0.4246	0.42453
10	1.23964	1.87	0.0099	1.6014	1.60140

Using 5th order $p(x) = a_0 + a_1x + a_2x^2 + \ldots$

$a_0 = 0.03284697 \quad a_3 = 1.3733233$

$a_1 = -0.06904819 \quad a_4 = -0.71879184$

$a_2 = -0.18301974 \quad a_5 = 0.34729856$

TABLE IV

TOTAL MASS ATTENUATION COEFFICIENTS FOR C, H, C_2H_4
(cm^2/g)

Source: Grodstein[a] & McGinnies[b]

Energy (kv)	(A)	H[a]	C[b]	Polyethylene C_2H_4 (Literature)	C_2H_4 (Fitted)
100	0.12396	0.295	0.152	0.173	0.1726
80	0.15496	0.309	0.161	0.183	0.1814
60	0.20661	0.326	0.174	0.196	0.1960
50	0.24793	0.335	0.184	0.206	0.2079
40	0.30991	0.345	0.205	0.225	0.2273
30	0.47321	0.357	0.253	0.268	0.2677
20	0.61982	0.369	0.424	0.417	0.4118
15	0.82643	0.377	0.755	0.701	0.7049
10	1.23964	0.385	2.22	1.95	1.953
8	1.62055	0.395	4.30	3.73	3.734

Using 5th order $p(x) = a_0 + a_1x + a_2x^2 + \ldots$

$a_0 = 0.13456500 \quad a_3 = -0.11398787$

$a_1 = 0.32984349 \quad a_4 = 1.5537852$

$a_2 = -0.19491743 \quad a_5 = -0.59536183$

of the x-ray beam by the polyethylene samples during checks of the predictive ability of the deduced x-ray spectrum.

Table V shows the literature and curve fitted values of the total mass attenuation coefficients of aluminum and beryllium and the data for air without the coherent contribution. A good fit of the aluminum data is particularly important here since the derivative of this curve plays an important role in establishing the x-ray spectrum in Eq. (23) where it appears as $dt/d\lambda$. The beryllium data in this table is used to specify the filtration by the x-ray tube window in reconstructing the x-ray spectrum at the tube target. The use of the air attenuation data w/o the coherent contribution was an arbitrary attempt to obtain an "effective" coefficient over the entire air path from the tube window to the dosimeter window. The choice for air did not sensitively affect the target referenced spectrum $[f_o(\lambda)]$ that was generated.

Table VI shows the literature and curve fitted mass energy transfer coefficients for beryllium. These data were applied to the specification of the effective filtration of the beryllium dosimeter window in reconstructing the x-ray spectrum at the tube target.

The curve fitting in every case appears to be satisfactory for the purpose of this study. Data were always extended to energies up to 100 Kv so that any slope data required from 50 Kv to lower energies would be dependable at the 50 Kv point.

E. Fabrication and Preparation of Attenuator Samples

With the interdependence of the geometrical configuration of the detector system and the selection of the various x-ray mass attenuation coefficients thus noted, samples of ∿2 inch diameter polyethylene and

TABLE V

MASS ATTENUATION COEFFICIENTS FOR Al (TOTAL), Be (TOTAL), AIR (W/O COHERENT) (cm^2/g)

Source: McGinnies, 1961

Energy		Al		Be		Air	
		Total		Total		w/o coherent	
(kv)	(A)	(Lit)	(Fitted)	(Lit)	(Fitted)	(Lit)	(Fitted)
100	0.12396	0.169	0.1647	0.133	0.1316	0.151	0.1506
80	0.15496	0.197	0.1947	0.140	0.1393	0.161	0.1601
60	0.20661	0.268	0.2697	0.148	0.1493	0.177	0.1774
50	0.24793	0.353	0.3595	0.154	0.1555	0.193	0.1940
40	0.30991	0.543	0.5556	0.162	0.1634	0.225	0.2268
30	0.41321	1.11	1.097	0.178	0.1763	0.315	0.3135
20	0.61982	3.37	3.363	0.219	0.2174	0.683	0.6811
15	0.82643	7.91	7.919	0.291	0.2925	1.44	1.442
10	1.23964	26.2	26.21	0.586	0.5857	4.76	4.760
8	1.62055	52.3	52.30	1.10	1.100	9.4	9.40

Al	Be	Air
a_0 = 0.13344217	a_0 = 0.08033692	a_0 = 0.10590459
a_1 = -0.18691079	a_1 = 0.59281896	a_1 = 0.46507523
a_2 = 3.0331828	a_2 = -1.7728069	a_2 = -1.2538133
a_3 = 2.3878178	a_3 = 2.8840037	a_3 = 3.3026251
a_4 = 14.595038	a_4 = -1.9289895	a_4 = -0.12352080
a_5 = -5.9335757	a_5 = 0.53142876	

TABLE VI

MASS ENERGY TRANSFER OR ABSORPTION COEFFICIENTS FOR BERYLLIUM (cm^2/g)

Source: McGinnies with Berger

Energy (kv)	λ (A)	(Lit)	(Fitted)
100	0.12396	0.018	0.0182
80	0.15496	0.016	0.0163
60	0.20661	0.014	0.0143
50	0.24793	0.013	0.0134
40	0.30991	0.013	0.0134
30	0.47321	0.017	0.0170
20	0.61982	0.040	0.0404
15	0.82643	0.094	0.0939
10	1.23964	0.353	0.3528
8	1.62055	0.755	0.7547

Using 5th order $p(x) = a_0 + a_1x + a_2x^2 + \ldots$

$a_0 = 0.02997959$ $a_3 = -0.21661733$

$a_1 = -0.12733652$ $a_4 = 0.24333794$

$a_2 = 0.28285558$ $a_5 = -0.03972112$

pure[1] aluminum with a known mass/area quantity were mounted on 2 x 4 inch plastic cards. The mounted attenuator samples could then be interposed between the x-ray source and the detector by placing them in the attenuator chamber (C) in Fig. (5) as depicted in Plate I. The diameter of the aluminum samples was precisely measured to within 0.0005 inch since the disks were turned on a machinist's lathe while the polyethylene samples were cut from a machined die of known diameter (known to within 0.001 inch). One 0.6 inch polyethylene sample was obtained from a cylindrical rod stock; this sample, however, was also turned on the lathe. Each of the samples of the aluminum and polyethylene attenuator material was individually weighed on a Sartorius semi-micro analytical balance to determine the sample mass to within 0.01 mg.

F. Regression Analysis of Attenuation Data

Using the five-parameter function described by Eq. (17) in a nonlinear regression analysis of the normalized ion current data, the parameters a, b, c, α, and γ were obtained. The computer logic for this analysis is listed in Appendix IV. Initial attempts to curve fit Eq. (17) by adjusting all five parameters simultaneously proved unrewarding; however, by having the IBM 360 computer print the values of the two terms contributing to $j(x)$, it was then possible to interpret the characteristics of each term. The second term of Eq. (17), $(1-a)\cdot[\alpha/(x+\alpha)]^{\gamma}$, was observed to contribute significantly to the curve fitting throughout the entire range of attenuator thickness values; whereas the first term,

$$a\cdot\exp[-b(\sqrt{x+c} - \sqrt{c})] \quad ,$$

---

[1] 99.993% pure by analysis; courtesy of Consolidated Aluminum Corp.

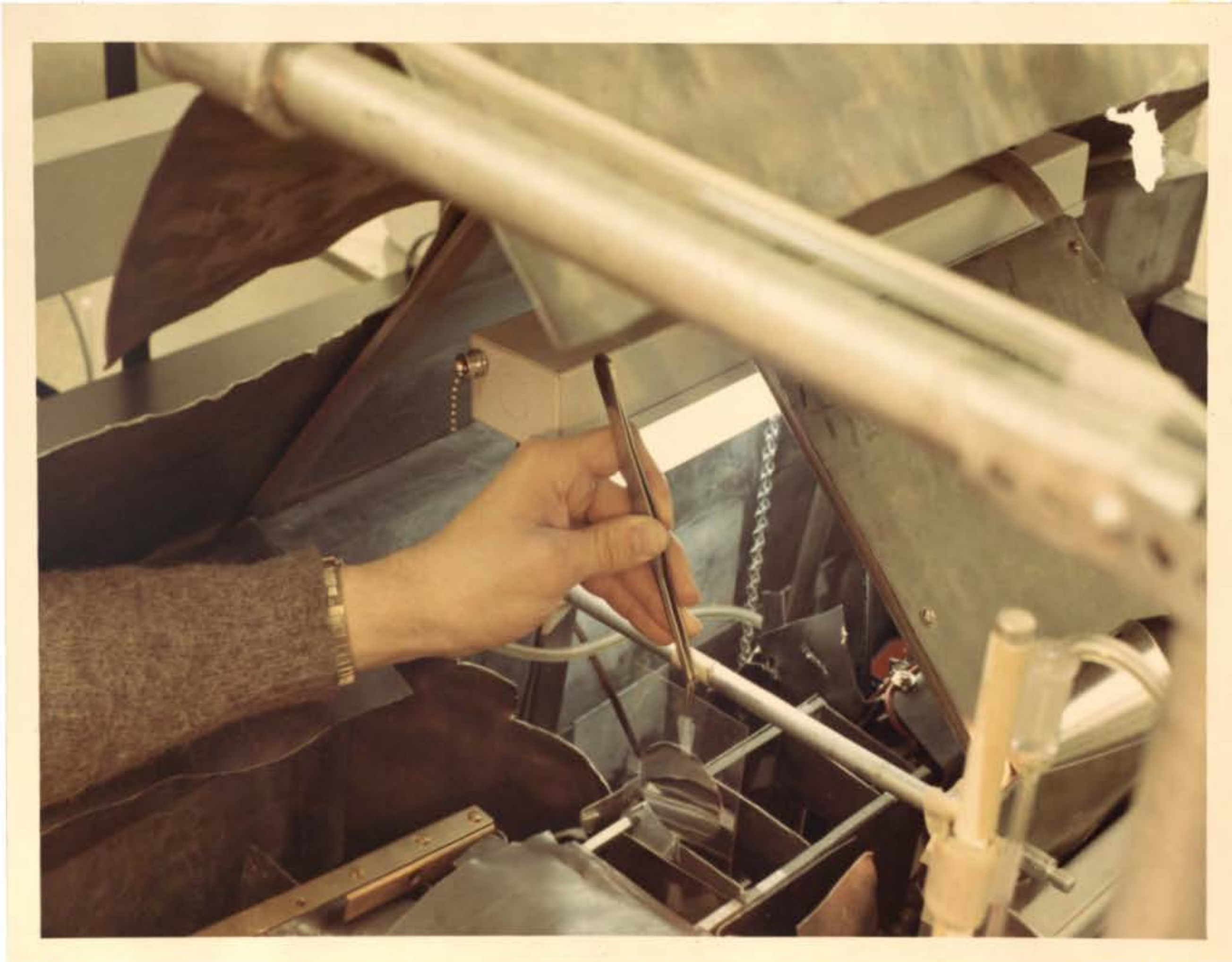

PLATE I. INSERTING MOUNTED SAMPLE OF Al ATTENUATOR INTO X-RAY BEAM contributed only at smaller values of thickness. Therefore, a simpler model containing only three adjustable parameters [a, α, γ] was fitted to the attenuation data at large thickness since the estimates of $j(x)$ did not exceed the experimental values toward the smaller values of x (attenuator thickness).

Trials of fitting the second term of Eq. (17) to the last nineteen, thirty-three, and the last thirty-five data sets of the forty-two experimental points indicated that the "last 33" trial, coupled with the results of adjusting only b and c in the entire function over the complete set of Al-attenuation data, provided the best over-all curve fit.

G. Evaluation of Spectral Absorbance and Total Spectral Distribution

Having obtained the parameters of Eq. (17) and the estimates [$j(x)$] of the experimental data, the Laplace transform [$\Psi(t)$] of Eq. (17), defined as Eq. (18), can be used to reconstruct the modified absolute spectrum $f_Y(\lambda)$. In addition to the normalized relative spectral intensity which is generated by

$$f_Y^*(\lambda) = \frac{[\Psi_Y(t)(dt/d\lambda)]\cdot[\mu_D(\lambda)L]}{[W\beta_0 i_{Eo})/(eI\cdot d\Omega)]} \quad , \qquad (40)$$

it will be found useful during comparison with other experimental work to have a description of the normalized relative spectral absorbance generated by

$$F_Y^*(\lambda) = F_Y(\lambda)\cdot\left[\int_{\lambda_0}^{\infty} F_Y(\lambda)d\lambda\right]^{-1} \quad . \qquad (41)$$

These forms were generated and the integrals evaluated by computer techniques for a series of upper limits on wavelength until a residual area of less than 5 parts per 10,000 was obtained.

H. Evaluation of Target Referenced Absolute Bremsstrahlung

Although one never directly measures the spectral distribution referenced to the target position within the x-ray tube [$f_o(\lambda)$], it is necessary to generate this information if one wishes to compare the experimental results with the theoretical predictions of KRAMERS (1923) and EHRLICH (1955). For the purposes of comparison, the absolute x-ray spectrum emanating from the tube target [$f_o^E(\lambda)$] was recovered from the filtered absolute spectrum $f_Y(\lambda)$.

The "recovery" process only involved accounting for the contributions to the inherent filtration (y) which modifies $f_o^E(\lambda)$. There are four pertinent contributions to the filtration which can be referred to as (a) Y1 = the 0.030 inch thick beryllium x-ray window, (b) Y2 = the 0.032 inch thick beryllium dosimeter window, (c) Y3 = the 9.17 inches of air between the two windows, and (d) Y4 = the aluminum "filter" of 0.1315 g/cm^2 thickness. Converting these dimensions to compatible units with the mass attenuation coefficients, $f_o^E(\lambda)$ is generated by

$$f_o^E(\lambda) = f_Y(\lambda)\cdot\exp[Y1\cdot\mu_{Y1}(\lambda) + Y2\cdot\mu_{Y2}(\lambda) + Y3\cdot\mu_{Y3}(\lambda) + Y4\cdot\mu_{Y4}(\lambda)], \quad (42)$$

where the quantities Yn (n = 1→4) represent the respective amounts of filter in g/cm^2 and $\mu_{Yn}(\lambda)$ represent their respective mass attenuation coefficients. (The mass attenuation coefficients for Y1, Y3, and Y4 are listed in Table V, while the mass energy transfer coefficients for Y2 are shown in Table VI.) The bremsstrahlung [$f_o^{EB}(\lambda)$] and characteristic radiation [$f_o^{EC}(\lambda)$] components of the target-referenced absolute x-ray spectrum [$f_o^E(\lambda)$] may therefore be evaluated and plotted[1] by modifying Eqs. (24)

---

[1]FORTRAN logic to accomplish this task is listed in Appendix IV.

and (25), respectively to yield

$$f_o^{EC}(\lambda) = f_Y^C(\lambda)\cdot\exp\left[\sum_{n=1}^{4} Yn\cdot\mu_{Yn}(\lambda)\right] \tag{43}$$

and

$$f_o^{EB}(\lambda) = f_Y^B(\lambda)\cdot\exp\left[\sum_{n=1}^{4} Yn\cdot\mu_{Yn}(\lambda)\right] \quad . \tag{44}$$

We can at this point compare the experimentally deduced bremsstrahlung emanating from the target $[f_o^{EB}(\lambda)]$ with Kramers' theoretical spectrum $[f_o^K(\lambda)]$ by evaluating the constant C in

$$f_o^K(\lambda) = C\cdot[1/\lambda^2(1/\lambda_0 - 1/\lambda)] \quad . \tag{45}$$

Recognizing that a meaningful method of comparison would be effected by requiring the integrated intensity or area under each spectral curve to be equal, we establish the definite integrals

$$\int_{\lambda_0}^{\varepsilon\lambda_0} f_o^{EB}(\lambda)d\lambda \equiv \int_{\lambda_0}^{\varepsilon\lambda_0} f_o^K(\lambda)d\lambda = C\cdot\left[(1/\lambda_0^2\ )\ \frac{(\varepsilon-1)^2}{2\varepsilon^2}\right] \tag{46}$$

from which one obtains

$$C = \frac{2\varepsilon^2\lambda_0^2}{(\varepsilon-1)^2}\cdot\int_{\lambda_0}^{\varepsilon\lambda_0} f_o^{EB}(\lambda)d\lambda \quad . \tag{47}$$

Permitting $\lambda_0 = 0.24792$ A and $\lambda_{max} = 1.7380$ [the final value of lambda in the evaluation of $f_y(\lambda)$], the parameter (ε) defined as

$$\varepsilon = \frac{\lambda_{max}}{\lambda_0} \tag{48}$$

would be 7.0103. Investigations have indicated that this upper bound leaves $\sim$26% of the total bremsstrahlung unaccounted for.

Evaluation of the definite integrals in the above statements was accomplished by employing Simpson's method in a FORTRAN IV logic similar to the integration program listed in Appendix IV. Since the integration of $f_o^{EB}(\lambda)$ was performed over the range of $0.24792 \leq \lambda \leq 1.7380$ angstrom, while polynomial representation of the attenuation coefficients, which determine $f_o^{EB}(\lambda)$, were available for lambda from λ_0 to $\lambda \leq 1.6$ angstrom, a lambda-cubed approximation was assumed for the extension $1.5 \leq \lambda \leq 1.7380$ angstrom. Integrating $f_o^{EB}(\lambda)$, the integrated intensity under $f_o^{EB}(\lambda)$ is $6.1023 \cdot 10^{16}$ $ev \cdot s^{-1} \cdot ma^{-1} \cdot sr^{-1}$. Eq. (45) can now be explicitly written as

$$f_o^K(\lambda) = [1.03806 \cdot 10^{16} \ ev \cdot s^{-1} \cdot ma^{-1} \cdot sr^{-1} \cdot A^2] \cdot [(1/\lambda^2) \cdot (1/\lambda_0 - 1/\lambda)], \quad (49)$$

allowing the two spectra to be expressed in compatible units.

IV. EXPERIMENTAL RESULTS

The regression analysis described in the previous chapter was applied to the aluminum attenuation data to obtain the results shown in Table VII. The deduced spectrum is extremely sensitive to the quality of the fit that is obtained. An examination of the experimental and predicted values shows a maximum difference of 0.7% over the entire set of data. This small variation, which represents the maximum of the error oscillation, is particularly gratifying in that it does not occur at the extremes of the thickness data and hence the hard and soft portions of the spectrum are assumed to be appropriately weighted. It should be noted that the computer generated data carries more significant figures than are available from the experimental data, but the fitting function assumes maximum absolute significance for the data presented and the resultant values of a,b,c,α,γ are presented with this implied reservation.

Fig. (7) shows a comparison of the normalized 50 KvCP spectral intensity $[f_Y^*(\lambda)]$ with the normalized detector spectral absorbance $[F_Y^*(\lambda)]$ for the beam subjected to an inherent filtration of 0.062 inch of beryllium, 0.1315 g/cm^2 aluminum and 9.17 inches of air. It is apparent that some residual characteristic radiation is still present after filtration by approximately 0.5 mm of aluminum. This value of filtration has been employed [WANG, *et. al.* (1957) and NORMAN & GREENFIELD (1955)] to remove by definition the characteristic contribution to the recorded integrated intensity. A large fraction of the response of a typical ionization detector such as the unit employed here, however, is associated with this residual characteristic spectrum, as may be seen from the peak in $F_Y^*(\lambda)$ centered at about 1.12 A.

The individual contributions of each of the two terms of the trans-

TABLE VII

EXPERIMENTAL AND TRANSFORM PREDICTED NORMALIZED ION CHAMBER CURRENTS AS A FUNCTION OF ALUMINUM ATTENUATOR THICKNESS (x)

Transform Constants

$\mu_0 = 0.3595\ cm^2/g$ $a = 0.19749987$ $b = 22.62371826$ $c = 0.27262676$ $\alpha = 0.27051646$ $\gamma = 1.07769299$

					$[(\beta_x i_{Ex})/(\beta_0 i_{Eo})] * \exp[\mu_0(x-x_o)]$			
						j(x), fitted		
x (g/cm^2)	β_x (L=0.360in)	$\beta_x i_{Ex}$ (nano-amp)	$(\beta_x i_{Ex})*\exp[\mu_0 x]$ (nano-amp)	$(x - x_o)$ (g/cm^2)	Experimental	Total	1st Term	2nd Term
0.0	0.9076	8.141	8.141					
0.0219	0.878	3.861	3.891					
0.0439	0.852	2.215	2.250					
0.0659	0.826	1.454	1.488					
0.0877	0.801	1.060	1.093					
0.1096	0.774	0.8267	0.8593					
0.1315	0.7463	0.6770	0.7091	0.0	1.0000	1.00000	0.19750	0.80250
0.1534	0.728	0.5798	0.6121	0.0219	0.8632	0.86147	0.12379	0.73768
0.1754	0.711	0.5089	0.5414	0.0439	0.7634	0.76118	0.07893	0.68225
0.1974	0.695	0.4535	0.4862	0.0659	0.6857	0.68547	0.05112	0.63435
0.2193	0.682	0.4108	0.4439	0.0878	0.6260	0.62641	0.03365	0.59276
0.2412	0.670	0.3763	0.4097	0.1097	0.5778	0.57835	0.02239	0.55596
0.2632	0.660	0.3471	0.3809	0.1317	0.5371	0.53838	0.01506	0.52332
0.2851	0.650	0.3221	0.3562	0.1536	0.5023	0.50447	0.01025	0.49422
0.3069	0.643	0.3010	0.3355	0.1754	0.4731	0.47525	0.00705	0.46820
0.3289	0.635	0.2819	0.3166	0.1974	0.4464	0.44945	0.00489	0.44456
0.3508	0.629	0.2656	0.3006	0.2193	0.4239	0.42657	0.00342	0.42315
0.3728	0.623	0.2506	0.2859	0.2413	0.4031	0.40605	0.00241	0.40364
0.3948	0.6175	0.2374	0.2729	0.2633	0.3848	0.38744	0.00171	0.38573

TABLE VII (continued)

x	β_x	$\beta_x i_{Ex}$	$(\beta_x i_{Ex})$*exp$[\mu_0 x]$	$(x - x_o)$	$[(\beta_x i_{Ex})/(\beta_0 i_{Eo})]$ * exp$[\mu_0(x-x_o)]$			
						j(x), fitted		
(g/cm^2)	(L=0.360in)	(nano-amp)	(nano-amp)	(g/cm^2)	Experimental	Total	1st Term	2nd Term
0.4159	0.614	0.2261	0.2619	0.2844	0.3693	0.37119	0.00124	0.36995
0.4376	0.6095	0.2151	0.2511	0.3061	0.3541	0.35583	0.00089	0.35494
0.4808	0.601	0.1959	0.2328	0.3493	0.3283	0.32870	0.00030	0.32840
0.5246	0.594	0.1793	0.2158	0.3931	0.3043	0.30533	0.00026	0.30507
0.5686	0.587	0.1648	0.2015	0.4371	0.2841	0.28482	0.00014	0.28468
0.6116	0.5805	0.1526	0.1893	0.4801	0.2670	0.26725	0.00008	0.26717
0.6554	0.5745	0.1415	0.1783	0.5239	0.2515	0.25136	0.00004	0.25132
0.6986	0.569	0.1318	0.1687	0.5671	0.2379	0.23740	0.00003	0.23737
0.7419	0.5635	0.1230	0.1598	0.6104	0.2254	0.22484	0.00002	0.22482
0.7851	0.558	0.1151	0.1518	0.6536	0.2141	0.21354	0.00001	0.21353
0.8289	0.553	0.1078	0.1445	0.6974	0.2038	0.20314	0.00001	0.20313
0.8729	0.548	0.1011	0.1375	0.7414	0.1939	0.19363	0.0	0.19363
0.9169	0.5435	0.0950	0.1313	0.7854	0.1852	0.18495	0.0	0.18495
0.9594	0.539	0.0897	0.1258	0.8279	0.1775	0.17725	0.0	0.17725
1.002	0.535	0.0847	0.1207	0.8713	0.1703	0.16999	0.0	0.16999
1.045	0.531	0.0803	0.1161	0.9136	0.1637	0.16346	0.0	0.16346
1.088	0.527	0.0759	0.1115	0.9572	0.1573	0.15722	0.0	0.15722
1.175	0.520	0.0683	0.1035	1.044	0.1459	0.14601	0.0	0.14601
1.263	0.513	0.0617	0.0964	1.131	0.1359	0.13622	0.0	0.13622
1.349	0.5075	0.0560	0.0902	1.217	0.1272	0.12776	0.0	0.12776
1.445	0.502	0.0506	0.0844	1.313	0.1190	0.11945	0.0	0.11945
1.539	0.4975	0.0461	0.0793	1.407	0.1119	0.11225	0.0	0.11225
1.629	0.4935	0.0422	0.0751	1.497	0.1059	0.10611	0.0	0.10611
1.723	0.490	0.0387	0.0710	1.592	0.1002	0.10032	0.0	0.10032
1.815	0.487	0.0356	0.0677	1.683	0.0954	0.09526	0.0	0.09526
1.909	0.484	0.0329	0.0645	1.777	0.0909	0.09057	0.0	0.09057
2.003	0.482	0.0303	0.0614	1.871	0.0866	0.08628	0.0	0.08628
2.237	0.476	0.0249	0.0549	2.106	0.0775	0.07716	0.0	0.07716
2.469	0.4715	0.0208	0.0498	2.337	0.0703	0.06979	0.0	0.06979

FIGURE 7

50 KvCP NORMALIZED SPECTRAL INTENSITY DISTRIBUTION $[f_y^*(\lambda)]$ AND THE ASSOCIATED NORMALIZED DOSIMETER SPECTRAL ABSORBANCE $[F_y^*(\lambda)]$. Inherent filtration: 0.062 inches beryllium, 9.17 inches air, and 0.1315 g/cm^2 aluminum. FSD = 10.25 inches.

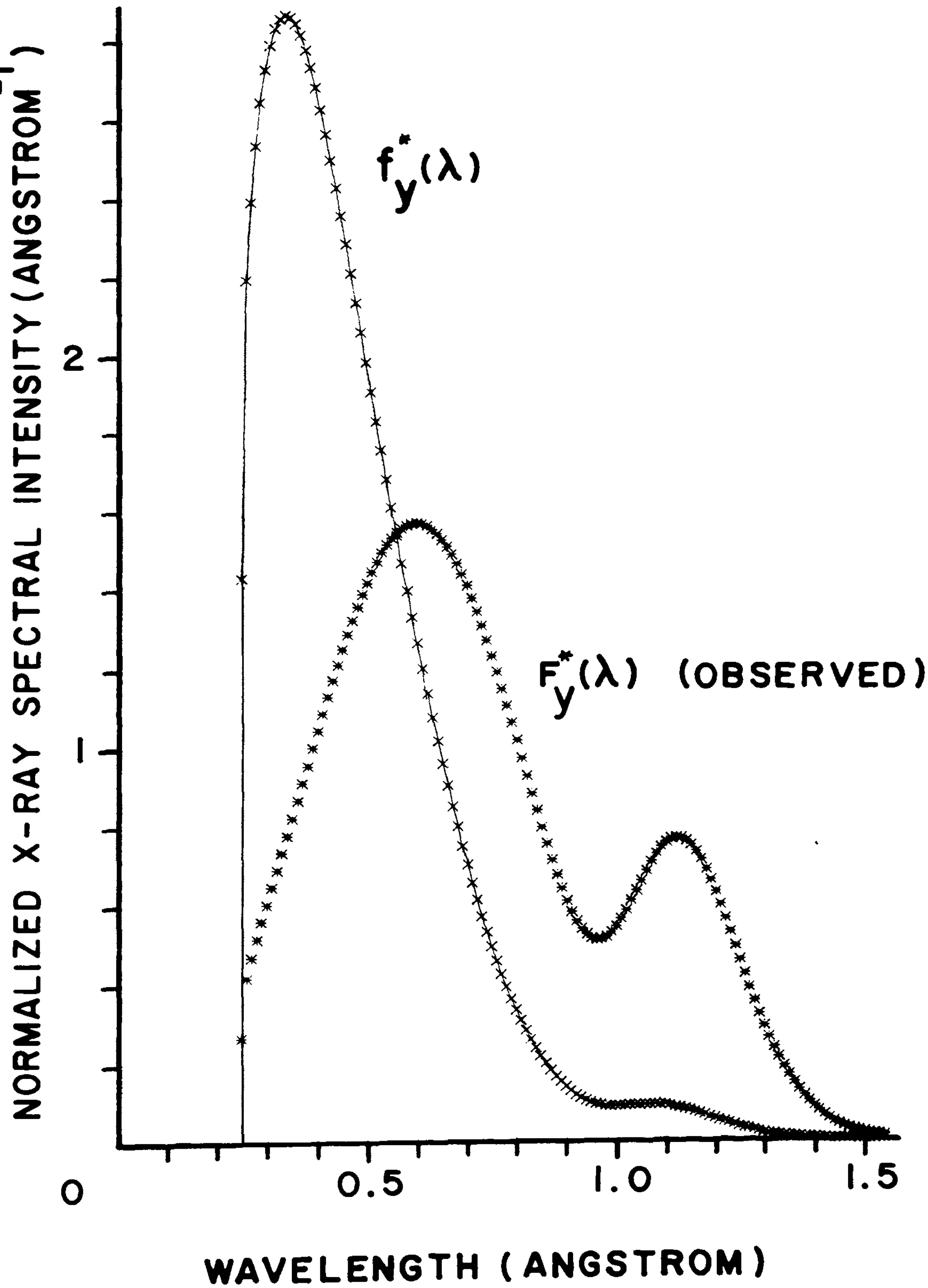

NORMALIZED X-RAY SPECTRAL INTENSITY (ANGSTROM^{-1})
2
1
0
0.5
1.0
1.5
$f_y^*(\lambda)$
$F_y^*(\lambda)$ (OBSERVED)
WAVELENGTH (ANGSTROM)

form generated spectrum to the absolute x-ray spectral intensity referenced to the tube target are tabulated in Table VIII and plotted in Fig. (8). It is apparent here that one of the terms associated with $f_o^{EB}(\lambda)$ attempts to fit the bremsstrahlung and the other, the characteristic spectrum $f_o^{EC}(\lambda)$ of the tube target material. The tungsten L_α and L_β lines lie at 1.476 and 1.267 A, respectively, with an intensity ratio $I_\beta/I_\alpha = 0.646$. The present fit appears to center on a wavelength of 1.22 A which is displaced to slightly shorter wavelengths than the average of the characteristic lines would suggest. The noticeable discontinuity at 1.538 A is caused by replacing the polynomially fitted wavelength dependence of the attenuation coefficients with a simple, data fitted λ^3 dependence for the longer wavelengths. The absolute spectrum values are based upon a W value of 26.3 ±0.3 ev per ion pair for ethylene, which is quoted in a survey article by WHYTE (1963).

If the spectrum that has been generated here represents a reasonable empirical approximation to the true spectrum, then it should be useful in predicting the energy deposition in any material for which adequate data on energy transfer coefficients are available. This point was checked by using the transform generated spectrum to predict the detector integrated spectral absorbance as a function of aluminum and polyethylene attenuator thickness.[1] The results for aluminum are shown in Table IX. The good results in this case ($\tilde{<}$0.7%) are not unexpected, since the same aluminum data are employed in generating the spectrum.

The data for polyethylene are presented in Table X. The predicted values agree with the experimental data to within less than 1% for poly-

---

[1]The "predictive FORTRAN logic" listed in Appendix IV was employed to achieve these predictions; again, a Simpson's numerical integration was incorporated into the program.

TABLE VIII

50 KvCP ABSOLUTE X-RAY SPECTRAL INTENSITIES AT TUBE TARGET

(10^{16}ev*s^{-1}*ma^{-1}*sr^{-1}*A^{-1})

λ(A)	$f_o^E(\lambda)$	$f_o^{EC}(\lambda)$	$f_o^{EB}(\lambda)$	$f_o^K(\lambda)$
0.248	6.663	0.0	6.663	0.019
0.258	10.237	0.0	10.237	2.455
0.268	11.216	0.0	11.216	4.366
0.278	11.940	0.0	11.940	5.860
0.288	12.517	0.0	12.517	7.023
0.298	12.980	0.0	12.980	7.922
0.308	13.347	0.0	13.347	8.608
0.318	13.628	0.0	13.628	9.123
0.328	13.830	0.0	13.830	9.500
0.338	13.962	0.0	13.962	9.766
0.348	14.032	0.0	14.032	9.942
0.358	14.046	0.0	14.046	10.044
0.368	14.011	0.0	14.011	10.088
0.378	13.933	0.0	13.933	10.083
0.388	13.818	0.0	13.818	10.040
0.398	13.672	0.0	13.672	9.966
0.408	13.500	0.000	13.500	9.868
0.418	13.305	0.000	13.305	9.750
0.428	13.092	0.000	13.092	9.616
0.438	12.863	0.000	12.863	9.471
0.448	12.622	0.000	12.622	9.316
0.458	12.371	0.000	12.371	9.155
0.468	12.112	0.000	12.112	8.989
0.478	11.847	0.000	11.847	8.820
0.488	11.578	0.000	11.578	8.649
0.498	11.305	0.000	11.305	8.477
0.508	11.030	0.000	11.030	8.306
0.518	10.754	0.000	10.754	8.138
0.528	10.478	0.000	10.478	7.966

TABLE VIII (continued)

50 KvCP ABSOLUTE X-RAY SPECTRAL INTENSITIES AT TUBE TARGET

($10^{16}ev*s^{-1}*ma^{-1}*sr^{-1}*A^{-1}$)

λ (A)	$f_o^E(\lambda)$	$f_o^{EC}(\lambda)$	$f_o^{EB}(\lambda)$	$f_o^K(\lambda)$
0.538	10.202	0.000	10.202	7.799
0.548	9.926	0.000	9.926	7.634
0.558	9.652	0.000	9.652	7.472
0.568	9.379	0.000	9.379	7.313
0.578	9.109	0.000	9.109	7.157
0.588	8.841	0.000	8.841	7.004
0.598	8.575	0.000	8.575	6.854
0.608	8.312	0.000	8.312	6.708
0.618	8.052	0.000	8.052	6.565
0.628	7.795	0.000	7.795	6.425
0.638	7.541	0.000	7.541	6.289
0.648	7.290	0.000	7.290	6.156
0.658	7.044	0.000	7.044	6.027
0.668	6.800	0.000	6.800	5.900
0.678	6.561	0.000	6.561	5.778
0.688	6.325	0.000	6.325	5.658
0.698	6.094	0.000	6.094	5.541
0.708	5.866	0.000	5.866	5.428
0.718	5.643	0.000	5.643	5.317
0.728	5.424	0.000	5.424	5.210
0.738	5.210	0.000	5.210	5.105
0.748	5.000	0.000	5.000	5.003
0.758	4.794	0.000	4.794	4.904
0.768	4.593	0.000	4.593	4.807
0.778	4.397	0.000	4.397	4.713
0.788	4.206	0.000	4.206	4.621
0.798	4.020	0.001	4.019	4.532
0.808	3.839	0.002	3.837	4.445
0.818	3.663	0.003	3.660	4.361
0.828	3.494	0.006	3.488	4.278

TABLE VIII (continued)

50 KvCP ABSOLUTE X-RAY SPECTRAL INTENSITIES AT TUBE TARGET

(10^{16}ev*s^{-1}*ma^{-1}*sr^{-1}*A^{-1})

λ(A)	$f_o^E(\lambda)$	$f_o^{EC}(\lambda)$	$f_o^{EB}(\lambda)$	$f_o^K(\lambda)$
0.838	3.331	0.010	3.321	4.198
0.848	3.175	0.016	3.159	4.120
0.858	3.027	0.024	3.003	4.044
0.868	2.889	0.038	2.851	3.970
0.878	2.760	0.056	2.704	3.898
0.888	2.644	0.082	2.562	3.827
0.898	2.542	0.116	2.426	3.759
0.908	2.456	0.162	2.294	3.692
0.918	2.389	0.221	2.168	3.626
0.928	2.342	0.296	2.046	3.563
0.938	2.317	0.388	1.929	3.501
0.948	2.318	0.501	1.817	3.440
0.958	2.346	0.636	1.710	3.381
0.968	2.402	0.795	1.607	3.324
0.978	2.487	0.978	1.509	3.268
0.988	2.602	1.187	1.415	3.213
0.998	2.748	1.422	1.326	3.159
1.008	2.922	1.681	1.241	3.107
1.018	3.123	1.963	1.160	3.056
1.028	3.349	2.265	1.084	3.006
1.038	3.596	2.585	1.011	2.958
1.048	3.862	2.920	0.942	2.910
1.058	4.142	3.265	0.877	2.864
1.068	4.432	3.616	0.816	2.819
1.078	4.726	3.968	0.758	2.774
1.088	5.019	4.316	0.703	2.731
1.098	5.306	4.654	0.652	2.689
1.108	5.583	4.980	0.603	2.647
1.118	5.845	5.287	0.558	2.607
1.128	6.088	5.572	0.516	2.567

TABLE VIII (continued)

50 KvCP ABSOLUTE X-RAY SPECTRAL INTENSITIES AT TUBE TARGET

(10^{16}ev*s^{-1}*ma^{-1}*sr^{-1}*A^{-1})

λ (A)	$f_o^E(\lambda)$	$f_o^{EC}(\lambda)$	$f_o^{EB}(\lambda)$	$f_o^K(\lambda)$
1.138	6.306	5.830	0.476	2.529
1.148	6.499	6.060	0.439	2.491
1.158	6.661	6.257	0.404	2.454
1.168	6.793	6.421	0.372	2.418
1.178	6.892	6.550	0.342	2.382
1.188	6.957	6.643	0.314	2.347
1.198	6.988	6.700	0.288	2.314
1.208	6.986	6.722	0.264	2.280
1.218	6.951	6.709	0.242	2.248
1.228	6.885	6.664	0.221	2.216
1.238	6.789	6.587	0.202	2.185
1.248	6.666	6.482	0.184	2.154
1.258	6.519	6.351	0.168	2.124
1.268	6.350	6.197	0.153	2.095
1.278	6.160	6.021	0.139	2.066
1.288	5.955	5.828	0.127	2.038
1.298	5.735	5.620	0.115	2.010
1.308	5.505	5.400	0.104	1.983
1.318	5.266	5.171	0.095	1.957
1.328	5.020	4.934	0.086	1.931
1.338	4.772	4.694	0.078	1.905
1.348	4.521	4.451	0.070	1.880
1.358	4.272	4.208	0.064	1.856
1.368	4.024	3.967	0.057	1.832
1.378	3.782	3.730	0.052	1.808
1.388	3.544	3.497	0.047	1.785
1.398	3.313	3.271	0.042	1.762
1.408	3.090	3.052	0.038	1.740
1.418	2.875	2.841	0.034	1.718
1.428	2.669	2.638	0.031	1.697

TABLE VIII (continued)

50 KvCP ABSOLUTE X-RAY SPECTRAL INTENSITIES AT TUBE TARGET

($10^{16}ev*s^{-1}*ma^{-1}*sr^{-1}*A^{-1}$)

λ (A)	$f_o^E(\lambda)$	$f_o^{EC}(\lambda)$	$f_o^{EB}(\lambda)$	$f_o^K(\lambda)$
1.438	2.473	2.445	0.028	1.676
1.448	2.286	2.261	0.025	1.655
1.458	2.109	2.087	0.022	1.635
1.468	1.943	1.923	0.020	1.615
1.478	1.786	1.768	0.018	1.595
1.488	1.639	1.623	0.016	1.576
1.498	1.502	1.488	0.014	1.557
1.508	1.375	1.362	0.013	1.538
1.518	1.256	1.244	0.012	1.520
1.528	1.145	1.135	0.010	1.502
1.538	1.340	1.328	0.012	1.485
1.548	1.215	1.204	0.011	1.467
1.558	1.097	1.088	0.009	1.450
1.568	0.989	0.981	0.008	1.434
1.578	0.889	0.882	0.007	1.417
1.588	0.797	0.791	0.006	1.401
1.598	0.713	0.707	0.006	1.385
1.608	0.636	0.631	0.005	1.369
1.618	0.566	0.562	0.004	1.354
1.628	0.503	0.499	0.004	1.339
1.638	0.445	0.442	0.003	1.324
1.648	0.393	0.390	0.003	1.310
1.658	0.347	0.344	0.003	1.295
1.668	0.304	0.302	0.002	1.281
1.678	0.267	0.265	0.002	1.267
1.688	0.234	0.232	0.002	1.254
1.698	0.203	0.202	0.001	1.240
1.708	0.177	0.176	0.001	1.227
1.718	0.154	0.153	0.001	1.214
1.728	0.134	0.133	0.001	1.201
1.738	0.116	0.115	0.001	1.188

FIGURE 8

50KvCP EXPERIMENTAL, TARGET-REFERENCED, ABSOLUTE X-RAY SPECTRA: BREMSSTRAHLUNG [$f_o^{EB}(\lambda)$], CHARACTERISTIC [$f_o^{EC}(\lambda)$], AND TOTAL [$f_o^{E}(\lambda)$].

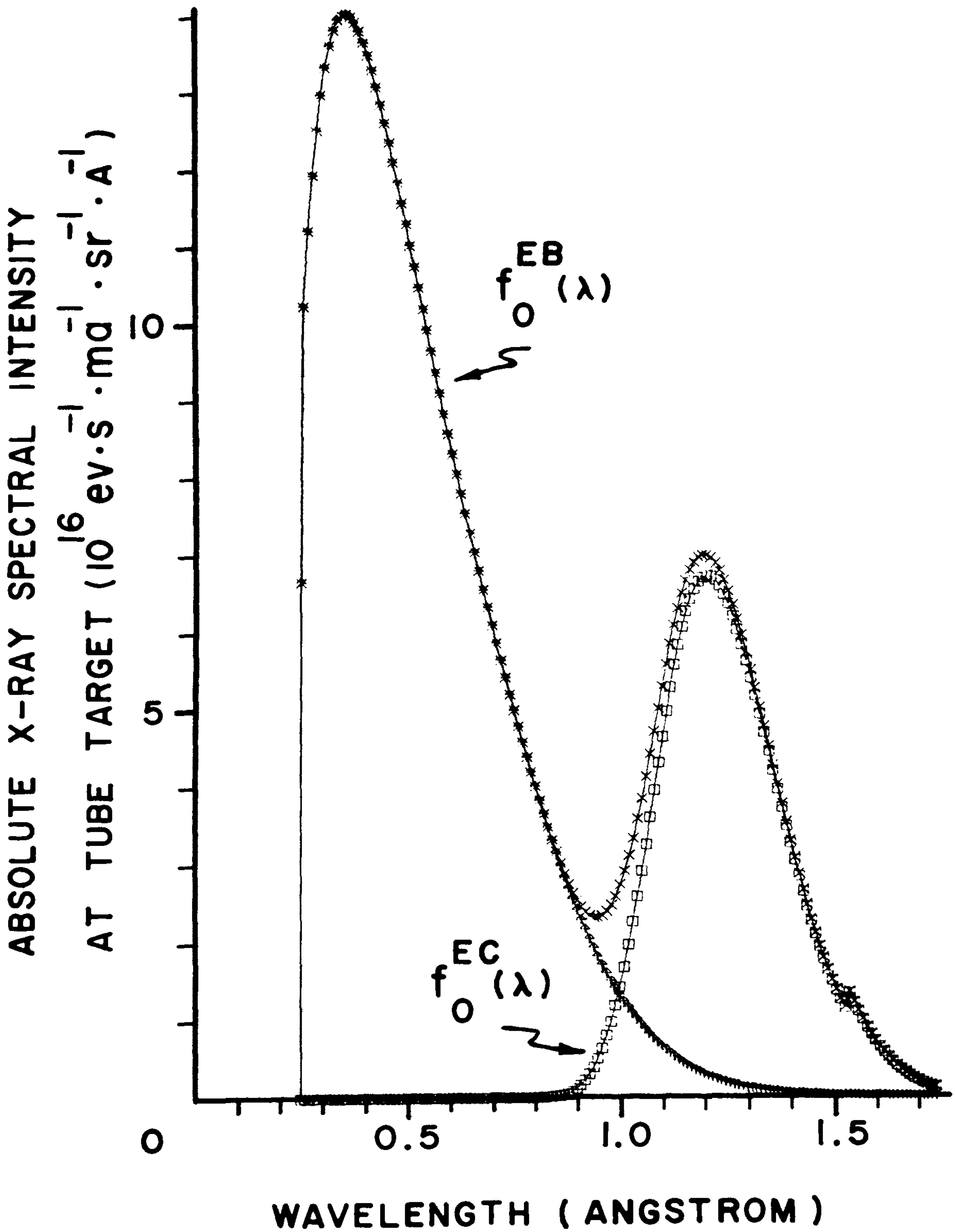
ABSOLUTE X-RAY SPECTRAL INTENSITY
AT TUBE TARGET (10^{16} ev·s^{-1}·ma^{-1}·sr^{-1}·A^{-1})
10
5
0
0.5
1.0
1.5
WAVELENGTH (ANGSTROM)
$f_0^{EB}(\lambda)$
$f_0^{EC}(\lambda)$

TABLE IX

COMPARISON OF 50 KvCP EXPERIMENTAL AND TRANSFORM PREDICTED RELATIVE INTEGRATED DETECTOR ABSORBANCE AS A FUNCTION OF ALUMINUM ATTENUATOR THICKNESS

(Inherent Filtration: 0.062 in. Be, 9.17 in. Air, x_o = 0.1315 g/cm^2 Al)

Al attenuator thickness $(x-x_o)$ (g/cm^2)	$\dot{D}_x/\dot{D}_{xo}$ $\left[\frac{\beta_x i_{Ex}}{\beta_{xo} i_{Eo}}\right]$ Experimental	$\dot{D}_x/\dot{D}_{xo}$ $\left[\frac{\beta_x i_{Ex}}{\beta_{xo} i_{Eo}}\right]$ Predicted	$\left[\frac{E-P}{E}\right]$ Relative Difference
0.0	1.0000	1.0000	-----
0.0219	0.8564	0.8546	-0.0021
0.0439	0.7514	0.7492	-0.0029
0.0659	0.6696	0.6694	-0.0003
0.1097	0.5554	0.5559	+0.0009
0.1537	0.4753	0.4773	+0.0042
0.1974	0.4158	0.4186	+0.0067
0.2633	0.3500	0.3524	+0.0068
0.6536	0.1693	0.1688	-0.0029
1.131	0.0907	0.0907	-----
2.337	0.0303	0.0301	-0.0066

TABLE X

COMPARISON OF 50 KvCP EXPERIMENTAL AND TRANSFORM PREDICTED RELATIVE INTEGRATED DETECTOR ABSORBANCE AS A FUNCTION OF POLYETHYLENE ATTENUATOR THICKNESS

(Inherent Filtration: 0.062 in. Be, 9.17 in. Air, 0.1315 g/cm^2 Al)

Polyethylene attenuator thickness (x) (g/cm^2)	$\dot{D}_x/\dot{D}_o$ $\left[\frac{\beta_x i_{Ex}}{\beta_o i_{Eo}}\right]$ Experimental	$\dot{D}_x/\dot{D}_o$ $\left[\frac{\beta_x i_{Ex}}{\beta_o i_{Eo}}\right]$ Predicted	$\left[\frac{E-P}{E}\right]$ Relative Difference
0.0	1.0000	1.0000	-----
0.0091	0.9901	0.9934	+0.0033
0.0261	0.9755	0.9816	+0.0062
0.0434	0.9623	0.9697	+0.0077
0.0916	0.9292	0.9380	+0.0095
0.1401	0.8996	0.9077	+0.0090
0.1878	0.8722	0.8795	+0.0084
0.2610	0.8329	0.8387	+0.0069
0.3585	0.7849	0.7890	+0.0052
0.6761	0.6601	0.6558	-0.0065
1.317	0.4888	0.4736	-0.0311
2.594	0.2928	0.2752	-0.0601

ethylene areal densities extending to approximately 1 g/cm^2 or 1 cm thickness. At larger thicknesses the difference increases to approximately 6% at the maximum areal density of 2.595 g/cm^2. The experimental data appears to be larger than the predicted value and this could be caused by either or both of two effects. The true x-ray spectrum could be softer than that predicted by the transform, or the β_x data for polyethylene could be smaller than the average value employed at these larger thicknesses.

If one notes that the dosimeter monitors the energy deposition in an equivalent thickness of solid corresponding to about 0.0003 inch, then one may appreciate that the absolute error integrated over the <u>entire</u> thickness of the sample will be considerably less than the difference observed at the back face of the polyethylene slab. Based on its behavior in this case, the transform generated spectrum shows considerable promise for predictions of energy deposition in material systems for which homogeneous ion chamber construction is not feasible.

In the experimental configuration employed here, the polyethylene was placed in the attenuator chamber shown in Fig. (5) and the values of the mass attenuation coefficients employed to modify the target-referenced spectrum were those listed in Table IV which contain contributions from all of the scattering and absorption processes for the polyethylene. If one placed the polyethylene samples immediately in front of the dosimeter window, then some fraction of the previously scattered radiation would remain in the beam and be intercepted by the detector as evidenced in the previous chapter. Careful attention must be given to the choice of attenuation coefficients to be employed in a particular geometrical configuration in order to obtain a correct description of the energy deposition process.

V. DISCUSSION

The experimentally deduced 50 KvCP absolute x-ray spectrum $[f_o^E(\lambda)]$ can be utilized to predict the absolute total rate of energy deposition in any desired material system of thickness x g/cm^2 whose wavelength dependent energy-transfer coefficients $\mu_x(\lambda)$ are known by simply specifying the sample thickness x and the steradians of solid angle subtended by the sample referenced to the x-ray target and computing

$$\int_{\lambda_0}^{\infty} \exp[-\sum_n Yn \cdot \mu_{Yn}(\lambda)] \cdot f_o^E(\lambda) \cdot \{1-\exp[-\mu_x(\lambda)x]\} d\lambda \quad .$$

We have denoted the inherent filtration components Yn and their respective appropriate attenuation coefficients $\mu_{Yn}(\lambda)$ in a generalized format to accommodate any changes in the experimental configuration.

In cases where one is concerned with specifying the depth-dose profile in a sample material, one may employ a modification of Eq. (4) to obtain

$$\dot{D}_x = \int_{\lambda_0}^{\infty} \exp[-\sum_n Yn \cdot \mu_{Yn}(\lambda)] \cdot f_o^E(\lambda) \cdot \exp[-\mu_x(\lambda)x] \cdot \{1-\exp[-\mu_x(\lambda)\Delta x]\} d\lambda \qquad (50)$$

where the $\mu_x(\lambda)$ defines the mass energy transfer coefficients of the material. In practical cases, it is extremely important to examine the contributions that are to be included in this $\mu_x(\lambda)$ term. Ordinarily, one is concerned with a variety of potential sample thicknesses and geometries which might require some appropriately weighted contributions to $\mu_x(\lambda)$ by the scattering events which will occur in the sample. However, no specific statements can be offered that are universally applicable.

In the event that one is satisfied with the shape of the present spectral distribution, but has some reservations about the absolute values generated herein, it is possible to employ a well-characterized standard ionization chamber to renormalize the present data. To accomplish this task, the standard detector would be positioned behind a thickness (x) of the material of interest and the monitored resultant detector response ($\dot{D}_{xs}$) would be given by

$$\dot{D}_{xs} = \int_{\lambda_0}^{\infty} \exp[-\sum_n Yn \cdot \mu_{Yn}(\lambda)] \cdot f_o^E(\lambda) \cdot \exp[-\mu_x(\lambda)x] \cdot \{1-\exp[-\mu_s(\lambda)L]\} d\lambda \qquad (51)$$

where $\mu_s(\lambda)$ is the mass energy transfer coefficient for the standard detector material of thickness L. The numerically evaluated integrals, together with the monitored $\dot{D}_{xs}$ data, permits one to compute $\dot{D}_x$ by ratioing the two expressions.

The present study has been restricted to the use of the transform generated spectrum to predict the energy deposition rates in polyethylene. It has demonstrated an accuracy of better than 1% for thickness extending up to 1 centimeter, which is typical of material samples employed in radiation chemistry studies. It would be of interest to extend this data to include a judicious variety of additional materials in order to establish the relative confidence which one may place in these predictions. Any such additional experimental checks would require that β_x data be generated for the material of interest, since the hardening of the impinging spectrum depends sensitively upon the composition of the attenuating material.

Any spectrum deductions based upon ion chamber detection methods must include a β_x analysis to generate correct ionization current data for the curve fitting of the transform function. This can only be obtained with a variable plate separation chamber, and conventional detectors do not incorporate this capability. In view of these considerations, the literature generated to-date employing window type, fixed plate separation ion chambers would appear to include this inherent error since β_x for aluminum in this study changes by a factor of two for the attenuator thicknesses employed, which are typical of the literature values.

Of equal importance is the observation that absolute specification of the spectrum must always be based upon satisfying the conditions of charged particle equilibrium in the cavity gas since the W value of the gas is the basic conversion factor in absolute data reduction. Generation of primary data describing these events originating in the cavity gas can only be obtained with window type ion chambers when these chambers are operated in a variable plate separation mode such as the method employed here.

As it was noted earlier, one of the contributions to the Laplace transform function utilized in this study was observed to represent the bremsstrahlung spectrum, while the other term attempted to describe the tungsten characteristic (L) radiation. If one were to employ an x-radiation source operating at exciting potentials beyond the threshold of the tungsten K-lines (~60 Kev), it would be interesting to extend the technique developed herein to incorporate a third term to the fitting function in order to describe the tungsten K-spectra that would then be present. Anticipating the general shape of the additional characteristic radiation superimposed on the tungsten L lines and bremsstrahlung, an exponential whose Laplace transform was sharply peaked, could possibly accommodate the additional characteristic radiation.

Comparison With Literature Results

The classical literature on theoretical predictions of the thick target x-ray bremsstrahlung is essentially the work of KRAMERS (1923). It does not take into account either electron backscatter or target self-absorption of the x-radiation produced at different depths in the material. Neglecting the absolute predictions of this theory and normalizing the relative spectrum in the manner described in Eqs. (45) - (49) to obtain an integrated spectral intensity equivalent to that predicted by the present transform method, one may compare these spectra in a meaningful way. The results are tabulated in Table VIII and a plot of the resultive data is shown in Fig. (9). It is apparent here that Kramers' theory predicts considerably more soft radiation than that generated by the transform. This would be expected since target self-absorption would tend to "harden" the spectrum emanating from the tube and this is not taken into account in this theory. In the case of heavily filtered x-radiation, the theory has been employed to generate useful empirical predictions [RAY, *et. al.* (1967) among others] for relative exposure dose rates in material systems.

EHRLICH (1955) extended Kramers' theory to include both electron backscatter and target self-absorption, and performed an experimental check of the resulting theory using scintillation detection techniques. Her results are one of the few pieces of absolute spectral distribution studies that are available for comparison with this work. Fig. (10) shows a comparison of both her theoretical and experimental results with those of the present study. It would appear that the transform generated spectrum in this study is in better agreement with her theory than are her own experimental results for which an uncertainty of ±30% was suggested. Problems associated with early scintillation work have been discussed in

FIGURE 9

COMPARISON OF 50 KvCP EXPERIMENTAL, TARGET-REFERENCED, ABSOLUTE BREMSSTRAHLUNG [$f_o^{EB}(\lambda)$] WITH KRAMERS' THEORETICAL BREMSSTRAHLUNG [$f_o^{K}(\lambda)$]. $f_o^{K}(\lambda)$ normalized to area under $f_o^{EB}(\lambda)$.

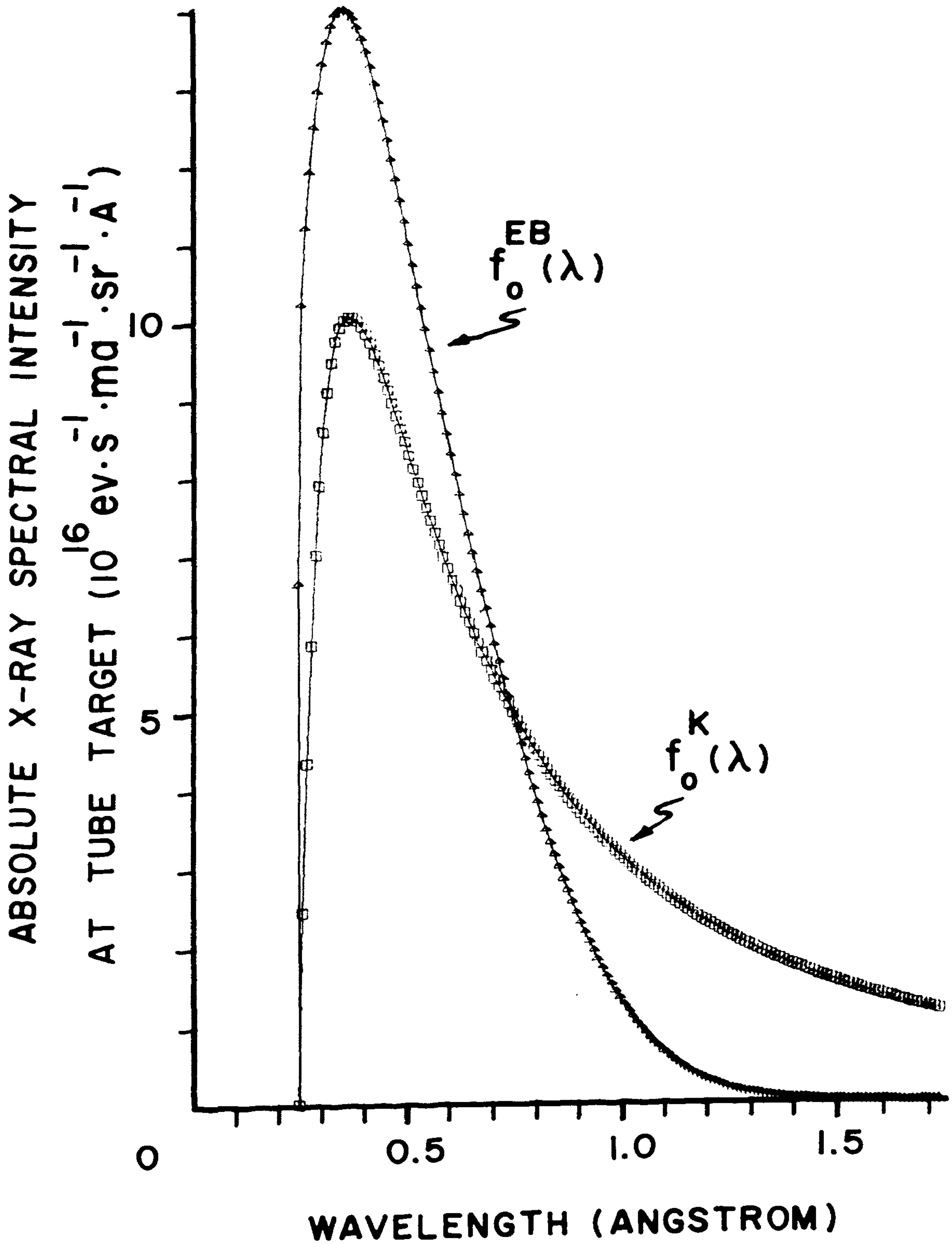

ABSOLUTE X-RAY SPECTRAL INTENSITY
AT TUBE TARGET (10^{16} ev·s^{-1}·ma^{-1}·sr^{-1}·Å^{-1})
10
5
0
0.5
1.0
1.5
WAVELENGTH (ANGSTROM)
$f_o^{EB}(\lambda)$
$f_o^{K}(\lambda)$

FIGURE 10

COMPARISON OF 50 KvCP EXPERIMENTAL, TARGET-REFERENCED, ABSOLUTE BREMSSTRAHLUNG [$f_o^{EB}(\lambda)$] WITH EHRLICH'S EXPERIMENTAL AND THEORETICAL BREMSSTRAHLUNG.

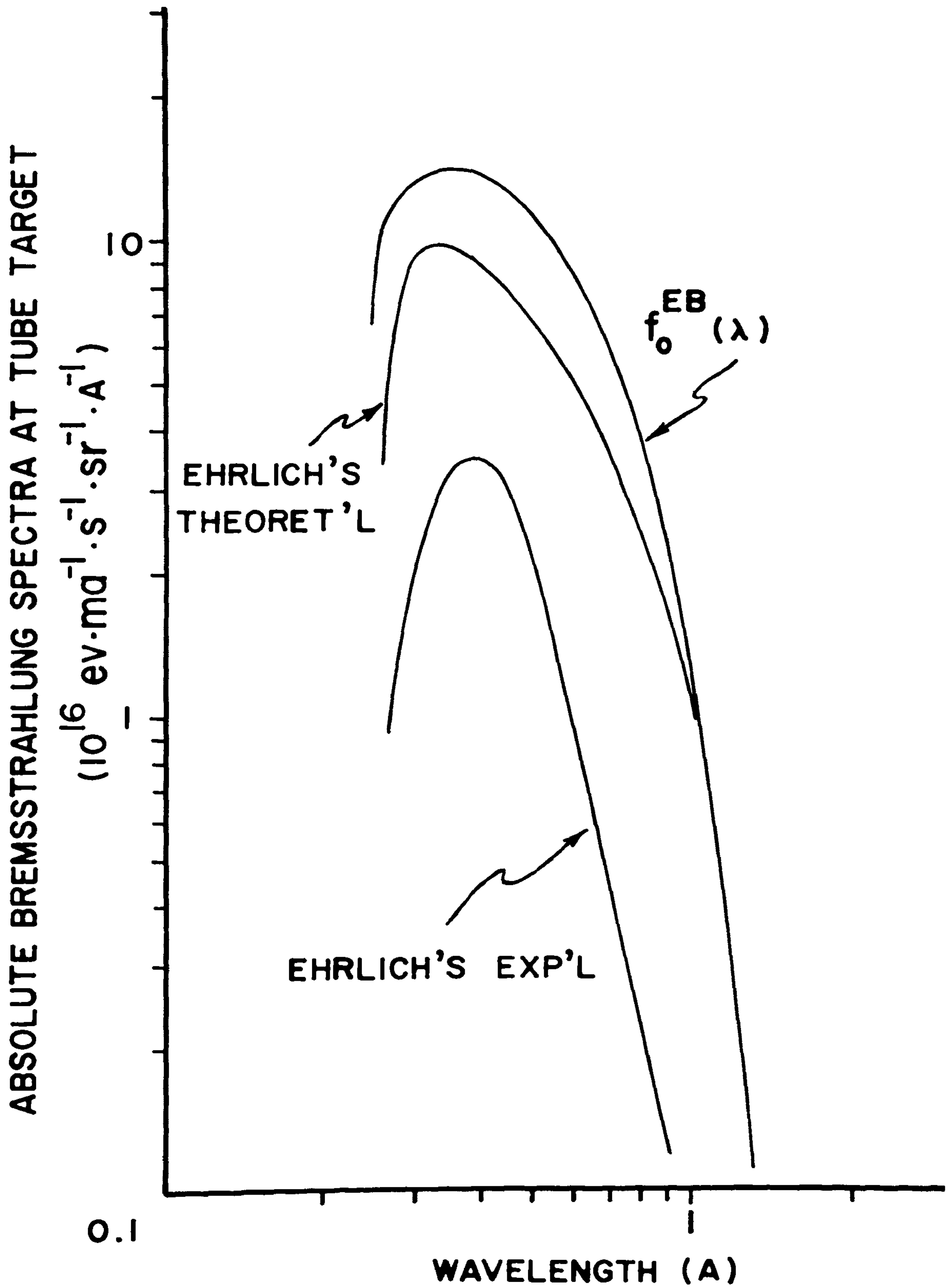
ABSOLUTE BREMSSTRAHLUNG SPECTRA AT TUBE TARGET
(10^{16} ev·ma^{-1}·s^{-1}·sr^{-1}·A^{-1})
10
1
0.1
$f_o^{EB}(\lambda)$
EHRLICH'S THEORET'L
EHRLICH'S EXP'L
1
WAVELENGTH (A)

detail by HETTINGER and STARFELT (1958a, 1958b).

In addition to the experimental work of Ehrlich, 50 KvCP spectra have been reported by KOLB (1955), JAEGER and KOLB (1956), WANG, *et. al.* (1957) and VILLFORTH, *et. al.* (1958). Jaeger and Kolb employed scintillation detection which was incorrect for iodine escape and the resulting spectra may be in error for this reason. Villforth and colleagues were concerned with heavily filtered spectra and their results are not readily comparable with the results of this study.

Wang, *et. al.* applied the Laplace transform suggested by EMIGH and MEGILL (1953) to the analysis of aluminum attenuation data obtained with a conventional Machlett OEG-50 x-ray tube operated at 50 KvCP, which was monitored with an NBS free-air standard ionization chamber. They also studied full wave rectified 50 KvP by the same data reduction technique, but employed a NaI(Tl) scintillation detector to monitor the total intensity of the x-ray beam. Only relative spectra were obtained for the case of inherent filtration consisting of 1 mm Be, 0.5 mm Al, and 8 cm of Air. The transform functions, tube operating specifications, and the imposed inherent aluminum filtration conditions are the same as those employed in the present study. There are a number of apparent errors in this paper which will be discussed in some detail.

Wang and colleagues are confused on several points. Their Fig. (3) implies that they do not make a distinction between the spectral distribution of the impinging radiation and the spectral absorbance of their ion chamber. They are unable to recover the spectrum at the x-ray target at longer wavelengths (>1 A) as indicated in their Fig. (4). This can be shown to be true only if they confused the spectral absorbance of their detector with the true impinging spectrum as is suggested in Fig. (3).

In the present study, this would correspond to referencing $F_Y^*(\lambda)$ rather than $f_Y^*(\lambda)$ in our Fig. (7) directly to the x-ray target. They failed to reconstruct the equivalent of $f_Y^*(\lambda)$ by including the wavelength dependence of their ion chamber cavity gas before proceeding to multiply by the $\exp\,[+\sum_n \mu_{Yn}(\lambda)\cdot Yn]$ factor.

Wang and colleagues are also in error in their attempts to use a GREENING (1947) plot to deduce the fraction of the total energy of the x-ray beam which is contributed by the characteristic radiation. First, their detector is not wavelength independent, which is one of the fundamental requirements specified by Greening in his analysis. Second, their plots are based upon the detector spectral absorbance data rather than the integrated intensity of the x-ray beam. Third, it is impossible to construct their Fig. (7) without assuming a sign error in their use of Greening's theory. Finally, the erroneous resulting curve should have been immediately suspect in view of the fact that the slope is such that it intercepts an incorrect axis. Their estimate of the fraction of the total energy associated with characteristic radiation is 65%. A comparison of the area under the transform fitted characteristic spectrum $f_o^{EC}(\lambda)$ to the total area under the curves in our Fig. (8) yields a prediction of approximately 28%.

EMIGH and MEGILL (1953), who suggested the form of the transforms employed in this study, used the transforms originally to specify the spectral distribution of the unfiltered output of a beryllium window, tungsten target tube operated at 50 KvP. A NaI(Tl) scintillation detector was used to monitor the total integrated intensity generated by the target. For reasons which are not apparent in their paper, their attenuation curves appear to differ substantially from our own and other literature. The spectrum that they deduce from fitting the equivalent of our a,b,c,α,γ parameters to this data exhibits only a single maximum and this occurs at approximately 0.45 A compared to 0.36 A in the present work.

There have been a number of studies of the 50 KvP, full or half wave rectified, x-ray spectra generated by conventional tubes. HETTINGER and STARFELT (1958b) employed a NaI(Tl) detector and pulse height analysis to obtain a relative spectrum for 0.7 mm Al inherent filtration which exhibited a maximum at approximately 20 Kev. AITKEN and DIXON (1958) also used a NaI(Tl) detector and pulse height analysis and 0.7 mm Al filtration to obtain a relative spectrum, but this data peaked at 28 Kev.

BURKE and PETIT (1960) used a Victoreen Model 651 ionization chamber as a detector and the attenuator technique together with a single-term Laplace transform identical to that employed to generate $f_y^{EB}(\lambda)$ in the present study. In an attempt to separate the continuous and characteristic components of the spectra, they collected absorption data on various tubes which differed from each other only in target material. Their deduced bremmstrahlung spectrum has a maximum value of 4.8×10^{16} $ev \cdot s^{-1} \cdot sr^{-1} \cdot ma^{-1} \cdot A^{-1}$ at 0.31 A compared to the present results shown in Fig. (8) of 14×10^{16} $ev \cdot s^{-1} \cdot sr^{-1} \cdot ma^{-1} \cdot A^{-1}$ which occurs at 0.36 A. One would expect the pulsating potential to peak at longer wavelengths than that observed for the constant potential mode.

EPP and WEISS (1966) have reported data on full wave rectified spectra at peak operating voltages of 45, 55 and higher intermediate values extending to 105 KvP. They employed a NaI(Tl) detector and performed a detailed analysis of their data to correct for the energy resolution and the non-linear response of their detector crystal, and the iodine K x-ray escape, as well as the contributions from the tungsten characteristic radiation. The target angle in the Machlett Dynamax No. 40 Tube is 15° compared to the more conventional 22° found in other units. The additional self-absorption of the softer radiation within the target, together with the 25% peak-to-peak ripple, makes comparison with the present data difficult. However, interpolating between the 45 and 55 KvP data, one obtains a maximum in the spectral distribution at 25 Kv which may be compared with the other data on pulsating spectra quoted previously.

The foregoing discussion should provide some indication of the variableness of the recorded literature in the field of thick target x-ray spectra. It would appear that some of the differences observed are due to misinterpretation of the physical quantity being measured, while in other cases the work can be criticized on the basis of an incomplete appreciation of the properties of the radiation detector employed.

A primary purpose of this thesis was to evaluate the effect which a well characterized detector could bring to bear on resolving some of these literature differences. One may summarize the results as follows:

(1) Any window type ion chamber possesses an inherent wavelength dependence associated with the present β_x type correction which can be removed by operating in a variable plate separation mode.

(2) Multi-term Laplace transforms can be fitted to attenuation data generated by a well characterized detector and the resulting spectra demonstrated to possess physical significance in the sense that the individual terms correspond to contributions from the bremsstrahlung and characteristic radiation.

(3) The absolute spectrum which can be obtained with the

simple device employed here together with the transform technique is a sufficiently adequate empirical approximation to the true spectrum to make it useful in predicting energy deposition rates in arbitrary materials with uncertainties of a few percent.

It would be interesting to employ this detection system to examine its ability to predict the energy deposition in other material systems and to generate by Laplace transform techniques an empirical spectrum for other material systems.

APPENDIX I

EQUIPMENT & MATERIALS

The following is a listing of the major equipment and materials used in this investigation.

1. X-RAY SOURCE. General Electric EA-75 x-ray tube unit. Operated anode grounded at constant potential. Water cooling jacket built into tube permits generous continuous duty ratings. Tube has projected focal spot 5mm square. Tungsten target angle is 22.5°.

2. X-RAY POWER SUPPLY. Universal Voltronics Corp., Model #BAL-75-50-UM, Serial # 4-12-1286. Specifications:

Input:	208/230 V AC, 1 phase, 60 Hz
Output:	0-75 Kv DC @ 50 ma DC
Polarity:	Reversible
Regulation:	Line - 0.1%, 190v - 260v AC input Ripple - 0.1% rms
Current Regulation:	0.1% over range of 10-50 ma DC

3. DUAL CHANNEL STRIP CHART RECORDER. Hewlett Packard/Moseley Div. Model # 7100B with input modules #17501A. Utilizes 120 ft. chart rolls 11 inches wide with 10 inch calibrated writing width, #9270-1010. Specifications:

Response Time:	maximum 0.5 seconds
Chart Speeds:	1,2 in/hr; 0.1, 0.2, 0.5, 1,2 in/min; 0.1, 0.2, 0.5, 1,2 in/sec.
Voltage Spans:	(16) 1,2,5,10,20,50,100,200,500 mV; 1,2,5,10,20,50,100 V f.s. Continuously variable mode on all spans.

Accuracy:	±0.2% f.s.
Linearity:	terminal based - 0.1% f.s.
Input Resistance:	1 meg-ohm at null on all fixed and variable spans
Zero-set:	continuously adjustable over full scale plus extended 5-scale suppression
Reference Supply:	continuous electronic references, Zener diode controlled

4. LINEAR PICOAMMETER. Keithley Instruments, Inc. Model 417 with remote housing facility Model 4172. Specifications:

Range:	10^{-13} - 3 x 10^{-5} ampere f.s. in eighteen 1x and 3x overlapping ranges, positive or negative currents.
Accuracy:	±2% f.s. on 3 x 10^{-5} to 10^{-8} ampere ranges; ±3% f.s. from 3 x 10^{-9} to 10^{-13} ampere.
Calibrated Current Suppression:	up to 1000 full scales; maximum suppression, 10^{-4} ampere. Accuracy is ±5% of reading or ±5% of decade setting, whichever is greater, except for the 10^{-12} decade where it degrades to ±10% with multiplier settings between 50 and 100.
Input:	Grid current <2 x 10^{-14} ampere. Change in input voltage drop <1 millivolt for f.s. deflection on any range. Input resistance increases from 100 ohms at 10^{-5} ampere range to 10,000 megohms at 10^{-13} ampere range in decade steps.
Output:	±3 volt output at up to 1 milliampere for f.s. meter deflection. Output polarity is opposite to input polarity. Impedance <5 ohms. Noise <3% rms of f.s. on 10^{-13} ampere range with minimum dampening, decreasing to 0.3% rms with maximum dampening.

5. INTEGRATING DIGITAL VOLTMETER. Hewlett-Packard Model DY-2401C installed in data acquisition system, located in Electronics Research Center, UMR. Device used for calibration of Keithley Picoammeter.

Specifications:

Input Circuit:

Type:	Floated and guarded signal pair, may be operated up to 500 V above chasis ground.
Ranges:	5 ranges from 0.1 to 1000 V f.s.
Input Impedance:	10 MΩ on 10, 100, 1000 V ranges; 1 MΩ on 1 V range; 100 kΩ on 0.1 V range; 150 pF on all ranges.

Accuracy: 0.01% of reading ±0.005% f.s. ±1 digit at 25° C; temperature coefficient 0.001% of reading per °C, 10 to 40°C.

6. ANALYTICAL BALANCES. Sartorius, Model #2604 (single pan) semi-micro balance; 0-100 gm capacity with 0.01 mg sensitivity.

7. INSIDE MICROMETER. Brown & Sharp 1 to 12 inch and 12 to 24 inch micrometer, with 0.0001 inch sensitivity.

8. Inside-Outside DIAL CALIPERS. Craftsman cat. no. 9F40164. 6 inch capacity, accurate to 0.001 inch.

9. ALUMINUM SAMPLE MATERIAL. Consolidated Aluminum Corp., 1100 Richmond St., Jackson, Tennessee (ZIP 38301). 99.993% Al by analysis.

10. POLYETHYLENE SAMPLE MATERIAL. Phillips Petroleum Co., Bartlesville, Oklahoma (ZIP 74004). 2 mil: #6002; 3 mil and 10 mil: #5003.

11. POLYETHYLENE SAMPLE MATERIAL. Cope Plastics Missouri, Inc., 1157 S. Kingshighway, St. Louis, Mo. 60 mil and 2 inch DIA ROD stock polyethylene.

12. PORTABLE RADIATION-LEVEL SURVEY INSTRUMENT. "Cutie Pie" #519, Technical Associates, Burbank, California.

13. <u>VOLT-OHM-METER</u>. Tripolet Model 630-A. Range: 0-6000 V DC with ±1 1/2 % accuracy.

14. <u>HIGH VOLTAGE POWER SUPPLY</u>. Plastic Capacitors, Inc., Chicago, Ill. Model # HV50-502. Output: 6 Kv DC, 5.0 ma with Variac (type V5) control.

15. <u>ELECTROMETER</u>. Keithley Instruments, Inc. Cleveland, Ohio. Model 610 B.

As a voltmeter:

Range:	0.001 v to 100 v
Accuracy:	±1% f.s.

As an Ohmmeter:

Range:	100 ohms to 10^{14} ohms
Accuracy:	±3% f.s. 100 to 10^{9} ohms
	±5% f.s. on 3 x 10^{9} to 10^{14} ohm ranges

16. <u>COMPUTER FACILITIES</u>. Located in the Computer Science Center, University of Missouri - Rolla.

As of March, 1968, the following equipment and program libraries were implemented by the Computer Science staff at UMR:

An IBM 360 MODEL 50 H digital computing system with 262,144 bytes of core storage operating ØS 360 MFT release 13 (control of HASP initiated 2/1/68 at UMR); utilizing FORTRAN IV (G) language, form #C28-6515-5.

An IBM 2540 READER-PUNCH with capacity for reading 1000 cards/min. and punching 300 cards/min.

An IBM 1403 PRINTER which can print a maximum of 1100 lines/min.

Six IBM 2311 DISK STORAGE DRIVES with combined capacity of 43,500,000 bytes.

Two IBM 2415 IV MAGNETIC TAPE DRIVES, each with 2400 ft. tape capacity of recording density of 1600 bpi.

Off-line plotting facilities provided by a CALCOMP 566 drum plotter with step size of 0.005 inch driven by CALCOMP 750 tape drive; maximum available plotting area of 12" x 120'. Plot subroutines implemented by the Computer Science staff.

APPENDIX II

PLOTS OF BETA CALIBRATION DATA

Figures (11) - (16): Aluminum attenuated data

Figures (17) - (21): Polyethylene attenuated (Aluminum filtered) data

□ --Divergence (α) corrected ionization current density ($\alpha i_{Ex}/V$) vs. absolute plate separation (L). ○ , ○ --Differential divergence (α) corrected ionization current density ($\Delta\alpha i_{Ex}/\Delta V$) vs. average plate separation ($\bar{L}$): ○ → ΔL = 0.100 inches, ○ → ΔL = 0.040 inches. $L^3/V^2 = 1.372 \cdot 10^{-8}$ in^3/v^2. Ethylene flow rate = 180 cc/min.

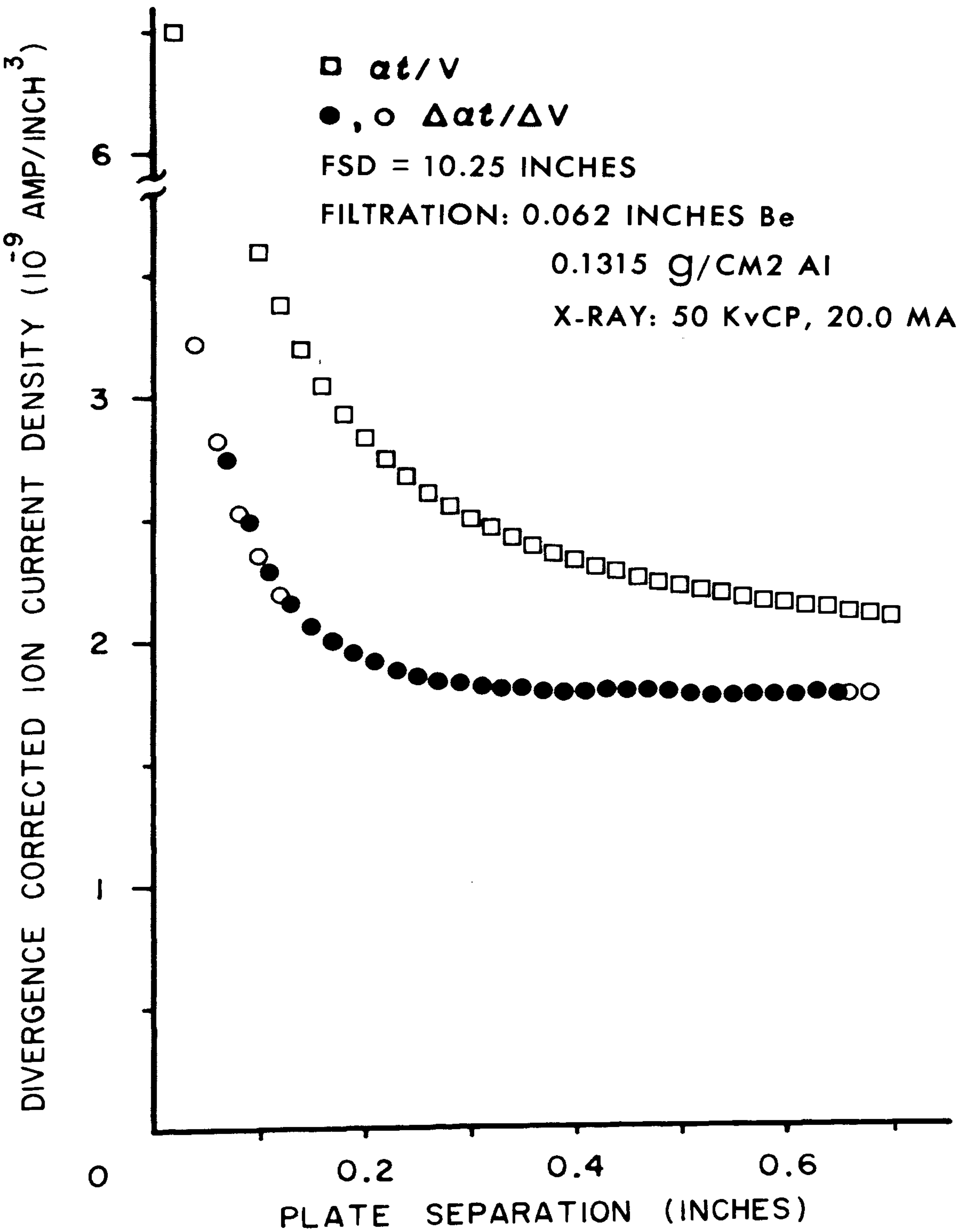

□ at/V
●, ○ $\Delta at/\Delta V$
FSD = 10.25 INCHES
FILTRATION: 0.062 INCHES Be
0.1315 g/CM2 Al
X-RAY: 50 KvCP, 20.0 MA
DIVERGENCE CORRECTED ION CURRENT DENSITY (10^{-9} AMP/INCH^3)
6
3
2
1
0
0.2
0.4
0.6
PLATE SEPARATION (INCHES)

FIGURE 11

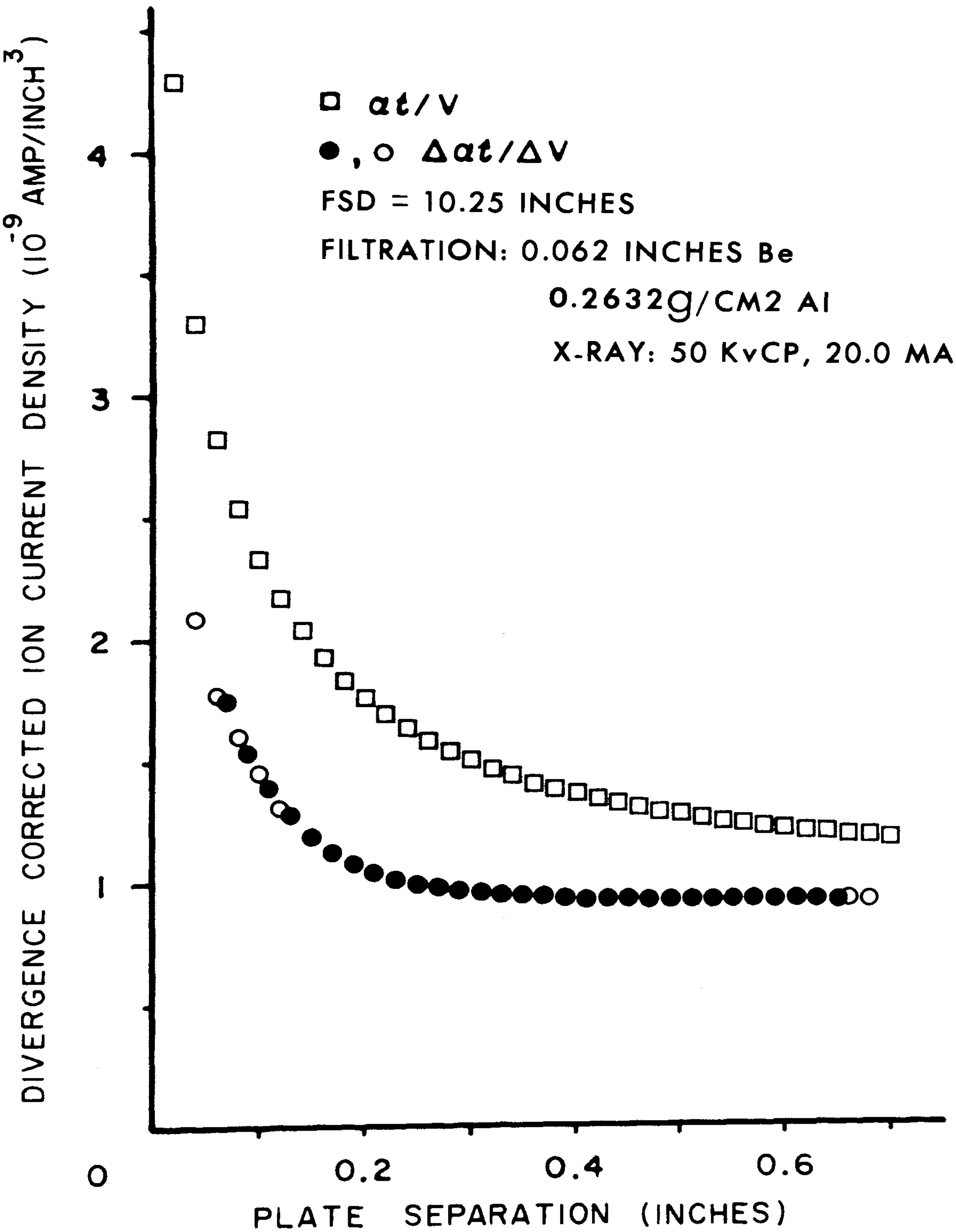
□ at/V
●, ○ $\Delta at/\Delta V$
FSD = 10.25 INCHES
FILTRATION: 0.062 INCHES Be
0.2632g/CM2 Al
X-RAY: 50 KvCP, 20.0 MA
DIVERGENCE CORRECTED ION CURRENT DENSITY (10^{-9} AMP/INCH^3)
PLATE SEPARATION (INCHES)
0
1
2
3
4
0.2
0.4
0.6

FIGURE 12

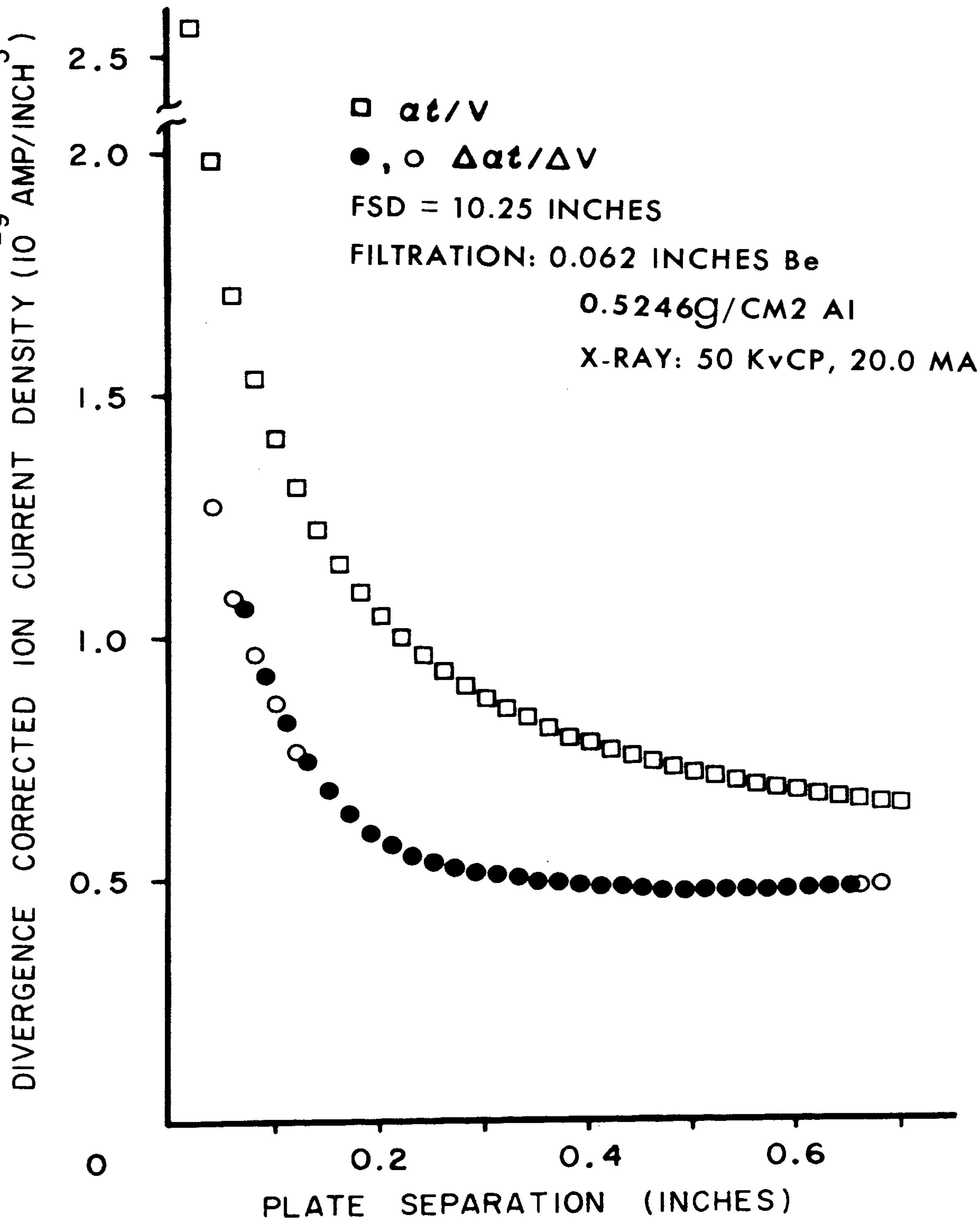

□ at/V
●, ○ $\Delta at/\Delta V$
FSD = 10.25 INCHES
FILTRATION: 0.062 INCHES Be
0.5246g/CM2 Al
X-RAY: 50 KvCP, 20.0 MA
DIVERGENCE CORRECTED ION CURRENT DENSITY (10^{-9} AMP/INCH^3)
2.5
2.0
1.5
1.0
0.5
0
0.2
0.4
0.6
PLATE SEPARATION (INCHES)

FIGURE 13

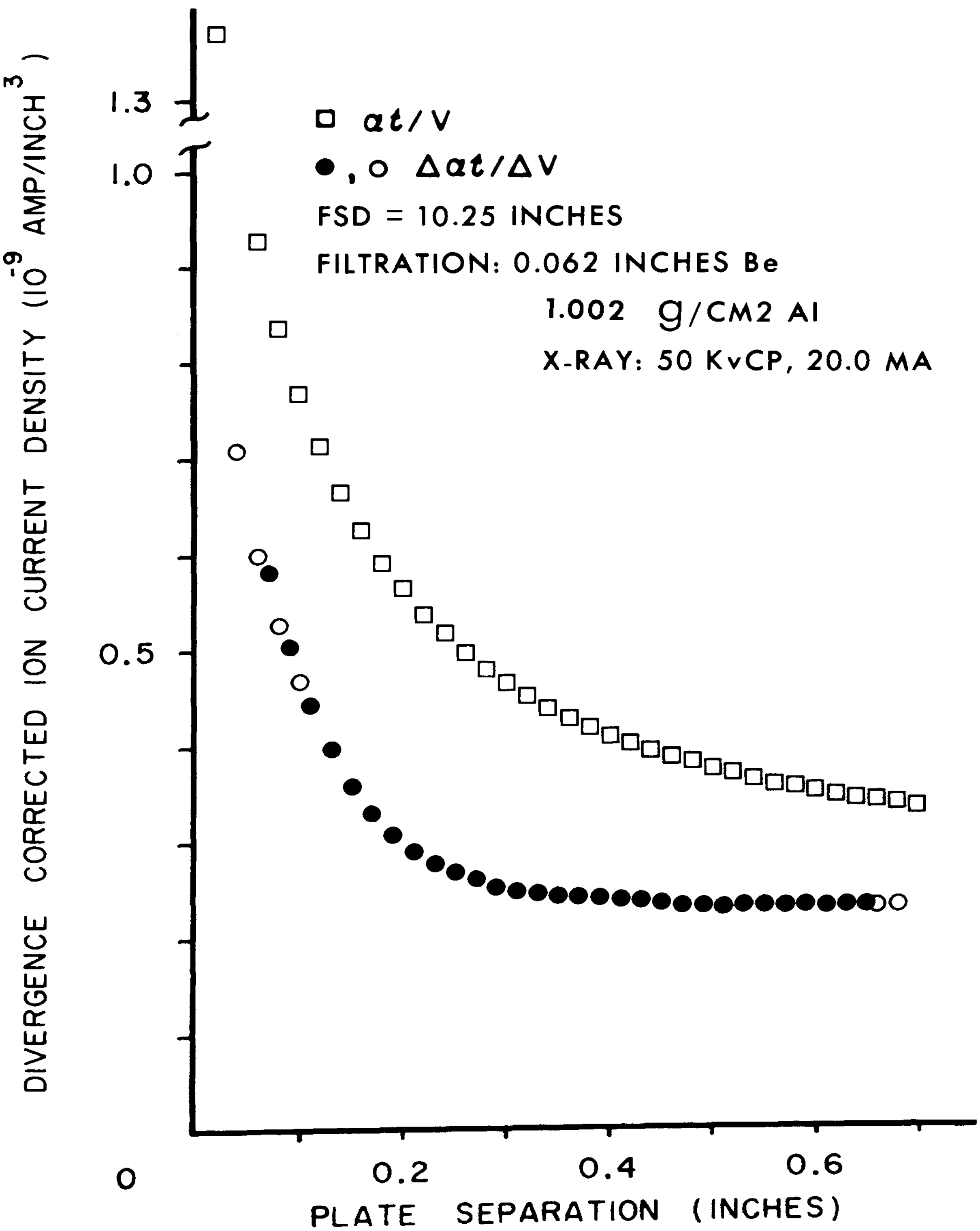
DIVERGENCE CORRECTED ION CURRENT DENSITY (10^{-9} AMP/INCH^3)
1.3
1.0
0.5
0
0.2
0.4
0.6
PLATE SEPARATION (INCHES)
□ $\alpha t/V$
●, ○ $\Delta\alpha t/\Delta V$
FSD = 10.25 INCHES
FILTRATION: 0.062 INCHES Be
1.002 g/CM2 Al
X-RAY: 50 KvCP, 20.0 MA

FIGURE 14

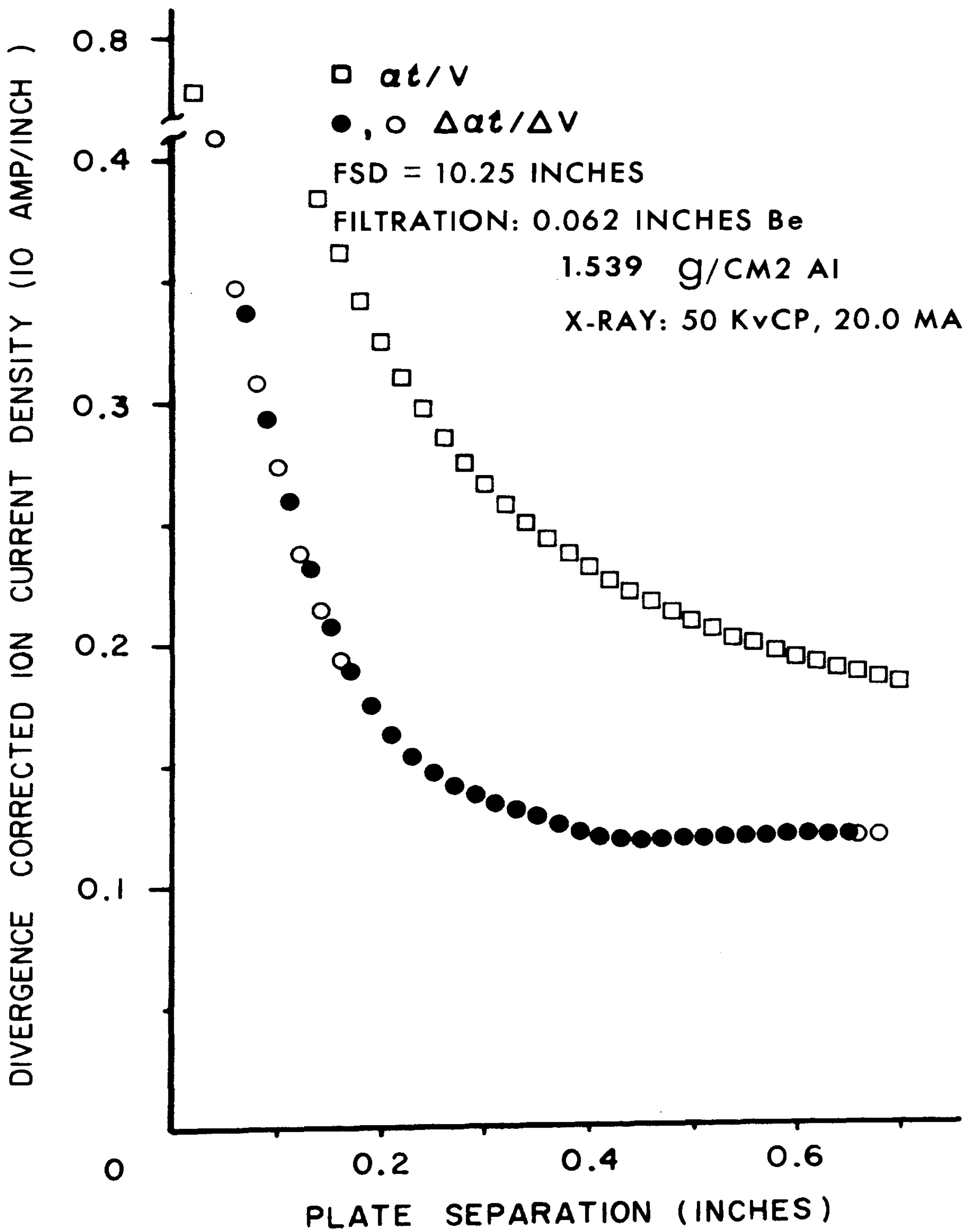

DIVERGENCE CORRECTED ION CURRENT DENSITY (10^{-9} AMP/INCH^3)
0.8
0.4
0.3
0.2
0.1
0
0.2
0.4
0.6
PLATE SEPARATION (INCHES)
□ αt/V
●, ○ Δαt/ΔV
FSD = 10.25 INCHES
FILTRATION: 0.062 INCHES Be
1.539 g/CM2 Al
X-RAY: 50 KvCP, 20.0 MA

FIGURE 15

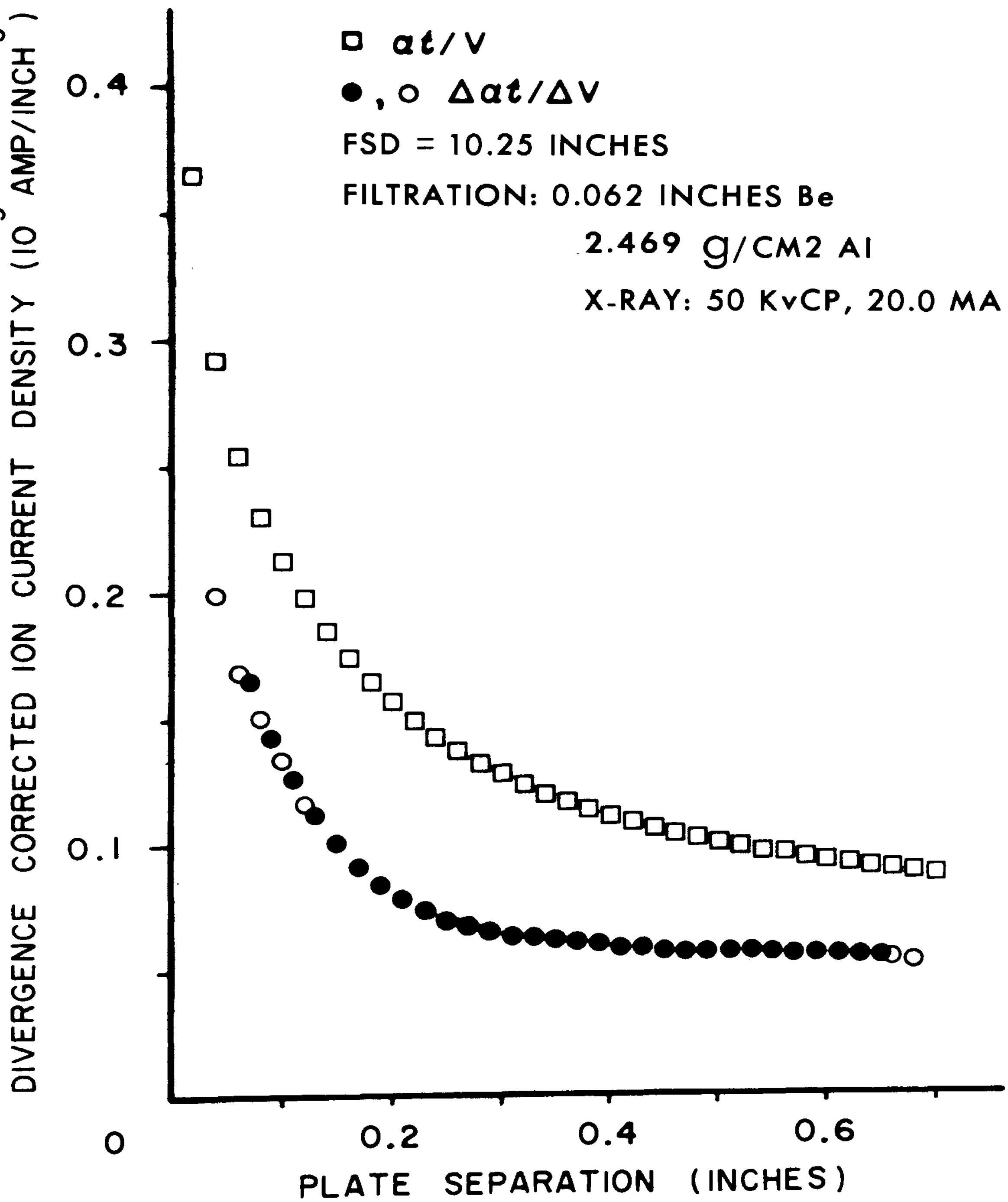
□ at/V
●, ○ Δat/ΔV
FSD = 10.25 INCHES
FILTRATION: 0.062 INCHES Be
2.469 g/CM2 Al
X-RAY: 50 KvCP, 20.0 MA
DIVERGENCE CORRECTED ION CURRENT DENSITY (10^-9 AMP/INCH^3)
0.4
0.3
0.2
0.1
0
0.2
0.4
0.6
PLATE SEPARATION (INCHES)

FIGURE 16

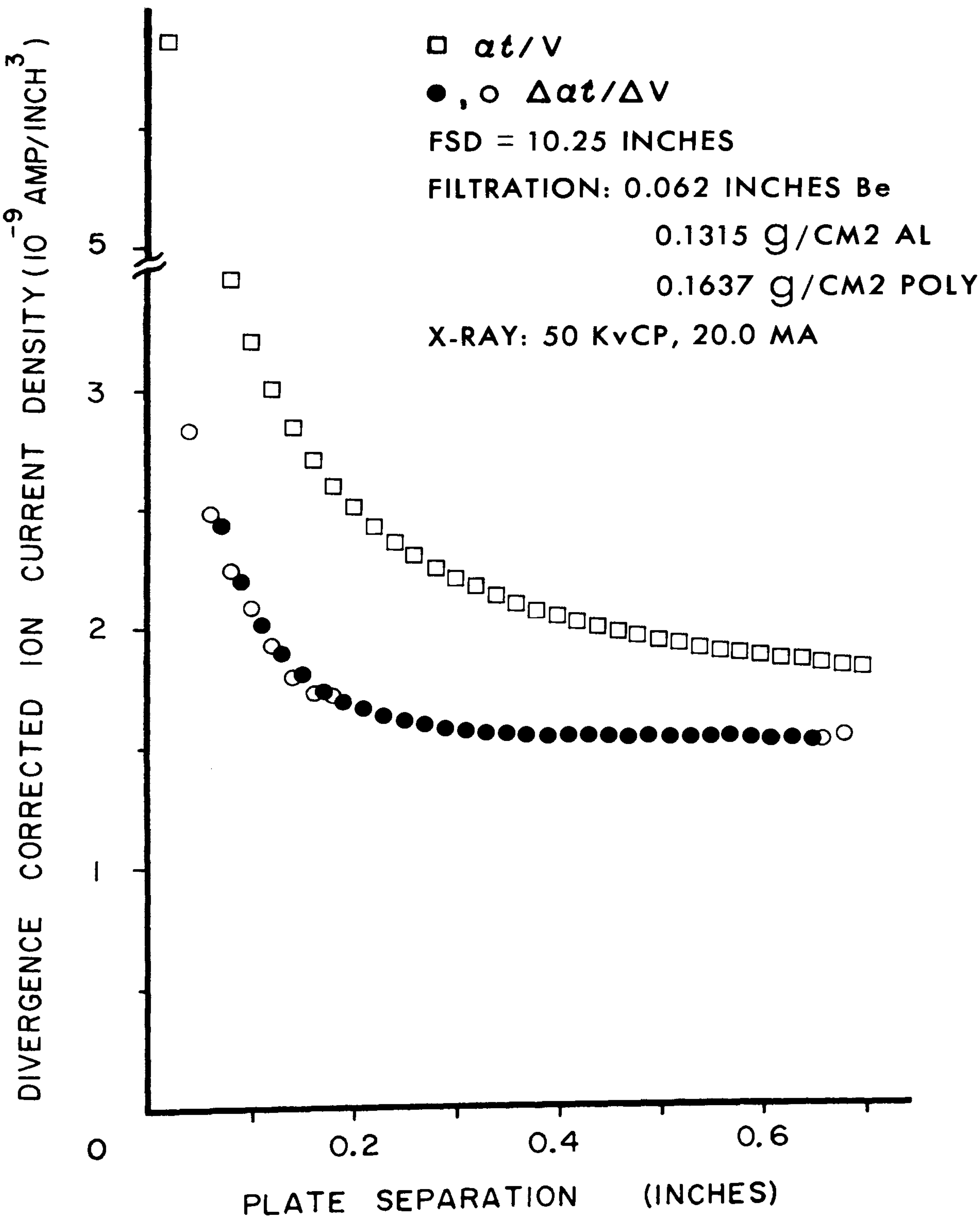

□ αt/V
●, ○ Δαt/ΔV
FSD = 10.25 INCHES
FILTRATION: 0.062 INCHES Be
0.1315 g/CM2 AL
0.1637 g/CM2 POLY
X-RAY: 50 KvCP, 20.0 MA
DIVERGENCE CORRECTED ION CURRENT DENSITY (10^{-9} AMP/INCH^3)
5
3
2
1
0
0.2
0.4
0.6
PLATE SEPARATION (INCHES)

FIGURE 17

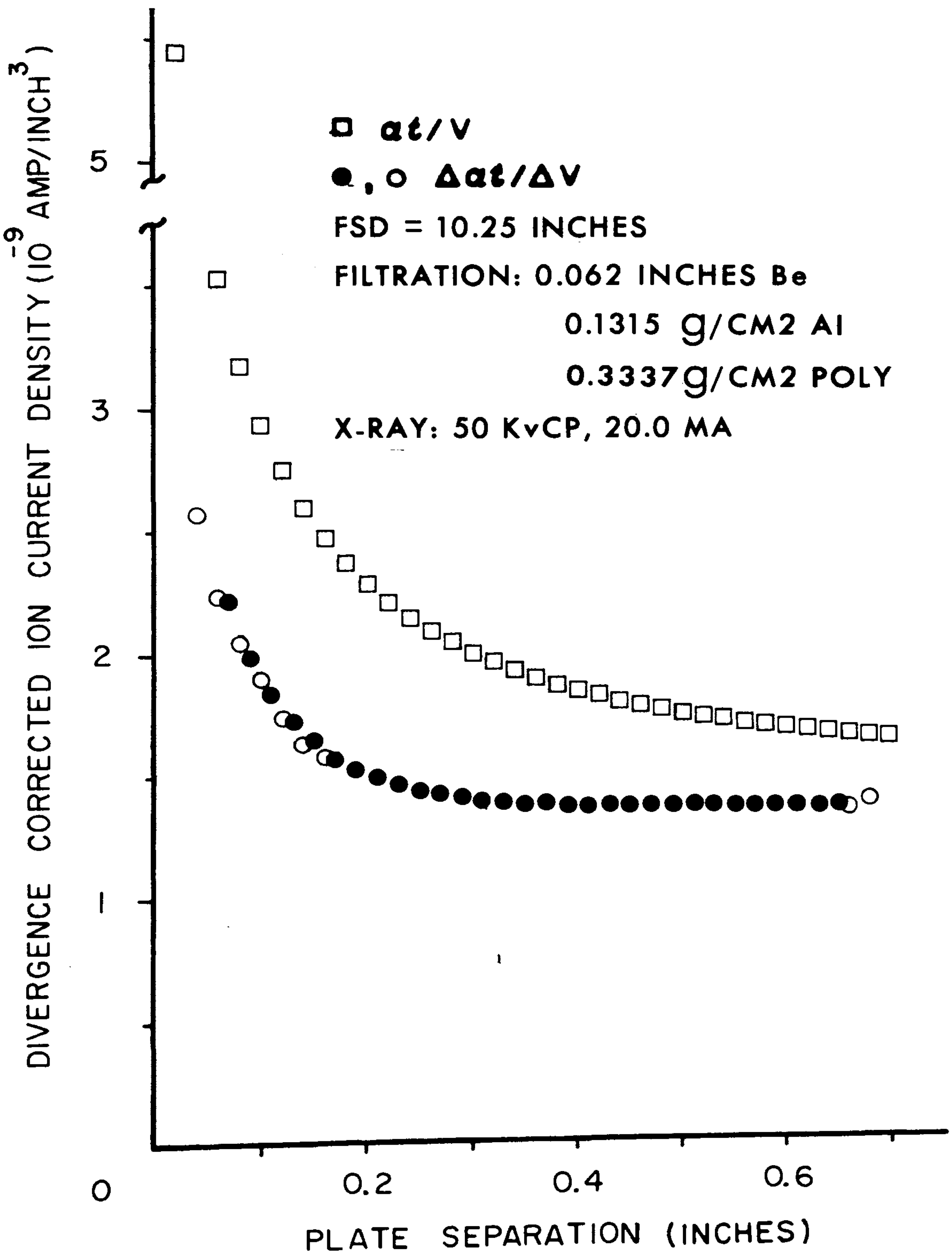
□ αt/V
●, ○ Δαt/ΔV
FSD = 10.25 INCHES
FILTRATION: 0.062 INCHES Be
0.1315 g/CM2 Al
0.3337 g/CM2 POLY
X-RAY: 50 KvCP, 20.0 MA
DIVERGENCE CORRECTED ION CURRENT DENSITY (10^-9 AMP/INCH^3)
PLATE SEPARATION (INCHES)
0
1
2
3
5
0.2
0.4
0.6

FIGURE 18

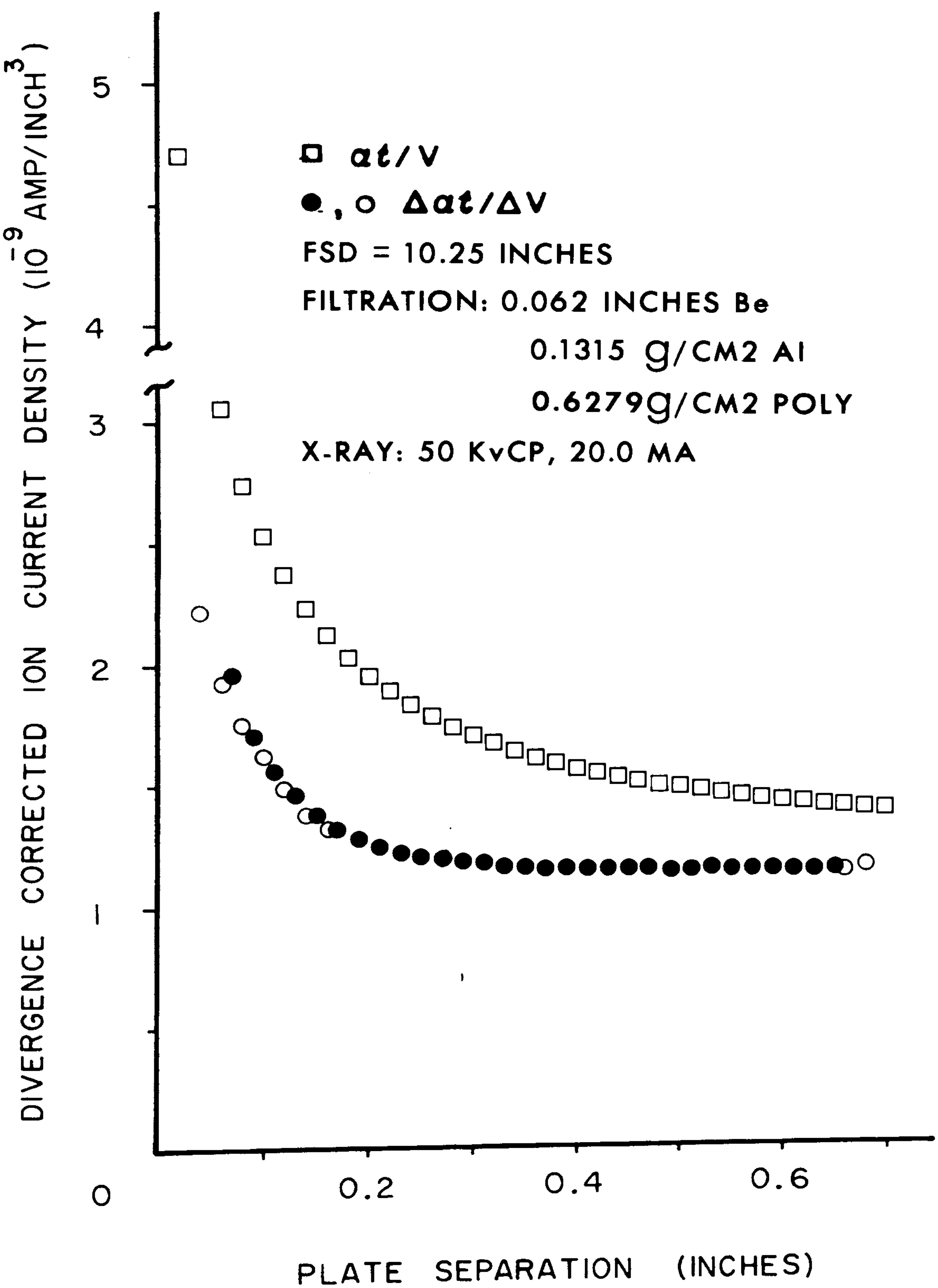
DIVERGENCE CORRECTED ION CURRENT DENSITY (10^{-9} AMP/INCH^3)
5
4
3
2
1
0
0.2
0.4
0.6
PLATE SEPARATION (INCHES)
□ at/V
●, ○ $\Delta at/\Delta V$
FSD = 10.25 INCHES
FILTRATION: 0.062 INCHES Be
0.1315 g/CM2 Al
0.6279 g/CM2 POLY
X-RAY: 50 KvCP, 20.0 MA

FIGURE 19

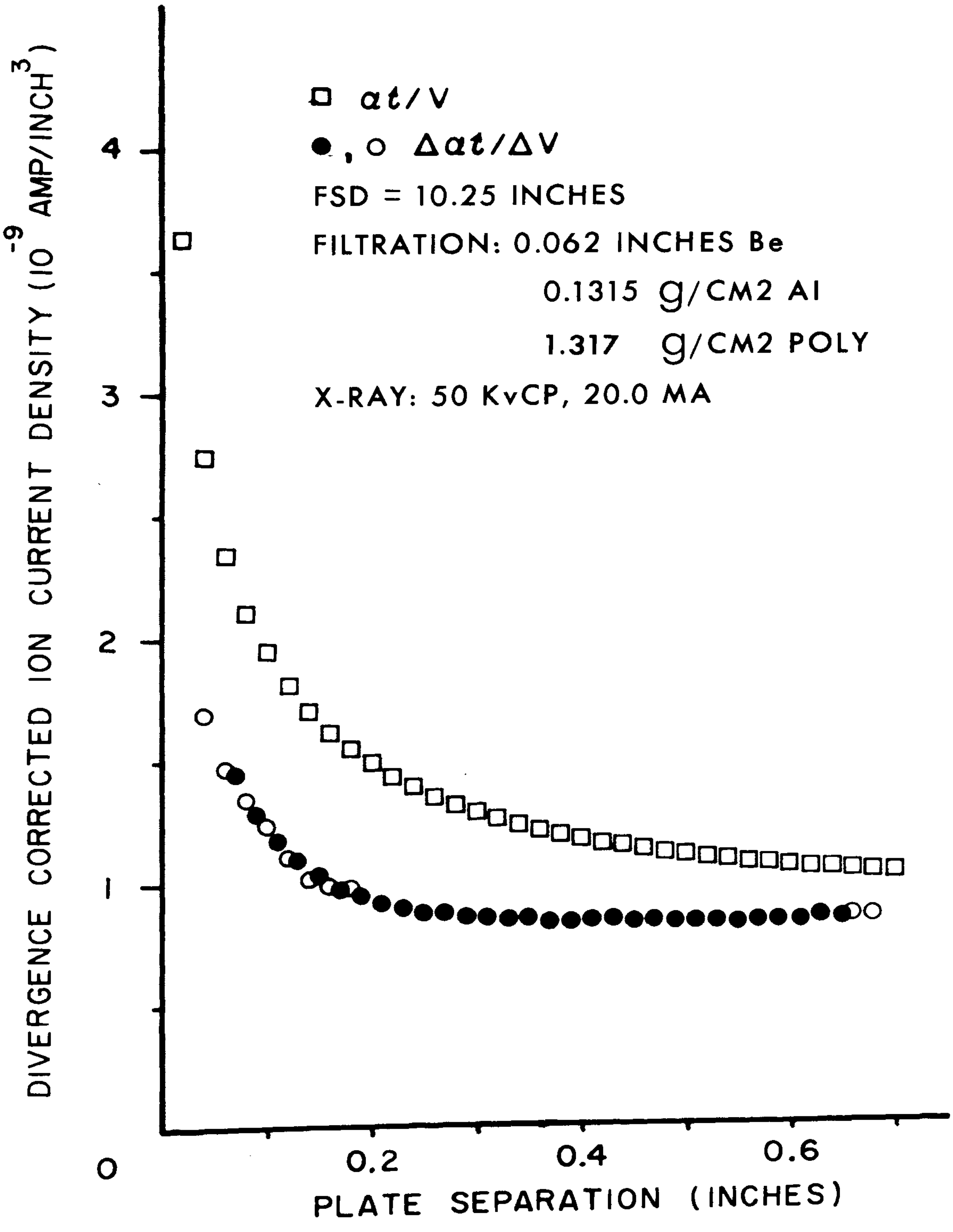

□ αt/V
●, ○ Δαt/ΔV
FSD = 10.25 INCHES
FILTRATION: 0.062 INCHES Be
0.1315 g/CM2 Al
1.317 g/CM2 POLY
X-RAY: 50 KvCP, 20.0 MA
DIVERGENCE CORRECTED ION CURRENT DENSITY (10^-9 AMP/INCH^3)
0
1
2
3
4
0.2
0.4
0.6
PLATE SEPARATION (INCHES)

FIGURE 20

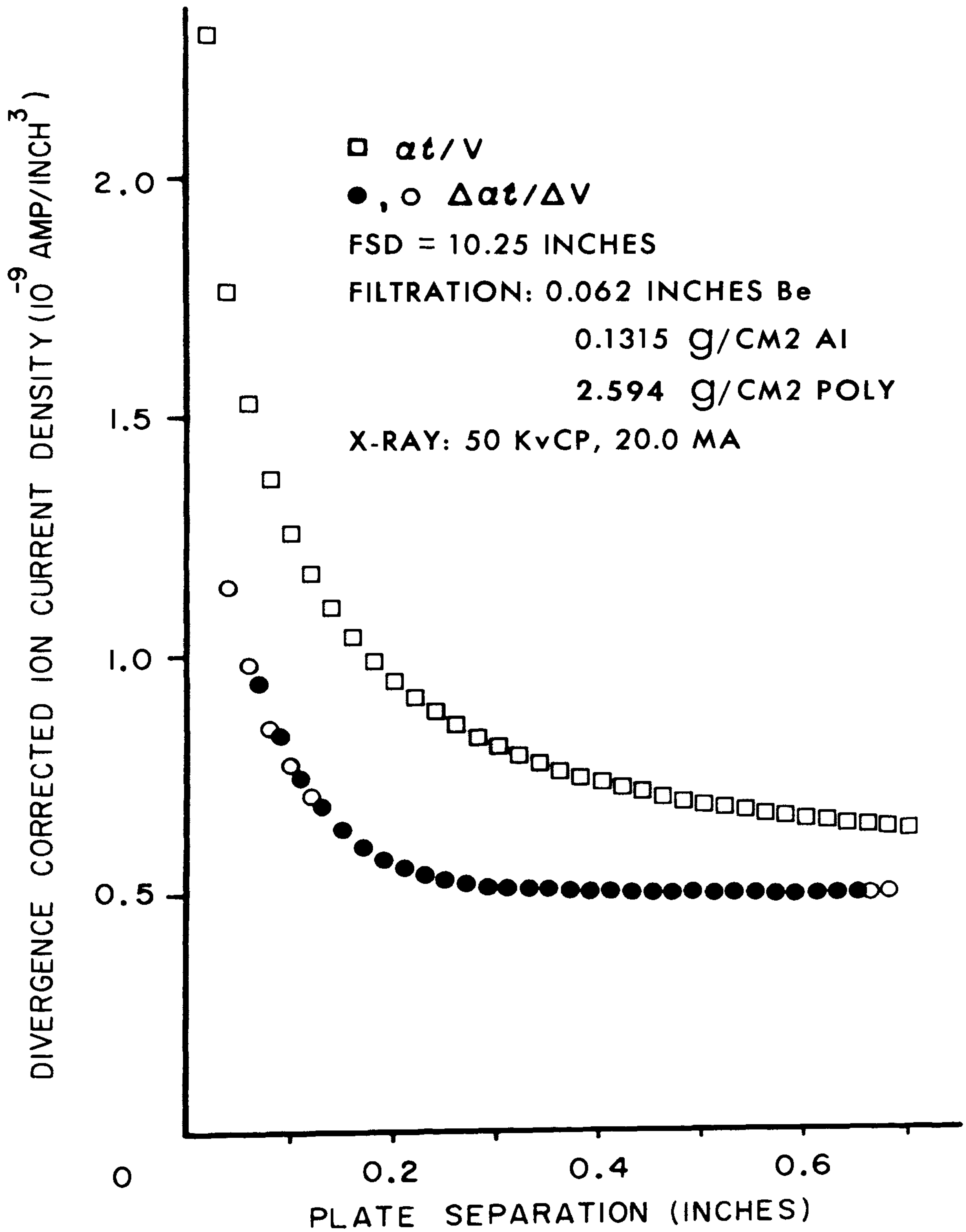
□ αt/V
●, ○ Δαt/ΔV
FSD = 10.25 INCHES
FILTRATION: 0.062 INCHES Be
0.1315 g/CM2 Al
2.594 g/CM2 POLY
X-RAY: 50 KvCP, 20.0 MA
DIVERGENCE CORRECTED ION CURRENT DENSITY (10^-9 AMP/INCH^3)
2.0
1.5
1.0
0.5
0
0.2
0.4
0.6
PLATE SEPARATION (INCHES)

FIGURE 21

APPENDIX III

TABULAR BETA CALIBRATION DATA

A. Table XI: Divergence Corrected Integral Ion Current Density (Aluminum attenuated)

B. Table XII: Divergence Corrected Differential Ion Current Density (Aluminum attenuated)

C. Table XIII: Divergence Corrected Integral Ion Current Density (Polyethylene attenuated, aluminum filtered)

D. Table XIV: Divergence Corrected Differential Ion Current Density (Polyethylene attenuated, aluminum filtered)

TABLE XI

$\left(\frac{\alpha i}{V}\right)$; DIVERGENCE CORRECTED INTEGRAL ION CURRENT DENSITY
(nano-amperes/cubic inch)

Abs. L (inch)	Aluminum Attenuator Thickness (g/cm^2) -0-	0.1315	0.2632	0.5246	1.002	1.539	2.469
0.020	33.06	6.503	4.290	2.564	1.371	0.7783	0.3648
0.040	25.36	4.953	3.297	1.985	1.073	0.6124	0.2922
0.060	22.44	4.313	2.824	1.706	0.9292	0.5327	0.2546
0.080	20.88	3.887	2.536	1.534	0.8359	0.4798	0.2304
0.100	19.95	3.597	2.336	1.411	0.7691	0.4428	0.2131
0.120	19.31	3.373	2.176	1.312	0.7137	0.4111	0.1983
0.140	18.82	3.197	2.041	1.226	0.6665	0.3843	0.1856
0.160	18.45	3.045	1.929	1.155	0.6262	0.3619	0.1744
0.180	18.13	2.927	1.839	1.097	0.5926	0.3419	0.1649
0.200	17.89	2.830	1.764	1.047	0.5646	0.3252	0.1572
0.220	17.67	2.749	1.697	1.003	0.5393	0.3101	0.1497
0.240	17.48	2.677	1.640	0.9647	0.5175	0.2969	0.1433
0.260	17.31	2.610	1.589	0.9309	0.4977	0.2851	0.1376
0.280	17.16	2.553	1.545	0.9013	0.4802	0.2747	0.1324
0.300	17.05	2.505	1.508	0.8768	0.4657	0.2656	0.1281
0.320	16.94	2.465	1.474	0.8543	0.4523	0.2575	0.1242
0.340	16.84	2.426	1.443	0.8331	0.4397	0.2499	0.1205
0.360	16.75	2.388	1.414	0.8142	0.4287	0.2431	0.1173
0.380	16.65	2.356	1.389	0.7971	0.4186	0.2369	0.1142
0.400	16.59	2.330	1.368	0.7822	0.4100	0.2313	0.1115
0.420	16.53	2.303	1.348	0.7682	0.4024	0.2258	0.1092
0.440	16.47	2.281	1.328	0.7547	0.3947	0.2208	0.1068
0.460	16.41	2.258	1.310	0.7428	0.3875	0.2163	0.1046
0.480	16.35	2.239	1.295	0.7316	0.3809	0.2122	0.1025
0.500	16.31	2.222	1.281	0.7214	0.3751	0.2085	0.1007
0.520	16.37	2.205	1.268	0.7122	0.3697	0.2051	0.0992
0.540	16.23	2.189	1.255	0.7034	0.3643	0.2019	0.0976
0.560	16.19	2.173	1.243	0.6954	0.3594	0.1989	0.0961
0.580	16.15	2.158	1.232	0.6878	0.3552	0.1962	0.0947
0.600	16.12	2.146	1.223	0.6810	0.3511	0.1937	0.0934
0.620	16.10	2.135	1.214	0.6745	0.3474	0.1914	0.0923
0.640	16.07	2.124	1.204	0.6684	0.3436	0.1891	0.0911
0.660	16.04	2.112	1.196	0.6628	0.3401	0.1870	0.0900
0.680	16.01	2.103	1.188	0.6576	0.3369	0.1851	0.0889
0.700	15.99	2.093	1.180	0.6527	0.3338	0.1832	0.0879

TABLE XII

$\left(\frac{\Delta\alpha i}{\Delta V}\right)$; DIVERGENCE CORRECTED DIFFERENTIAL ION CURRENT DENSITY (nano-amperes/cubic inch)

	Aluminum Attenuator Thickness (g/cm^2)						
Ave. L (inch)	-0-	0.1315	0.2632	0.5246	1.002	1.539	2.469
0.070	16.56	2.746	1.752	1.061	0.5820	0.3375	0.1650
0.090	16.20	2.495	1.539	0.9235	0.5041	0.2932	0.1430
0.110	16.06	2.284	1.393	0.8249	0.4445	0.2595	0.1263
0.130	15.93	2.159	1.281	0.7467	0.3979	0.2316	0.1125
0.150	15.84	2.062	1.191	0.6830	0.3600	0.2074	0.1011
0.170	15.70	2.001	1.123	0.6339	0.3305	0.1892	0.0915
0.190	15.62	1.948	1.080	0.5985	0.3090	0.1746	0.0842
0.210	15.49	1.912	1.043	0.5715	0.2920	0.1623	0.0786
0.230	15.40	1.879	1.016	0.5498	0.2780	0.1538	0.0739
0.250	15.37	1.855	0.9947	0.5361	0.2679	0.1465	0.0699
0.270	15.34	1.839	0.9833	0.5255	0.2604	0.1414	0.0680
0.290	15.30	1.823	0.9683	0.5171	0.2530	0.1371	0.0657
0.310	15.28	1.814	0.9615	0.5110	0.2494	0.1339	0.0644
0.330	15.25	1.806	0.9548	0.5054	0.2461	0.1310	0.0631
0.350	15.18	1.803	0.9488	0.4983	0.2430	0.1282	0.0619
0.370	15.21	1.786	0.9448	0.4930	0.2428	0.1245	0.0611
0.390	15.20	1.790	0.9388	0.4882	0.2414	0.1219	0.0603
0.410	15.19	1.789	0.9364	0.4857	0.2391	0.1199	0.0589
0.430	15.20	1.796	0.9351	0.4827	0.2374	0.1186	0.0584
0.450	15.19	1.792	0.9319	0.4783	0.2355	0.1175	0.0574
0.470	15.20	1.790	0.9296	0.4772	0.2323	0.1182	0.0570
0.490	15.19	1.784	0.9328	0.4774	0.2305	0.1187	0.0571
0.510	15.18	1.780	0.9324	0.4777	0.2300	0.1190	0.0571
0.530	15.21	1.766	0.9300	0.4775	0.2322	0.1194	0.0573
0.550	15.22	1.766	0.9333	0.4787	0.2307	0.1197	0.0569
0.570	15.19	1.775	0.9328	0.4785	0.2312	0.1198	0.0564
0.590	15.17	1.771	0.9294	0.4797	0.2318	0.1201	0.0561
0.610	15.22	1.773	0.9326	0.4799	0.2319	0.1204	0.0561
0.630	15.19	1.782	0.9320	0.4826	0.2304	0.1202	0.0552
0.650	15.16	1.775	0.9358	0.4829	0.2305	0.1201	0.0550

TABLE XIII

$\left(\frac{\alpha i}{V}\right)$; DIVERGENCE CORRECTED INTEGRAL ION CURRENT DENSITY

(nano-amperes/cubic inch)

Polyethylene Attenuator Thickness (g/cm^2)

(with 0.1315 g/cm^2 Al Filtration)

Abs. L (inch)	-0-	0.1637	0.3337	0.6279	1.317	2.594
0.020	6.503	5.861	5.442	4.695	3.639	2.301
0.040	4.953	4.445	4.123	3.554	2.744	1.762
0.060	4.313	3.842	3.532	3.046	2.344	1.532
0.080	3.886	3.460	3.179	2.738	2.105	1.371
0.100	3.597	3.201	2.938	2.530	1.943	1.259
0.120	3.373	3.001	2.753	2.367	1.815	1.172
0.140	3.197	2.837	2.598	2.233	1.704	1.100
0.160	3.045	2.698	2.473	2.121	1.615	1.040
0.180	2.927	2.590	2.373	2.032	1.543	0.9908
0.200	2.830	2.501	2.291	1.957	1.488	0.9495
0.220	2.749	2.424	2.215	1.893	1.433	0.9128
0.240	2.676	2.358	2.151	1.836	1.387	0.8823
0.260	2.610	2.298	2.098	1.786	1.347	0.8548
0.280	2.553	2.246	2.049	1.743	1.312	0.8306
0.300	2.505	2.204	2.009	1.707	1.282	0.8100
0.320	2.465	2.165	1.969	1.675	1.258	0.7913
0.340	2.425	2.127	1.935	1.644	1.232	0.7751
0.360	2.388	2.093	1.904	1.616	1.209	0.7597
0.380	2.356	2.063	1.875	1.591	1.189	0.7463
0.400	2.330	2.040	1.852	1.570	1.173	0.7353
0.420	2.303	2.016	1.830	1.551	1.157	0.7241
0.440	2.281	1.993	1.809	1.533	1.142	0.7141
0.460	2.258	1.972	1.789	1.515	1.129	0.7047
0.480	2.239	1.954	1.772	1.499	1.116	0.6961
0.500	2.222	1.937	1.757	1.486	1.106	0.6885
0.520	2.205	1.922	1.743	1.474	1.095	0.6817
0.540	2.189	1.907	1.729	1.461	1.085	0.6748
0.560	2.173	1.893	1.716	1.450	1.076	0.6681
0.580	2.158	1.880	1.703	1.439	1.067	0.6624
0.600	2.146	1.869	1.692	1.430	1.059	0.6572
0.620	2.135	1.859	1.682	1.421	1.052	0.6524
0.640	2.124	1.847	1.673	1.412	1.046	0.6474
0.660	2.112	1.836	1.662	1.403	1.039	0.6426
0.680	2.103	1.827	1.655	1.396	1.035	0.6386
0.700	2.093	1.819	1.647	1.389	1.028	0.6347

TABLE XIV

$\left(\frac{\Delta\alpha i}{\Delta V}\right)$; DIVERGENCE CORRECTED DIFFERENTIAL ION CURRENT DENSITY

(nano-amperes/cubic inch)

Polyethylene Attenuator Thickness (g/cm^2)

(with 0.1315 g/cm^2 Al Filtration)

Ave. L (inch)	-0-	0.1637	0.3337	0.6279	1.317	2.594
0.070	2.746	2.428	2.214	1.901	1.450	0.9454
0.090	2.495	2.195	1.989	1.706	1.289	0.8361
0.110	2.284	2.013	1.839	1.565	1.178	0.7447
0.130	2.160	1.894	1.728	1.467	1.094	0.6865
0.150	2.062	1.801	1.644	1.384	1.033	0.6401
0.170	2.001	1.733	1.570	1.325	0.9746	0.6029
0.190	1.948	1.688	1.527	1.280	0.9438	0.5769
0.210	1.912	1.657	1.496	1.249	0.9175	0.5587
0.230	1.879	1.627	1.465	1.222	0.8959	0.5424
0.250	1.855	1.608	1.444	1.208	0.8714	0.5311
0.270	1.839	1.593	1.426	1.195	0.8742	0.5232
0.290	1.823	1.572	1.417	1.182	0.8580	0.5176
0.310	1.814	1.561	1.401	1.175	0.8501	0.5128
0.330	1.806	1.552	1.390	1.167	0.8428	0.5103
0.350	1.803	1.548	1.381	1.158	0.8458	0.5110
0.370	1.786	1.539	1.388	1.153	0.8322	0.5089
0.390	1.790	1.538	1.380	1.156	0.8370	0.5067
0.410	1.789	1.537	1.376	1.153	0.8399	0.5064
0.430	1.796	1.536	1.379	1.151	0.8410	0.5052
0.450	1.792	1.528	1.379	1.150	0.8348	0.5013
0.470	1.790	1.528	1.374	1.149	0.8359	0.5040
0.490	1.784	1.527	1.375	1.147	0.8330	0.5020
0.510	1.780	1.529	1.377	1.148	0.8314	0.5000
0.530	1.766	1.528	1.374	1.152	0.8325	0.5007
0.550	1.766	1.529	1.368	1.146	0.8276	0.5009
0.570	1.775	1.529	1.369	1.146	0.8287	0.4996
0.590	1.771	1.523	1.371	1.145	0.8376	0.4996
0.610	1.773	1.519	1.365	1.143	0.8316	0.4998
0.630	1.782	1.518	1.372	1.142	0.8463	0.5004
0.650	1.775	1.515	1.374	1.147	0.8397	0.4994

APPENDIX IV

FORTRAN COMPUTER LOGIC

The major FORTRAN IV computer programs which were utilized during this investigation are listed on the following pages. The logic was listed via the "THESIS DUMP" OPTION implemented by the Computer Science Center staff. Included in this listing are:

(1) a program which generates from the recorded variable plate separation ion current data (i_{Ex}) the divergence corrected ion current densities [$\alpha i_{Ex}/V$, $\Delta\alpha i_{Ex}/\Delta V$] which constitute the β_x Calibration Data

(2) a program to assimilate the attenuation data and reduce it into a format [Eq. (17)] compatible for curve-fitting using the non-linear model defined by Eq. (18)

(3) a program that generates a polynomial representation of the x-ray attenuation coefficients from a linear least squares curve fitting analysis

(4) a program that adjusts the three parameters a,α,γ of the second term in Eq. (18) to best fit the attenuation data at large attenuator thicknesses

(5) a program which curve fits the complete model defined by Eq. (18) but holds a,α,γ constant while adjusting b and c to best represent the attenuation data over the complete range of attenuator thickness

(6) a program to evaluate and plot the normalized spectral absorbance $F_y^*(\lambda)$ detected by the dosimeter and defined by Eqs. (6) and (41), and the normalized true x-ray spectrum $f_y^*(\lambda)$ impinging upon the dosimeter and defined by Eq. (2)

(7) a program that generates and plots the absolute x-ray spectrum referenced to the x-ray tube target $f_o^E(\lambda)$, defined by Eqs. (23) and (42), as the sum of the characteristic $[f_o^{EC}(\lambda)]$ and bremsstrahlung $[f_o^{EB}(\lambda)$ radiation components and also compares $f_o^{EB}(\lambda)$ with the theoretical Kramers' bremsstrahlung $[f_o^K(\lambda)]$ defined by Eq. (49)

(8) a program that employs Simpson's method to numerically integrate the experimentally deduced spectra $f_o^{EB}(\lambda)$ and $f_o^{EC}(\lambda)$ over the wavelength range of $0.248 \leq \lambda \leq 1.728$ angstrom

(9) a program that employs Eq. (7) and the deduced absolute spectrum [Eq. (23)] to "predict" attenuation data $(\dot{D}_x)$ when $f_y(\lambda)$ is modified by different attenuator materials

Program #1

```
C       ANALYZE RAW VARIABLE PLATE SEPARATION DATA: GENERATE
C       ALPHA*I/V AND DELTA ALPHA*I/DELTA V  DATA.
C       DETERMINE ALPHA AT VARIOUS PLATE SEPARATIONS AND
C       X-RAY DOSIMETRY CALC'NS FOR DELTA ALPHA*I, DELA*I/DELTAV
        DIMENSION X(36),C(35),V(35),ALPHA(35),AI(35),DIV(35),
       1  DELTAI(35),DELTV(35),SUPRDV(35),XX(30)
        READ(1,102) (V(I),I=1,35)
        READ(1,101) (C(I),I=1,35)
        WRITE(3,18)
        WRITE(3,19)
        WRITE(3,20)
        X(1) = 0.020
        DO 10 I=1,35
        Y = ( X(I)/2.0 ) + 10.246
        Z = Y**1.98
        BOTT = (10.246)**1.98
        ALPHA(I) = Z/BOTT
        WRITE(3,21) X(I),Y,Z,ALPHA(I)
        X(I+1) = X(I) +0.02
     10 CONTINUE
C
C       WITH X(I) AND ALPHA(I) THUS DERIVED, ANALYZE DATA
        WRITE(3,900)
        WRITE(3,901)
C       FIND ALPHA*I & (ALPHA*I)/V
        DO 1  J = 1,35
        AI(J)=ALPHA(J)*C(J)
        DIV(J)= AI(J)/V(J)
      1 WRITE(3,200) X(J),C(J),V(J),ALPHA(J),AI(J),DIV(J)
C
C       NOW FIND DELTA(ALPHA.I)FOR DELTA L =0.040 INCHES
        WRITE(3,809)
        WRITE(3,800)
        WRITE(3,801)
        DO 2 I = 2,34
        DELTAI(I)= ABS(AI(I-1)-AI(I+1))
        DELTV(I) = ABS(V(I-1)-V(I+1))
        SUPRDV(I)= DELTAI(I)/DELTV(I)
      2 WRITE(3,300) X(I),SUPRDV(I)
C
C       NOW FIND SAME, FOR DELTA L =0.080 INCHES
        WRITE(3,807)
        WRITE(3,800)
        WRITE(3,801)
        DO 3 I = 3,33
        DELTAI(I) = ABS(AI(I-2)-AI(I+2))
        DELTV(I)  = ABS(V(I-2)-V(I+2))
        SUPRDV(I) = DELTAI(I)/DELTV(I)
      3 WRITE(3,300) X(I), SUPRDV(I)
C
C       NOW FIND SAME, FOR DELTA L =0.100 INCHES
        WRITE(3,805)
        WRITE(3,800)
        WRITE(3,801)
```

```
      DO 4 I = 1,30
      XX(I) = X(I) + 0.05
      DELTAI(I) = ABS(AI(I)-AI(I+5))
      DELTV(I) = ABS(V(I)-V(I+5))
      SUPRDV(I)= DELTAI(I)/DELTV(I)
    4 WRITE(3,300) XX(I), SUPRDV(I)
      RETURN
   18 FORMAT(13X,'TABLE FOR FINDING ALPHA AT VARIOUS PLATE',
     1  ' SEPARATIONS')
   19 FORMAT(13X,'WITH WINDOW TO TARGET DISTANCE AT 10.246',
     1  ' INCHES')
   20 FORMAT(13X,'L',6X,'D + L/2',5X,'(D+ L/2)**1.98',4X,
     1  'ALPHA')
   21 FORMAT(10X,F5.3,5X,F7.3,5X,F9.4,9X,F6.4)
  101 FORMAT(7F10.4)
  102 FORMAT(6F10.4)
  900 FORMAT(1X,'ABSOL.PLATE',1X,'I',15X,'V',7X,'ALPHA'2X,
     1  'ALPHA*I',4X,'ALPHA*I/V')
  901 FORMAT(1X,'SEPN,INCHES',1X,'AMPS*E-10',4X,'CUBIC IN.',
     1  10X,'AMPS*E-10',2X,'AMP/VOL*E-10')
  200 FORMAT(/,F8.2,3X,F7.4,6X,F8.4,4X,F6.4,3X,F7.4,3X,F7.4,//)
  800 FORMAT(14X,'X',11X,'DELTA(ALPHA*I)/DELTA V')
  801 FORMAT(27X,'X10*-10AMP')
  300 FORMAT(/,12X,F5.2,12X,F7.4,//)
  807 FORMAT(5X,'DELTA L =0.080 INCHES')
  805 FORMAT(5X,'DELTA L =0.100 INCHES')
  809 FORMAT(5X,'DELTA L = 0.040 INCHES')
      END
```

Program #2

```
C     ABSORPTION DATA REDUCTION INTO CURVE-FITTING FORMAT.
      DIMENSION X(50),Y(50),DATA(50),AVALUE(50),RATIO(50),
     1  ALOGR(50),AMUOX(50),YY(50),GREEN(50),AX(50),BETA(50),
     2  BETAY(50),A(10),XNEW(50),ITHICK(50)
      READ(1,50 ) NNN
      READ(1,100)   (X(I),Y(I),I = 1,NNN )
      READ( 1,75 )   ( BETA(I), I = 1,NNN )
      UNOT = .353
      WRITE(3,150)
      DO 1 I = 1,NNN
      BETAY(I)=BETA(I)*Y(I)
      DATA(I)=BETAY(I)*EXP(UNOT*X(I))
    1 WRITE(3,200) X(I),Y(I),BETA(I),BETAY(I),DATA(I)
C   TAKE RAW DATA VALUES OF IONIZATION CURRENT AND NORMALIZE
C   TO UNITY.
      DO 9 I = 7,NNN
      AX(I) = X(I)/2.70
      XNEW(I) = X(I) - X(7)
    9 AVALUE(I) = DATA(I)/DATA(7)
      WRITE(3,98)
      WRITE(3,99)
      WRITE(3,250)(I,XNEW(I),AX(I),DATA(I),AVALUE(I),I = 7,NNN)
      WRITE(2,450)(XNEW(I),AVALUE(I), I = 7,NNN)
C     TAKE RAW DATA & GENERATE DATA FOR GREENING PLOT
      DO 11 I = 8,NNN
      RATIO(I) = BETAY(7)/BETAY(I)
      ALOGR(I) = ALOG( RATIO(I) )
      AMUOX(I) = UNOT*XNEW(I)
      YY(I) = ALOGR(I)-AMUOX(I)
      GREEN(I) = XNEW(I)/YY(I)
      ITHICK(I)= I - 7
   11 CONTINUE
      WRITE(3,500)
      WRITE(3,525)
      WRITE(3,550)( ITHICK(I),XNEW(I),RATIO(I),ALOGR(I),
     1  AMUOX(I),YY(I),GREEN(I),I = 8,NNN)
      RETURN
   50 FORMAT(I20 )
   75 FORMAT( 7F10.4 )
   98 FORMAT(6X,'I',11X,'X(I)',11X,'X(I)',7X,'RAW DATA',3X,
     1  'DATA NORMALIZED TO UNITY')
   99 FORMAT(13X,'GM/CM**2',11X,'CM',6X,'I*EXP(UNOT*X(I))')
  100 FORMAT( 2E18.8 )
  150 FORMAT(13X,'X(I)',14X,'Y(I)',12X,'BETA(I)',12X,
     1  'BETA(I)*Y(I)',7X,'Y(I)*EXP(UNOT*X(I))')
  200 FORMAT( 5F18.5 )
  250 FORMAT(5X,I3,5X,F10.6,6X,F10.6,5X,F8.4,7X,F8.4 )
  450 FORMAT( 2F15.6 )
  500 FORMAT(/,5X,'I',9X,'X(I)',10X,'I(O)/I(K)',5X,'LN(IO/I)',
     1  3X,'U(O)*X(I)',6X,'Y',12X,'X/Y')
  525 FORMAT(10X,'GM/CM**2',//)
  550 FORMAT( I5,5X,F10.6,8X,F10.6,5X,F8.5,5X,F8.5,5X,F8.5,
     1  5X,F8.5 )
      END
```

Program #3

```
C      LINEAR LEAST SQUARES APPROXIMATION: POLYNOMIAL TYPE.
C      N=NUMBER OF POINTS OF X AND Y
C      KM = DEGREE OF THE LEAST SQUARES POLYNOMIAL DESIRED
       DOUBLE PRECISION X(50),Y(50),S(20,21),A(50),B(50),AY(50),
      1  EY(50)
       DO 727 JACK = 1,3
       READ (1,100) N,KM
       READ(1,200) ( X(I),Y(I), I = 1,N )
       DO 99 M = 1,KM
       A(1)=N
       L=2*M
       DO 11 J=1,M
       D=0.
       DO 12 I=1,N
    12 D=D+X(I)**J*Y(I)
    11 B(J+1)=D
       DO 13 J=1,L
       C=0.
       DO 14 I=1,N
    14 C=C+X(I)**J
    13 A(J+1)=C
       K=M+1
       DO 15 J=1,K
       JJ=J
       DO 15 I=1,K
       S(I,J)=A(JJ)
       JJ=JJ+1
    15 CONTINUE
       C=0.
       DO 44 J=1,N
    44 C=C+Y(J)
       B(1)=C
       MM=K+1
       DO 55 J=1,K
    55 S(J,MM)=B(J)
    96 WRITE(3,900)
       DO 87 I=1,K
    87 WRITE(3,800)(S(I,J),J=1,MM)
       CALL LUSK(K,S)
       WRITE(3,500) M
       WRITE(3,300)(S(I,MM),I=1,K)
       WRITE(3,400)
       SUME=0.
       D=N-M-1
       DO 33 I = 1,N
       SUM=S(1,MM)
       DO 22 J = 2,K
       JJ=J-1
    22 SUM=SUM+S(J,MM)*X(I)**JJ
       AY(I)=SUM
       EY(I)=Y(I)-AY(I)
       EY(I)=EY(I)**2
       DM=EY(I)/D
       SUME=SUME+DM
```

```
   33 WRITE(3,300)X(I),Y(I),AY(I),FY(I)
      WRITE(3,600)SUME
   99 CONTINUE
  727 CONTINUE
      RETURN
  100 FORMAT(2I5)
  200 FORMAT( 2F18.8 )
  300 FORMAT(4D18.8)
  400 FORMAT(11X,1HX,17X,1HY,15X,4HAPPR,14X,4HDELK)
  500 FORMAT(10X,'THE',I3,' DEGREE LEAST SQUARES COEFFICIENTS'
     1   ,' ARE')
  600 FORMAT(10X,10HVARIANCE =,D18.8)
  800 FORMAT(5D18.8)
  900 FORMAT(/,10X,26HTHE LEAST SQUARE MATRIX IS)
      END
C
C     GAUJOR REDUCTION OF MATRIX
      SUBROUTINE LUSK (N,A)
      DOUBLE PRECISION A(20,21),X(20),LOC(20),CK(20),AMAX
      NP =N+1
      DO 1 I = 1,N
    1 CK(I) =0.
      DO 101 I = 1,N
      IP = I+1
C     FIND MAX ELEMENT IN I-TH COL
      AMAX = 0.
      DO 2 K = 1,N
      IF(AMAX-DABS(A(K,I)))3,2,2
C     IS NEW MAX IN ROW PREVIOUSLY USED AS PIVOT?
    3 IF(CK(K)) 4,4,2
    4 LOC(I) =K
      AMAX =DABS(A(K,I))
    2 CONTINUE
      IF(DABS(AMAX)-1.E-5) 99,99,7
C     MAX ELEMENT IN I-TH COL IS A(L,I)
    7 L =LOC(I)
      CK(L) = 1.0
C     PERFORM ELIMINATION,L IS PIVOT ROW,A(L,I) IS PIVOT ELEMENT
      DO 50 J=1,N
      IF(L-J) 6,50,6
    6 F=-A(J,I)/A(L,I)
      DO 40 K=IP,NP
   40 A(J,K) = A(J,K) +F*A(L,K)
   50 CONTINUE
  101 CONTINUE
      DO 201 I = 1,N
      L = LOC(I)
  201 X(I) = A(L,N+1)/A(L,I)
      DO 301 I = 1,N
      A(I,NP) = X(I)
  301 CONTINUE
   99 CONTINUE
      RETURN
      END
```

Program #4

```
C       NON-LINEAR REGRESSION: 3 PARAMETERS--A,ALPHA,GAMMA.
C       MAINLINE PROGRAM
        COMMONX(100),P(9),A(10,10),N,NP,M,ND,NV,MAX,TOL,PI(9,2)
        CALL CHAIN2
        CALL CHAIN3
        CALL CHAIN4
        CALL EXIT
        END
C     INITIALIZE
        SUBROUTINE CHAIN2
        DIMENSION HEADER(20)
        COMMONX(100),P(9),A(10,10),N,NP,M,ND,NV,MAX,TOL
 1001   FORMAT(4I5,E18.8)
 1002   FORMAT(20A4)
 2001   FORMAT(1H1,I2,13H-OBSERVATIONS,10X,I1,11H-PARAMETERS,
      1   10X,11HMAXIMUM OF ,I2,' ITERATIONS, WITH CUT-OFF',
      2   ' TOLERANCE',E18.8/6H MODEL,10X,20A4///5H ITER,
      3   9(7X,2HP(,I1,1H),3X))
        READ(1,1001) N,NP,ND,MAX,TOL
        IF(N.LE.0)STOP
        M=NP+1
        NV=ND+1
        READ(1,1002) HEADER
        WRITE(3,2001) N,NP,MAX,TOL,HEADER,(I,I=1,NP)
C    GET OBSERVATIONS
        CALLINPUT(N,NV,X)
C    INITIAL PARAMETER ESTIMATES
        CALL PARAM
        RETURN
        END
C     INPUT   READ DATA
        SUBROUTINEINPUT(N,NV,X)
        DIMENSIONX(1)
 1001   FORMAT( 2E18.8)
        K2 = 0
        DO 1 I=1,N
        K1 = K2+1
        K2 = K2+NV
      1 READ(1,1001) (X(K),K=K1,K2)
        RETURN
        END
C     PARAMETER
        SUBROUTINEPARAM
        INTEGERSCNTL,CNTL
        DIMENSIONSCNTL(9),CNTL(9)
        DIMENSION PV(9),THETA(9,2)
        COMMONX(100),P(9),A(10,10),N,NP,M,ND,NV,MAX,TOL,PI(9,2)
 1001   FORMAT(9F8.0)
        READ(1,1001) RDC
        IF(RDC .EQ.0.0) GO TO 100
        DO5J=1,2
      5 READ(1,1001) (PI(I,J),I=1,NP)
        J = 1
        F0=1.0
```

```
      F1=1.0
   10 F2 = F0+F1
      IF(F2 .GE. 2.0/RDC) GO TO 20
      F0 = F1
      F1 = F2
      J = J+1
      GO TO 10
   20 SS1 = 0.0
      DO 21 I=1,NP
      CNTL(I) = 1
      DELTA = (PI(I,2)-PI(I,1))*(F0/F2)
      THETA(I,1) = PI(I,1)+DELTA
      PV(I) = THETA(I,1)
   21 THETA(I,2) = PI(I,2)-DELTA
   22 CALL RSS(PV,SS2)
      IF(SS1.EQ.0.0) GO TO 30
      IF(SS2.GE.SS1) GO TO 33
   30 SS1 = SS2
      DO 32 I=1,NP
   32 SCNTL(I) = CNTL(I)
   33 I = NP
   35 IF(CNTL(I).EQ.1) GO TO 36
      CNTL(I) = 1
      IF(I.EQ.1) GO TO 40
      PV(I) = THETA(I,1)
      I = I-1
      GO TO 35
   36 CNTL(I) = 2
      PV(I) = THETA(I,2)
      GO TO 22
   40 J = J-1
      F2 = F1
      F1 = F0
      F0 = F2-F1
      DO 43 I=1,NP
      DELTA = (THETA(I,2)-PI(I,1))*(F0/F2)
      IF(SCNTL(I).EQ.1) GO TO 41
      PI(I,1) = THETA(I,1)
      THETA(I,1) = THETA(I,2)
      THETA(I,2) = PI(I,2)-DELTA
      GO TO 42
   41 PI(I,2) = THETA(I,2)
      THETA(I,2) = THETA(I,1)
      THETA(I,1) = PI(I,1)+DELTA
   42 PV(I) = THETA(I,1)
   43 CONTINUE
      IF(J.GT.1)GOTO22
   50 DO51I=1,NP
   51 P(I)=(PI(I,2)+PI(I,1))/2.
      RETURN
  100 READ(1,1001) (P(I),I=1,NP)
      DO 105 I=1,NP
      PI(I,2)=1.0E30
      PI(I,1)=-1.0E30
```

```
  105 CONTINUE
      RETURN
      END
C    ITERATE
      SUBROUTINE CHAIN3
      DIMENSIONPD2(9),D(10),UNIT(9)
      COMMONX(100),P(9),A(10,10),N,NP,M,ND,NV,MAX,TOL,PI(9,2)
 2002 FORMAT(2X,I2,3X,1P9E14.6)
 2003 FORMAT(5X,14HRESIDUAL SS = ,1PE14.7)
 2004 FORMAT(6X,1H(,1P3E14.7,I3,1H)/)
 2005 FORMAT(1X,' PARAMETER ESTIMATE OUT OF RANGE,LIMITS',
     1   ' SET BY FIBONACCI SEARCH ARE -',/)
 2006 FORMAT(7HSLEFT  ,1P9E14.6)
 2007 FORMAT(7HSRIGHT ,1P9E14.6)
 2090 FORMAT(7X,1P9E14.7)
 2080 FORMAT(33HL@MODIFIED@ G-N DOES NOT CONVERGE,5X,1P4E14.7)
      ICNT=0
      QO=1.0E30
      KTRIG=0
      KTEST=0
C   BEGIN ITERATION
   10 WRITE(3,2002) ICNT,(P(I),I=1,NP)
      IF(KTEST.EQ.0)GOTO19
      IF(KTRIG.EQ.1)GOTO19
      WRITE(3,2005)
      WRITE(3,2006) (PI(I,1),I=1,NP)
      WRITE(3,2007) (PI(I,2),I=1,NP)
      KTRIG=1
   19 DO20I=1,M
      DO20J=I,M
   20 A(I,J)=0.0
C   BUILD NORMAL EQUATIONS
      KY = 0
      DO30I=1,N
      KY = KY+NV
      L=KY-ND
      CALL DERIV(P,X,L,D)
      D(M)=X(KY)-YCAL(P,X,L)
      DO30J=1,M
      DO30K=J,M
   30 A(J,K)=A(J,K)+D(J)*D(K)
      DO40I=2,NP
      K=I-1
      DO40J=1,K
   40 A(I,J)=A(J,I)
C   SOLVE NORMAL EQUATIONS
      DO41I=1,NP
   41 WRITE(3,2090) (A(I,J),J=1,M)
      CALL CHRISA(NP,A)
C   TEST FOR CONVERGENCE
      WRITE(3,2003) A(M,M)
      QOO = ABS(QO-A(M,M) )
      IF( QOO.LE.TOL) RETURN
      QO = A(M,M)
```

```
C   CALCULATE PARAMETER ADJUSTMENTS
C   FIRST,NORMALIZE THETA VECTOR:I.E.,OBTAIN UNIT VECTOR.
       SUM = 0.
       DO 35 I = 1,NP
   35  SUM = SUM + A(I,M)**2
       SUM = SQRT( SUM )
       DO 36 I = 1,NP
   36  UNIT(I) = A(I,M)/SUM
       KITER = 0
       C = 1.
   55  DO 50 I = 1,NP
   50  PD2(I) = P(I) + UNIT(I)*C
       CALL RSS(PD2,Q2)
       QD = Q2-Q0
       IF(QD.LT.0.0) GO TO60
       KITER = KITER+1
       IF(KITER.GT.MAX) GO TO 58
       C = C*0.5
       GO TO 55
   58  WRITE(3,2080)
       RETURN
   60  WRITE(3,2004) Q0,Q2,C,KITER
       DO 61  I = 1,NP
   61  P(I) = PD2(I)
       ICNT = ICNT + 1
       GO TO 10
       END
C   GAUJOR
       SUBROUTINE CHRISA(N,A)
       DIMENSION A(10,10),X(20),LOC(20),CK(20)
       NP = N+1
       DO 1 I = 1,N
    1  CK(I) = 0.
       DO 101 I = 1,N
       IP = I + 1
       AMAX = 0.
       DO 2 K = 1,N
       IF( AMAX-ABS( A(K,I)) ) 3,2,2
    3  IF( CK(K) ) 4,4,2
    4  LOC(I) = K
       AMAX = ABS( A(K,I) )
    2  CONTINUE
       IF( ABS(AMAX)-1.E-5) 99,99,7
    7  L = LOC(I)
       CK(L) = 1.0
       DO 50 J = 1,N
       IF( L -J) 6,50,6
    6  F = -A(J,I)/A(L,I)
       DO 40 K = IP,NP
   40  A(J,K) = A(J,K) + F*A(L,K)
   50  CONTINUE
  101  CONTINUE
       DO 201 I = 1,N
       L = LOC(I)
```

```
  201 X(I) = A(L,N+1)/A(L,I)
      DO 301 I = 1,N
      A(I,NP) = X(I)
  301 CONTINUE
   99 CONTINUE
      RETURN
      END
C     RESIDUAL SUM OF SQUARES
      SUBROUTINERSS(V,Q)
      DIMENSIONV(1)
      COMMONX(100),P(9),A(10,10),N,NP,M,ND,NV,MAX,TOL
      Q=0.0
      KY = 0
      DO1I=1,N
      KY = KY+NV
      K=KY-ND
      YR = X(KY)-YCAL(V,X,K)
    1 Q=Q+YR*YR
      RETURN
      END
C     OUTPUT
      SUBROUTINE CHAIN4
      COMMONX(100),P(9),A(10,10),N,NP,M,ND,NV,MAX,TOL
 2004 FORMAT(3H1 I,13X,8HOBSERVED,15X,10HCALCULATED,15X,
     1  8HRESIDUAL//)
 2005 FORMAT(1X,I2,3(10X,1PE14.7))
 2006 FORMAT(22HLGREATEST RESIDUAL OF ,1PE14.7,5H, AT ,I2,
     1   14HTH OBSERVATION/1H1,9X.10HPARAMETER ,9X,
     2   14H.95 CONFIDENCE/2X,1HI,8X,8HESTIMATE,13X,8HINTERVAL//)
 2007 FORMAT(1HK,I2,5X,1PE14.7,3X,1H*,3X,E14.7)
 2008 FORMAT(///19HLSTANDARD ERROR OF ,1PE14.7,7H, WITH ,0PF3.0,
     1   19H DEGREES OF FREEDOM)
  100 WRITE(3,2004)
      BIGD=0.0
      KY = 0
      DO110I=1,N
        KY = KY+NV
      K=KY-ND
      YC = YCAL(P,X,K)
      YR=X(KY)-YC
      WRITE(3,2005) I,X(KY),YC,YR
      IF(ABS(BIGD).GT.ABS(YR))GOTO110
  109 BIGD=YR
      J=I
  110 CONTINUE
      WRITE(3,2006) BIGD,J
      DF=N-NP
      VAR=A(M,M)/DF
      T=(1.96*DF+0.60033+0.9591/DF)/(DF-0.90259+0.11588/DF)
      DO120I=1,NP
      CI=T*SQRT(A(I,I)*VAR)
  120 WRITE(3,2007) I,P(I),CI
      SE=SQRT(VAR)
      WRITE(3,2008) SE,DF
```

```
      RETURN
      END
C     Y ESTIMATED
      FUNCTION YCAL(P,X,L)
      DIMENSIONP(1),X(1)
      F(X,A,ALPHA,GAMMA) = (1.-A)*((ALPHA/(X+ALPHA))**GAMMA)
      DO 1 I = 1,3
    1 P(I) = ABS( P(I) )
      YCAL=F(X(L),P(1),P(2),P(3))
      RETURN
      END
C     DERIVATIVES OF MODEL
      SUBROUTINEDERIV(P,X,L,D)
      DIMENSIONP(1),D(1),X(1)
      FA(X,ALPHA,GAMMA) = -((ALPHA/(X+ALPHA))**GAMMA)
      FALPHA(X,A,ALPHA,GAMMA)=(1.-A)*GAMMA*((ALPHA/(X+ALPHA))
     Q               **(GAMMA-1.))
     W                           *(X/((X+ALPHA)**2))
      FGAMMA(X,A,ALPHA,GAMMA) = (1.-A)*((ALPHA/(X+ALPHA))**GAMMA)
     3                          *ALOG( ALPHA/(X+ALPHA) )
      DO 1 I = 1,3
    1 P(I) = ABS( P(I) )
      D(1)=FA(X(L),P(2),P(3))
      D(2) = FALPHA(X(L),P(1),P(2),P(3) )
      D(3) = FGAMMA(X(L),P(1),P(2),P(3) )
      RETURN
      END
```

Program #5

```
C       NON-LINEAR REGRESSION: 2 PARAMETERS.
C       MODEL:   F = A*EXP( -B*(SQRT(X+C)-SQRT(C) ) )+
C                    (1.-A)*( ALPHA/(X+ALPHA) )**GAMMA
C       DEFINE A,ALPHA, AND GAMMA IN THE ROUTINES:YCAL,DERIV,TERM.
C       READ IN X,Y AS FORMATED: 2E18.8 I.E., ANY FORM WITHIN
C       COLUMNS 18&36.
C       ORDER OF DATA CARDS
C        1:  LIST # OF DATA PTS,ETC.
C       2:  HEADER CARD
C       3:  THE DATA POINTS--OBSERVED VALUES--
C       4:  RDC--SOME FRACTION; THEN DO NOT PUT IN STARTING
C           VALUES FOR PARAMETERS.
C       5:  LOWER BOUND
C       6:  UPPER BOUND
C       IF IT IS DESIRED TO READ IN STARTING VALUES,SET RDC EQUAL
C       TO ZERO;I.E., A BLANK CARD IS INSERTED IN THE LAST
C       PLACE, THEN THE FOLLOWING CARD YIELDS THE DESIRED START-
C       ING VALUES TO BE READ IN.
C       MAINLINE PROGRAM
        COMMONX(100),P(9),A(10,10),N,NP,M,ND,NV,MAX,TOL,PI(9,2)
        CALL CHAIN2
        CALL CHAIN3
        CALL CHAIN4
        CALL EXIT
        END
C     INITIALIZE
        SUBROUTINE CHAIN2
        DIMENSION HEADER(20)
        COMMONX(100),P(9),A(10,10),N,NP,M,ND,NV,MAX,TOL
 1001   FORMAT(4I5,E18.8)
 1002   FORMAT(20A4)
 2001   FORMAT(1H1,I2,13H-OBSERVATIONS,10X,I1,11H-PARAMETERS,
      1   10X,11HMAXIMUM OF ,I2,' ITERATIONS, WITH CUT-OFF',
      2   ' TOLERANCE', E18.8/' MODEL',10X,20A4///5H ITER,
      3   9(7X,2HP(,I1,1H),3X))
        READ(1,1001) N,NP,ND,MAX,TOL
        IF(N.LE.0)STOP
        M=NP+1
        NV=ND+1
        READ(1,1002) HEADER
        WRITE(3,2001) N,NP,MAX,TOL,HEADER,(I,I=1,NP)
C
C    GET OBSERVATIONS
        CALLINPUT(N,NV,X)
C    INITIAL PARAMETER ESTIMATES
        CALL PARAM
        RETURN
        END
C     INPUT    READ DATA
        SUBROUTINEINPUT(N,NV,X)
        DIMENSIONX(1)
 1001   FORMAT( 2E18.8)
        K2 = 0
        DO 1 I=1,N
```

```
      K1 = K2+1
      K2 = K2+NV
    1 READ(1,1001) (X(K),K=K1,K2)
      RETURN
      END
C     PARAMETER
      SUBROUTINEPARAM
      INTEGERSCNTL,CNTL
      DIMENSIONSCNTL(9),CNTL(9)
      DIMENSION PV(9),THETA(9,2)
      COMMONX(100),P(9),A(10,10),N,NP,M,ND,NV,MAX,TOL,PI(9,2)
 1001 FORMAT(9F8.0)
      READ(1,1001) RDC
      IF(RDC .EQ.0.0) GO TO 100
      DO5J=1,2
    5 READ(1,1001) (PI(I,J),I=1,NP)
      J = 1
      F0=1.0
      F1=1.0
   10 F2 = F0+F1
      IF(F2 .GE. 2.0/RDC) GO TO 20
      F0 = F1
      F1 = F2
      J = J+1
      GO TO 10
   20 SS1 = 0.0
      DO 21 I=1,NP
      CNTL(I) = 1
      DELTA = (PI(I,2)-PI(I,1))*(F0/F2)
      THETA(I,1) = PI(I,1)+DELTA
      PV(I) = THETA(I,1)
   21 THETA(I,2) = PI(I,2)-DELTA
   22 CALL RSS(PV,SS2)
      IF(SS1.EQ.0.0) GO TO 30
      IF(SS2.GE.SS1) GO TO 33
   30 SS1 = SS2
      DO 32 I=1,NP
   32 SCNTL(I) = CNTL(I)
   33 I = NP
   35 IF(CNTL(I).EQ.1) GO TO 36
      CNTL(I) = 1
      IF(I.EQ.1) GO TO 40
      PV(I) = THETA(I,1)
      I = I-1
      GO TO 35
   36 CNTL(I) = 2
      PV(I) = THETA(I,2)
      GO TO 22
   40 J = J-1
      F2 = F1
      F1 = F0
      F0 = F2-F1
      DO 43 I=1,NP
      DELTA = (THETA(I,2)-PI(I,1))*(F0/F2)
```

```
      IF(SCNTL(I).EQ.1) GO TO 41
      PI(I,1) = THETA(I,1)
      THETA(I,1) = THETA(I,2)
      THETA(I,2) = PI(I,2)-DELTA
      GO TO 42
   41 PI(I,2) = THETA(I,2)
      THETA(I,2) = THETA(I,1)
      THETA(I,1) = PI(I,1)+DELTA
   42 PV(I) = THETA(I,1)
   43 CONTINUE
      IF(J.GT.1)GOTO22
   50 DO51I=1,NP
   51 P(I)=(PI(I,2)+PI(I,1))/2.
      RETURN
  100 READ(1,1001) (P(I),I=1,NP)
      DO 105 I=1,NP
      PI(I,2)=1.0E30
      PI(I,1)=-1.0E30
  105 CONTINUE
      RETURN
      END
C    ITERATE
      SUBROUTINE CHAIN3
      DIMENSIONPD2(9),D(10),UNIT(9)
      COMMONX(100),P(9),A(10,10),N,NP,M,ND,NV,MAX,TOL,PI(9,2)
 2002 FORMAT(2X,I2,3X,1P9E14.6)
 2003 FORMAT(5X,14HRESIDUAL SS = ,1PE14.7)
 2004 FORMAT(6X,1H(,1P3E14.7,I3,1H)/)
 2005 FORMAT(1X,'PARAMETER ESTIMATE OUT OF RANGE, LIMITS SET',
     1   ' BY FIBONACCI SERCH ARE ',/)
 2006 FORMAT(7HSLEFT   ,1P9E14.6)
 2007 FORMAT(7HSRIGHT  ,1P9E14.6)
 2090 FORMAT(7X,1P9E14.7)
 2080 FORMAT(33HL@MODIFIED@ G-N DOES NOT CONVERGE,5X,1P4E14.7)
      ICNT=0
      QO = 1.E30
      KTRIG=0
      KTEST=0
C   BEGIN ITERATION
   10 WRITE(3,2002) ICNT,(P(I),I=1,NP)
      IF(KTEST.EQ.0)GOTO19
      IF(KTRIG.EQ.1)GOTO19
      WRITE(3,2005)
      WRITE(3,2006) (PI(I,1),I=1,NP)
      WRITE(3,2007) (PI(I,2),I=1,NP)
      KTRIG=1
   19 DO20I=1,M
      DO20J=I,M
   20 A(I,J)=0.0
C   BUILD NORMAL EQUATIONS
      KY = 0
      DO30I=1,N
      KY = KY+NV
      L=KY-ND
```

```
      CALL DERIV(P,X,L,D)
      D(M)=X(KY)-YCAL(P,X,L)
      DO30J=1,M
      DO30K=J,M
   30 A(J,K)=A(J,K)+D(J)*D(K)
      DO40I=2,NP
      K=I-1
      DO40J=1,K
   40 A(I,J)=A(J,I)
C   SOLVE NORMAL EQUATIONS
      DO41I=1,NP
   41 WRITE(3,2090) (A(I,J),J=1,M)
      CALL CHRISA(NP,A)
C   TEST FOR CONVERGENCE
      WRITE(3,2003) A(M,M)
      QQQ = ABS(QQ-A(M,M) )
      IF( QQQ.LE.TOL) RETURN
      QQ = A(M,M)
C   CALCULATE PARAMETER ADJUSTMENTS
C   FIRST,NORMALIZE THETA VECTOR:I.E.,OBTAIN UNIT VECTOR.
      SUM = 0.
      DO 35 I = 1,NP
   35 SUM = SUM + A(I,M)**2
      SUM = SQRT( SUM )
      DO 36 I = 1,NP
   36 UNIT(I) = A(I,M)/SUM
      KITER = 0
      C = 1.
   55 DO 50 I = 1,NP
   50 PD2(I) = P(I) + UNIT(I)*C
      CALL RSS(PD2,Q2)
      QD = Q2-QQ
      IF(QD.LT.0.0) GO TO60
      KITER = KITER+1
      IF(KITER.GT.MAX) GO TO 58
      C = C*0.5
      GO TO 55
   58 WRITE(3,2080)
      RETURN
   60 WRITE(3,2004) QQ,Q2,C,KITER
      DO 61  I = 1,NP
   61 P(I) = PD2(I)
      ICNT = ICNT + 1
      GO TO 10
      END
C   GAUJOR
      SUBROUTINE CHRISA(N,A)
      DIMENSION A(10,10),X(20),LOC(20),CK(20)
      NP = N+1
      DO 1 I = 1,N
    1 CK(I) = 0.
      DO 101 I = 1,N
      IP = I + 1
      AMAX = 0.
```

```
      DO 2 K = 1,N
      IF( AMAX-ABS( A(K,I)) ) 3,2,2
    3 IF( CK(K) ) 4,4,2
    4 LOC(I) = K
      AMAX = ABS( A(K,I) )
    2 CONTINUE
      IF( ABS(AMAX)-1.E-5) 99,99,7
    7 L = LOC(I)
      CK(L) = 1.0
      DO 50 J = 1,N
      IF( L -J) 6,50,6
    6 F = -A(J,I)/A(L,I)
      DO 40 K = IP,NP
   40 A(J,K) = A(J,K) + F*A(L,K)
   50 CONTINUE
  101 CONTINUE
      DO 201 I = 1,N
      L = LOC(I)
  201 X(I) = A(L,N+1)/A(L,I)
      DO 301 I = 1,N
      A(I,NP) = X(I)
  301 CONTINUE
   99 CONTINUE
      RETURN
      END
C    RESIDUAL SUM OF SQUARES
      SUBROUTINEERSS(V,Q)
      DIMENSIONV(1)
      COMMONX(100),P(9),A(10,10),N,NP,M,ND,NV,MAX,TOL
      Q=0.0
      KY = 0
      DO1I=1,N
      KY = KY+NV
      K=KY-ND
      YR = X(KY)-YCAL(V,X,K)
    1 Q=Q+YR*YR
      RETURN
      END
C    OUTPUT
      SUBROUTINE CHAIN4
      COMMONX(100),P(9),A(10,10),N,NP,M,ND,NV,MAX,TOL
 2004 FORMAT(1X,3H1 I,13X,'OBSERVED',15X,'CALCULATED',15X,
     1  'RESIDUAL',//)
 2005 FORMAT(1X,I2,3(10X,1PE14.7))
 2006 FORMAT(22HLGREATEST RESIDUAL OF ,1PE14.7,5H, AT ,I2,
     1  'TH OBSERVATION'/'1',9X,'PARAMETER ',9X,
     2  '.95 CONFIDENCE'/,2X,1HI,8X,'ESTIMATE',13X,'INTERVAL'//)
 2007 FORMAT(1HK,I2,5X,1PE14.7,3X,1H*,3X,F14.7)
 2008 FORMAT(///19HLSTANDARD ERROR OF ,1PE14.7,7H, WITH ,
     1 0PF3.0,19H DEGREES OF FREEDOM)
  100 WRITE(3,2004)
      BIGD=0.0
      KY = 0
      DO110I=1,N
```

```
      KY = KY+NV
      K=KY-ND
      YC = YCAL(P,X,K)
      YR=X(KY)-YC
      WRITE(3,2005) I,X(KY),YC,YR
      IF(ABS(BIGD).GT.ABS(YR))GOTO110
  109 BIGD=YR
      J=I
  110 CONTINUE
      WRITE(3,2006) BIGD,J
      DF=N-NP
      VAR=A(M,M)/DF
      T=(1.96*DF+0.60033+0.9591/DF)/(DF-0.90259+0.11588/DF)
      DO120I=1,NP
      CI=T*SQRT(A(I,I)*VAR)
  120 WRITE(3,2007) I,P(I),CI
      SE=SQRT(VAR)
      WRITE(3,2008) SE,DF
      CALL TERM(NV,P,X,N,ND)
      RETURN
      END
C     Y ESTIMATED
      FUNCTION YCAL(P,X,L)
      DIMENSIONP(1),X(1)
      Z(X,B,C)=(-B*(SQRT(ABS(X+C))-SQRT(ABS(C))))
      F(X,A,B,C,ALPHA,GAMMA)= A*EXP(Z(X,B,C))
     1                          +(1.-A)*((ALPHA/(X+ALPHA))**GAMMA)
      A     = .16951489
      ALPHA = .24643677
      GAMMA = 1.0498142
      DO 1 I = 1,2
    1 P(I) = ABS( P(I) )
      YCAL = F(X(L),A,P(1),P(2),ALPHA,GAMMA)
      RETURN
      END
C     DERIVATIVES OF MODEL
      SUBROUTINEDERIV(P,X,L,D)
      DIMENSIONP(1),D(1),X(1)
      Z(X,B,C)=(-B*(SQRT(ABS(X+C))-SQRT(ABS(C))))
      FB(X,A,B,C)=-A*( SQRT(ABS(X+C))- SQRT(ABS(C)))*EXP(Z(X,B,C))
      FC(X,A,B,C)=-((A*B)/2.)*((1./SQRT(ABS(X+C)))-
     1             (1./SQRT(ABS(C))))
     2                          * EXP(Z(X,B,C))
      A     = .16951489
      DO 1 I = 1,2
    1 P(I) = ABS( P(I) )
      D(1) = FB(X(L),A,P(1),P(2))
      D(2) = FC(X(L),A,P(1),P(2) )
      RETURN
      END
C   EVALUATION OF FUNCTION AS TWO TERMS
      SUBROUTINE TERM(NV,P,X,N,ND)
      DIMENSION X(100),P(9)
      Z(X,B,C) = (-B*(SQRT(ABS(X+C))-SQRT(ABS(C))))
```

```
      F1(X,A,B,C) = A*EXP(Z(X,B,C))
      F2(X,A,ALPHA,GAMMA) = (1.-A)*((ALPHA/(X+ALPHA))**GAMMA)
      A      = .16951489
      ALPHA = .24643677
      GAMMA = 1.0498142
      WRITE(3,150) A,P(1),P(2),ALPHA,GAMMA
      WRITE(3,175)
      KY = 0
      DO 1 I = 1,N
      KY = KY+NV
      K = KY-ND
      FT1 = F1(X(K),A,P(1),P(2) )
      FT2 = F2(X(K),A,ALPHA,GAMMA)
      FTTOT = FT1+FT2
    1 WRITE(3,200) X(K),FT1,FT2,FTTOT
  150 FORMAT(//,1X,'USING A=',F12.8,'B=',F12.8,'C=',F12.8,
     1  ' ALPHA = ',F12.8,' GAMMA = ',F12.8,' WE OBTAIN:')
  175 FORMAT(//,25X,'1ST TERM',9X,'2ND TERM',12X,'TOTAL',///)
  200 FORMAT(/,4X,'F(',F12.8,')',1X,'=',3X,F12.8,4X,'+',3X,
     1  F12.8,4X,' = ',2X,F12.8 )
      RETURN
      END
```

Program #6

```
C      SPECTRUM EVALUATION,INTERPOLATION, AND PLOT.
       DIMENSION AX(200),Y(200),AY(200)
       DOUBLE PRECISION X(200),AMUFCN,DMUFCN,AMUDFN,PI,
      U   AL,MUNOT,XX,A,B,C,ALPHA,GAMMA,A1,A2,A3,A4,A5,A6,B1,
      1  B2,B3,B4,B5,B6,AMU,DMU,AMUD,T,CAPF,BOT,FLAMBA,GX,
      2  EXPON1,EXPON2,CONVRT,TERM1,TERM2,GAMFCN
C   LET LAMBDA--HERE,X,--VARY FROM 0.24793 TO 1.5000 ANGSTROMS.
C   MUNOT HAS THE UNITS OF CM**2/GM.
C   AMUFCN IS THE FUNCTIONAL FORM OF TOTAL ATTENUATION COEFF.
C   DMUFCN IS THE FUNCTIONAL FORM OF THE DERIVATIVE OF AMUFCN.
C   AMUDFN IS THE FUNCTIONAL FORM OF THE DOSIMETER ABSORPTION
C    COEFFICIENT.
C   CAPF REPRESENTS THE OBSERVED SPECTRUM.
C   CAPF REPRESENTS THE OBSERVED SPECTRUM.
C   FLAMBA REPRESENTS THE CORRECTED  OR  TRUE  X-RAY SPECTRUM.
       AMUFCN(X,A1,A2,A3,A4,A5,A6) =
      1         (((((A6*X+A5)*X+A4)*X+A3)*X+A2)*X)+A1
       DMUFCN(X,A2,A3,A4,A5,A6)  =
      1         ((((5.*A6*X+(4.*A5))*X+(3.*A4))*X+(2.*A3))*X)+A2
       AMUDFN(X,B1,B2,B3,B4,B5,B6) =
      1         (((((B6*X+B5)*X+B4)*X+B3)*X+B2)*X)+B1
   19  READ(1,99) NP
       READ(1,100) PI,AL,MUNOT,XX,X(1)
       READ(1,100) A1,A2,A3,A4,A5,A6
       READ(1,100) B1,B2,B3,B4,B5,B6
       READ(1,100) A,B,C,ALPHA,GAMMA
       CALL FGAMMA(XX,GX,IER)
       WRITE(3,695) XX,GX,IER
  695  FORMAT(/,10X,'THE GAMMA FCN OF ',F12.8,2X,'IS ',F12.8,
      1  2X,' ERROR CODE IS ',I3,//)
       WRITE(3,200)
       WRITE(3,201)
       GAMFCN = GX
       DO 9 I=1,NP
       AMU = AMUFCN(X(I),A1,A2,A3,A4,A5,A6)
       DMU = DMUFCN(X(I),A2,A3,A4,A5,A6)
       AMUD= AMUDFN(X(I),B1,B2,B3,B4,B5,B6)
       T = AMU  - MUNOT
       EXPON1 = B*DSQRT(C)-C*T-((B*B)/(4.*T))
       EXPON2 = -ALPHA*T
       TERM1 = ((A*B)*DEXP(EXPON1)/(2.*DSQRT(PI)*T**1.5))
       TERM2 =   ((1.-A)*(ALPHA**GAMMA)*T**(GAMMA-1.)
      2         *DEXP(EXPON2))/GAMFCN
       CAPF = (TERM1 + TERM2)*DMU
       Y(I) =CAPF
       CONVRT = 2.85496D-03
       BOT = AMUD*AL*CONVRT*7817.4805D+00
       FLAMBA = CAPF/BOT
       AY(I) =FLAMBA
       AX(I) = X(I)
       WRITE(3,300) I,X(I),AMU,TERM1,TERM2,CAPF,AMUD,FLAMBA
    9  X(I+1) = X(I) +0.010
C    SEARCH FOR MAXIMUM VALUES
       XMAX = -1.E+30
```

```
      AYMAX = XMAX
      DO 1 I=1,NP
      IF( AX(I).LE.XMAX ) GO TO 1
      XMAX = AX(I)
    1 CONTINUE
      DO 3 I= 1,NP
      IF(AY(I).LE.AYMAX) GO TO 3
      AYMAX = AY(I)
    3 CONTINUE
      XMIN = 0.0
      AYMIN= 0.0
C    PLOT ROUTINE
      CALL PENPOS('LUSK,GERALD R.',14,1)
      CALL NEWPLT(0.0,1.0,10.0)
      CALL ORIGIN( 0.0, 0.0)
      CALL XSCALE(XMIN,XMAX, 5.0)
      CALL YSCALE(AYMIN,AYMAX, 8.0)
      DX = 0.1
      DY = 0.1
      CALL XAXIS(DX)
      CALL YAXIS(DY)
      CALL XYPLT(AX,AY,NP,1,4)
      CALL XYPLT(AX,Y,NP,2,11)
      CALL ENDPLT
      CALL LSTPLT
  909 RETURN
   99 FORMAT(I5)
  100 FORMAT(6F12.8)
  200 FORMAT(///,4X,'I',5X,'LAMBDA',2X,'MU-TOTAL',4X,'(TERM1',
     1  5X,'+',5X,'TERM2)*DMU =  CAPF',8X,'MU-DOSIM',4X,
     2  'REBUILT')
  201 FORMAT(7X,'ANGSTROMS  CM**2/GM',30X,'OBS.SPECTM',
     1  4X,'CM**2/GM',4X,'SPECTRUM',////)
  300 FORMAT(//,2X,I4,2X,F8.4,2X,F9.4,2X,F12.7,2X,F12.7,2X,
     1  F10.4,3X,F9.4,3X,F12.4)
      END
C    GAMMA FUNCTION
C
C    ------------------------------------------------------------
C
C    THIS SUBROUTINE COMPUTES THE GAMMA FUNCTION FOR A GIVEN
C    ARGUMENT.
C
C    INSTRUCTIONS
C         CALL FGAMMA(XX,GX,IER)
C
C    DESCRIPTION OF PARAMETERS
C         XX = THE ARGUMENT FOR THE GAMMA FCN
C         GX = THE RESULTANT GAMMA FUNCTION VALUE
C         IER= THE RESULTANT ERROR CODE WHERE
C              IER = 0 : NO ERROR
C              IER = 1 : XX IS WITHIN 0.000001 OF BEING A NEG-
C                        ATIVE INTEGER.
C
```

```
      SUBROUTINE FGAMMA(XX,GX,IER)
      DOUBLE PRECISION X,XX,GX,ERR,Y,GY
      X = XX
      ERR = 1.0E-06
      IER = 0
      GX = 1.0
      IF(X-2.0) 50,50,15
   10 IF(X-2.0) 110,110,15
   15 X = X-1.0
      GX = GX*X
      GO TO 10
   50 IF(X-1.0) 60, 120,110
C
C  SEE IF X IS NEAR NEGATIVE INTEGER OR ZERO
C
   60 IF(X-ERR) 62,62,80
   62 Y = DFLOAT(IDINT(X))-X
      IF( DABS(Y)-ERR ) 130,130,64
   64 IF(1.0-Y-ERR)  130, 130,70
C
C  X NOT NEAR A NEGATIVE INTEGER OR ZERO
C
   70 IF(X-1.0)80,80,110
   80 GX = GX/X
      X = X+1.0
      GO TO 70
  110 Y = X - 1.0
      GY=1.0+Y*(-0.5771017+Y*(+0.9858540+Y*(-0.8764218+Y*
     1  (+0.8328212+Y*(-0.5684729+Y*(+0.2548205+Y*(-0.05149930)
     2  ))))))
      GX = GX*GY
  120 RETURN
  130 IER = 1
      RETURN
      END
```

Program #7

```
C     GENERATE FUNCTION REPRESENTING X-RAY SPECTRA AT X-RAY
C     TARGET; THIS SPECTRUM IS IN ABSOLUTE UNITS OF ENERGY PER
C     SECOND PER MILLIAMPERE PER STERADIAN PER WAVELENGTH.
C     ALSO, GENERATE BREMSTRALUNG,PREDICTED BY KRAMER'S THEORY.
C     LET LAMBDA--HERE,X,--VARY FROM 0.248 TO 1.540 ANGSTROMS.
C     THEN USE THE CURVE-FITTED MU DATA POLYNOMIALS.
C     FROM LAMBDA > 1.54 ANGSTROMS, LET THE MU-POLYNOMIALS BE A
C     LAMBDA-CUBED FUNCTION--A CONTINUOUS EXTENSION OF THE
C     CURVE-FITTED POLYNOMIALS. THEN LAMBDA WILL VARY TO ABT 5
C     ANGSTROMS.
C     BETOT = POLYNOMIAL REPRESENTING ATTENUATION COEFF FOR
C       BE-TOTAL.
C     BEABS = POLYNOMIAL REPRESENTING ABSORPTION COEFF FOR BE.
C     AIR = POLYNOMIAL FOR ATTENUATION BY AIR.
C     ALUM = POLYNOMIAL REPRESENTING ATTENUATION BY ALUMINUM.
C     DMUFCN IS THE FUNCTIONAL FORM OF THE DERIVATIVE OF ALUM.
C     AMUDFN IS THE FUNCTIONAL FORM OF THE DOSIMETER ABSORPTION.
C     THESE COEFFICIENTS HAVE UNITS OF CM**2/GM.
C
C     CAPF REPRESENTS THE OBSERVED SPECTRUM.
C     FLAMBA REPRESENTS THE CORRECTED  OR  TRUE  X-RAY SPECTRUM.
C     FOKRAM REPRESENTS ABSOLUTE KRAMER'S SPECTRUM AT X-RAY
C     TUBE TARGET.
C
      DIMENSION AX(200),Y(200),YA(200),YB(200),Z(200)
      DOUBLE PRECISION X(600),A1,A2,A3,A4,A5,A6,B1,B2,B3,B4,
     1  B5,B6,P1,P2,P3,P4,P5,P6,R1,R2,R3,R4,R5,R6,S1,S2,S3,
     2  S4,S5,AA,BB,CC,DD,EE,FF,ALUM,BETOT,BEABS,AIR,DER,DOS,
     3  UBET,UBEA,UAIR,UALUM,UDOS,T,CAPF,BOT,EXPON1,EXPON2,
     4  CONVRT,TERM1,TERM2,MUNOT,GAMFCN,A,B,C,ALPHA,GAMMA,PI,
     5  SEP,DMUFCN,AMUDFN,ALU,AT,BE1,BE2,SEPC,FLAMBA,FA
      DOUBLE PRECISION CAPF1,CAPF2,FLAMB1,FLAMB2,FA1,FA2,Y1,Y2,
     1    CNORM,REF,FOKRAM,DEX,FAE,DEXX
C
      DMUFCN(X,A2,A3,A4,A5,A6)  =
     1         ((((5.*A6*X+(4.*A5))*X+(3.*A4))*X+(2.*A3))*X)+A2
      AMUDFN(X,B1,B2,B3,B4,B5,B6) =
     1         (((((B6*X+B5)*X+B4)*X+B3)*X+B2)*X)+B1
      BETOT(X,P1,P2,P3,P4,P5,P6) =
     1         (((((P6*X+P5)*X+P4)*X+P3)*X+P2)*X)+P1
      BEABS(X,R1,R2,R3,R4,R5,R6) =
     1         (((((R6*X+R5)*X+R4)*X+R3)*X+R2)*X)+R1
      ALUM(X,A1,A2,A3,A4,A5,A6) =
     1         (((((A6*X+A5)*X+A4)*X+A3)*X+A2)*X)+A1
      AIR(X,S1,S2,S3,S4 ,S5) =
     1       ((((S5*X+S4)*X+S3)*X+S2)*X)+S1
C
C     NP = NUMBER OF INCREMENTS TO LAMBDA,(X).
C     SEP = PLATE SEPARATION OF VARIABLE PLATE SEPARATION ION
C     CHAMBER AT WHICH ABSORPTION DATA WAS COLLECTED.
C     GAMFCN = THE GAMMA FUNTION-VALUE OF THE CONSTANT, GAMMA.
C     MUNOT = THE VALUE OF MU-ALUM( TOTAL ) AT 50 KV.
C     CONVRT = VALUE OF A UNIT CONVERSION CONSTANT.
C
```

```
  111 READ(1,99) NP,X(1)
      READ(1,101)PI,SEP,GAMFCN,MUNOT,CONVRT
      READ(1,100) A,B,C,ALPHA,GAMMA
      READ(1,100) A1,A2,A3,A4,A5,A6
      READ(1,100) B1,B2,B3,B4,B5,B6
      READ(1,100) P1,P2,P3,P4,P5,P6
      READ(1,100) R1,R2,R3,R4,R5,R6
      READ(1,100) S1,S2,S3,S4,S5
      READ(1,100) REF,CNORM
C
   39 WRITE(3,200)
      WRITE(3,201)
C
      BB = 4.0334D+00
      CC =  .141D+00
      DD =  .150D+00
      EE =  .0300D+00
      FF =  .13146D+00
      DO 9 I = 1,NP
C
C   CHECK ON THE VALUE OF LAMBDA; DETERMINE FUNCTIONAL FORM
C   OF POLYNOMIAL.
      IF( X(I).GE. 1.538 ) GO TO 1
C
C   POLYNOMIALS FROM CURVE FITTING.
      BE1 = BETOT( X(I),P1,P2,P3,P4,P5,P6 )
      BE2 = BEABS( X(I),R1,R2,R3,R4,R5,R6 )
      AT = AIR( X(I),S1,S2,S3,S4,S5 )
      ALU = ALUM( X(I),A1,A2,A3,A4,A5,A6 )
      DER = DMUFCN( X(I),A2,A3,A4,A5,A6 )
   40 DOS = AMUDFN( X(I),B1,B2,B3,B4,B5,B6 )
      GO TO 3
C
    1 UBET = 0.2943D+00*X(I)*X(I)*X(I)
   41 UBEA = 0.2020D+00*X(I)*X(I)*X(I)
   42 UAIR = 2.5230D+00*X(I)*X(I)*X(I)
   43 UALUM=12.6400D+00*X(I)*X(I)*X(I)
   44 UDOS = 0.9502D+00*X(I)*X(I)*X(I)
   45 DER = 37.92D+00*X(I)*X(I)
      ALU = UALUM
      DOS = UDOS
      BE1 = UBET
      BE2 = UBEA
      AT  = UAIR
C
C   GENERATE SPECTRUM
    3 T = ALU  - MUNOT
   51 EXPON1 = B*DSQRT(C)-C*T-((B*B)/(4.*T))
   52 EXPON2 = -ALPHA*T
   53 TERM1 = ((A*B)*DEXP(EXPON1)/(2.*DSQRT(PI)*T**1.5))
   54 TERM2 =  ((1.-A)*(ALPHA**GAMMA)*T**(GAMMA-1.)
     1         *DEXP(EXPON2))/GAMFCN
      CAPF = (TERM1 + TERM2)*DER
   55 CAPF1 = TERM1*DER
```

```
   56 CAPF2 = TERM2*DER
      SEPC=SEP*CONVRT
   57 BOT = SEPC*DOS*7817.4805D+00
      FLAMBA = CAPF/BOT
      DEXX = DEXP(-CC*BE1-DD*BE2-EE*AT-FF*ALU)
      DEX = DEXP(CC*BE1+DD*BE2+EE*AT+FF*ALU)
      FA = FLAMBA*4.305D+00
      FAE = FA*DEX
   58 FLAMB1 = CAPF1/BOT
   59 FLAMB2 = CAPF2/BOT
   60 FA1 = FLAMB1*4.305D+00
   61 FA2 = FLAMB2*4.305D+00
   62 Y1 = FA1*DEXP(+CC*BE1+DD*BE2+EE*AT+FF*ALU)
   63 Y2 = FA2*DEXP(+CC*BE1+DD*BE2+EE*AT+FF*ALU)
   64 Y(I) = Y1+Y2
   65 YA(I) = Y1
   66 YB(I) = Y2
   67 FOKRAM = REF*CNORM*(1./(X(I)*X(I)))*(BB-(1./X(I)))
   68 Z(I) = FOKRAM
   69 AX(I) = X(I)
      WRITE(3,300) I,X(I),YA(I),YB(I),Y(I),Z(I)
    9 X(I+1) = X(I) + 0.010
C
C    SEARCH FOR MAXIMUM VALUES.
      XMAX = -1.E+30
      YMAX = XMAX
      DO 2 I = 1,NP
      IF( AX(I).LE.XMAX ) GO TO 2
      XMAX = AX(I)
    2 CONTINUE
      DO 4 I = 1,NP
      IF( Y(I).LE.YMAX ) GO TO 4
      YMAX = Y(I)
    4 CONTINUE
C
C    PLOT ROUTINE
      XMIN = 0.0
      YMIN = 0.0
      CALL PENPOS('LUSK,GERALD R.',14,1)
      CALL NEWPLT(0.0,1.0,10.0)
      CALL ORIGIN(0.0,0.0)
      CALL XSCALE( XMIN,XMAX,5.0 )
      CALL YSCALE( YMIN,YMAX,8.0 )
      DX = 0.1
      DY = 1.0
      CALL XAXIS(DX)
      CALL YAXIS(DY)
      CALL XYPLT(AX,YA,NP,1,0)
      CALL XYPLT( AX,Y,NP,1,4 )
      CALL XYPLT(AX,YB,NP,1,6)
      CALL SYM(2.0,9.0,0.14,'EXPERIMENTAL SPECTRUM OF',
     1 0.0,24)
      CALL SYM(2.0,8.65,0.14,'X-RAY INTENSITY, REBUILT AND',
     1 0.0,28)
```

```
      CALL SYM(2.0,8.20,0.14,'RECOVERED TO X-RAY TARGET',
     1  0.0,25)
      CALL ENDPLT
      CALL LSTPLT
      RETURN
   99 FORMAT( I5,E20.5 )
  100 FORMAT( 6E12.8 )
  101 FORMAT( 4E12.8,D12.8 )
  200 FORMAT('1',9X,'I',14X,'LAMBDA',5X,'( TERM1',8X,'+  TERM2)'
     1   ,6X,'=',5X,'RECOVERED SPECTRUM',8X,'KRAMER''S SPECTRUM')
  201 FORMAT(20X,'ANGSTROMS',40X,'*E+10*MEV/SEC/MA/STERAD''N',
     1   5X,'*E+10*MEV/SEC/MA/STERAD''N'///)
  300 FORMAT(/,8X,I4,6X,F12.4,5X,F12.4,3X,F12.4,6X,F12.4,
     1 11X,F15.4)
      END
```

Program #8

```
C    EVALUATION OF THE INTEGRAL OF THE EXPERIMENTALLY
C    DETERMINED CHARACTERISTIC RADIATION SPECTRA AND THE
C    BREMSTRALUNG STECTRA.
C
C    AO    = LOWER BOUND OF INTEGRATION; THE LAMBDA-NOT;
C    HERE LAMBDA-NOT = 50KV---0.2480
C    BO    = UPPER BOUND OF INTEGRATION = 1.538 ANGSTROMS.
C    CO = THE SECOND UPPER BOUND;
C
C - - - - - - - - - - - - - - - - - - - - - - - - - - - - -
C
      EXTERNAL G,H,BR1,BR2
      REAL MUNOT
      COMMON A1,A2,A3,A4,A5,A6,P1,P2,P3,P4,P5,P6,R1,R2,R3,
     1  R4,R5,R6,S1,S2,S3,S4,S5,B1,B2,B3,B4,B5,B6,AA,BB,CC,
     2   DD,EE,FF,A,B,C,ALPHA,GAMMA,SEP,PI,CONVRT,MUNOT,GAMFCN
  100 FORMAT( 6E12.8 )
   19 READ(1,100) AO,BO,CO
      READ(1,100) A,B,C,ALPHA,GAMMA
      READ(1,100) A1,A2,A3,A4,A5,A6
      READ(1,100) B1,B2,B3,B4,B5,B6
      READ(1,100) P1,P2,P3,P4,P5,P6
      READ(1,100) R1,R2,R3,R4,R5,R6
      READ(1,100) S1,S2,S3,S4,S5
      READ(1,100)PI,SEP,GAMFCN,MUNOT,CONVRT
      READ(1,100) AA,BB,CC,DD,EE,FF
C
C  - - - - - - - - - - - - - - - - - - - - - - - - - - - -
C
   51 CALL SIMPSN( BR1  ,AO,BO,1.E-04,14,SIL,S,N,IER )
   52 WRITE(3,900) S,N,IER
   53 BREM1 = S
   54 CALL SIMPSN( BR2 ,BO,CO,1.E-04,14,SIL,S,N,IER )
   55 WRITE(3,900) S,N,IER
   56 BREM2 = S
   57 BREM = BREM1+BREM2
   58 WRITE(3,975) BREM
   59 CALL SIMPSN( G    ,AO,BO,1.E-04,14,SIL,S,N,IER )
   60 WRITE(3,900) S,N,IER
   61 CHAR1 = S
   62 CALL SIMPSN( H    ,BO,CO,1.E-04,14,SIL,S,N,IER )
   63 WRITE(3,900) S,N,IER
   64 CHAR2 = S
   65 CHAR = CHAR1 + CHAR2
   66 WRITE(3,950) CHAR
  975 FORMAT(//,10X,'TOTAL AREA UNDER BREMSTRALUNG CURVE =',
     1   F16.4//)
  950 FORMAT(//,10X,'TOTAL AREA UNDER CHARACTERISTIC CURVE =',
     1   F16.4//)
  900 FORMAT(//,10X,'INTEGRAL OF EXP ABS SPECTRUM = ',
     1  F16.6,/,15X,'AFTER USING',I6,' SUBINTERVALS TO',
     2   ' INTEGRATE   ERROR CODE = ',I3,///)
  190 RETURN
      DEBUG TRACE
```

```
      AT 19
      TRACE ON
      AT 190
      TRACE OFF
      END
C
C   - - - - - - - - - - - - - - - - - - - - - - - - - - - - - -
C
C    SUBROUTINE  SIMPSN
C
C    PURPOSE:
C      INTEGRATES THE GIVEN FUNCTION OVER THE PRESCRIBED RANGE
C
C    INSTRUCTIONS:
C    CALL SIMPSN( ?(X),A ,B ,DEL,IMAX,SIL,S,N,IER )
C
C    DESCRIPTION OF PARAMETERS:
C    F = NAME OF USER FUNCTION SUBPROGRAM WHICH CONTAINS THE
C    FUNCTION TO BE INTEGRATED.
C    AO= LOWER INTEGRATION LIMIT
C    BO= UPPER INTEGRATION LIMIT
C    DEL = REQUIRED ACCURACY OR TOLERANCE
C    IMAX= MAXIMUM NUMBER OF RECOMPUTATIONS OF THE INTEGRAL VALUE
C    SIL = RESULTANT VALUE OF INTEGRAL JUST PRIOR TO FINAL VALUE
C    S = RESULTANT FINAL VALUE OF INTEGRAL
C    N = RESULTANT NUMBER OF INTERVALS USED IN COMPUTING S
C    IER = RESULTANT ERROR CODE WHERE:
C          IER = 0  NO ERROR
C          IER = 1  A = B
C          IER = 2  DEL = ZERO
C          IER = 3  IMAX LESS THAN 2
C          IER = 4  REQUIRED ACCURACY NOT MET IN IMAX STEPS.
C
C    SUBROUTINES AND FUNCTION SUBPROGRAMS REQUIRED
C    F = FUNCTION SUBPROGRAM WHICH COMPUTES F(X) FOR X BETWEEN
C    A AND B.
C
C    METHOD:
C    SIMPSON'S RULE IS PERFORMED WITH INTERVAL HALVING UNTIL
C    DIFFERENCE BETWEEN SUCCESSIVE VALUES OF THE INTEGRAL IS
C    LESS THAN DEL. FAILURE TO REACH THE TOLERANCE AFTER IMAX
C    TRIES TERMINATES THE SUBROUTINE,
C    EXECUTION.
C
C    - - - - - - - - - - - - - - - - - - - - - - - - - - - - -
C
      SUBROUTINE SIMPSN( F    ,A,B,DEL,IMAX,SIL,S,N,IER )
C
C    ----- - - - - - - - - - - - - - - - - - - - - - - - - - -
C
C    IF A DOUBLE PRECISION VERSION OF THIS ROUTINE IS DESIRED,
C    THE C IN COLUMN 1 SHOULD BE REMOVED FROM THE DOUBLE
C    PRECISION STATEMENT WHICH FOLLOWS:
C
```

```
C     DOUBLE PRECISION A,B,DEL,SIL,S,BA,X,SUMK,FRSTX,XK,FINC,F
C
C   THE C MUST ALSO BE REMOVED FROM DOUBLE PRECISION STATE-
C   MENTS APPEARING IN OTHER ROUTINES USED IN CONJUNCTION
C   WITH THIS ROUTINE.
C
C   THE DOUBLE PRECISION VERSION OF THIS SUBROUTINE MUST ALSO
C   CONTAIN DOUBLE PRECISION FORTRAN FUNCTIONS. THE ABS IN
C   STATEMENT 27 MUST BE CHANGED TO DABS.
C
C   - - - - - - - - - - - - - - - - - - - - - - - - - - - - -
C
C
   41 SIL = 0.0
   42 S = 0.0
   43 N = 0
   44 BA =B-A
   45 IF(BA)20,19,20
   19 IER = 1
   46 RETURN
   20 IF(DEL)22,22,23
   22 IER = 2
   47 RETURN
   23 IF(IMAX-1) 24,24,25
   24 IER= 3
   48 RETURN
C
C   COMPUTE SIGMA(1)
   25 X =BA/2. + A
   49 NHALF = 1
   50 SUMK = F(X)*BA*2./3.
   70 S = SUMK+ (F(A)+F(B))*BA/6.
C
C   DIVIDE (A,B) INTO 2,4,6,.....,2**I INTERVALS,
C   COMPUTE SIGMA(2),SIGMA(4),....., SIGMA(I)
C
   71 DO 28 I = 2,IMAX
   72 SIL = S
   73 S = (S-SUMK/2.)/2.
   74 NHALF = NHALF*2
   75 ANHLF = NHALF
   76 FRSTX = A+(BA/ANHLF)/2.
   77 SUMK = F(FRSTX)
   78 XK = FRSTX
   79 KLAST = NHALF-1
   80 FINC = BA/ANHLF
   81 DO 26  K=1,KLAST
   82 XK =XK+FINC
   26 SUMK = SUMK +F(XK)
   83 SUMK = SUMK*2.*BA/(3.*ANHLF)
   84 S = S + SUMK
C
C   COMPARE THE I-TH AND (I-1)ST RESULTS.
C
```

```
   27 IF( ABS(S-SIL) - ABS(DEL*S) ) 29,28,28
   28 CONTINUE
      IER = 4
      GO TO 30
   29 IER = 0
   30 N = 2*NHALF
      RETURN
      DEBUG TRACE
      AT 41
      TRACE ON
      AT 42
      TRACE OFF
      END
C
C    THIS SUBPROGRAM DEFINES THE CHARACTERISTIC X-RAY SPECTRUM
C    FROM LAMBDA = 0.248 TO 1.548 ANGSTROMS; IT UTILIZES
C    POLYNOMIALS DERIVED FROM CURVE FITTING ANALYSIS.
C
C    BETOT = POLYNOMIAL REPRESENTING ATTENUATION COEFF FOR
C      BE-TOTAL.
C    BEABS = POLYNOMIAL REPRESENTING ABSORPTION COEFF FOR BE.
C    AIR = POLYNOMIAL FOR ATTENUATION BY AIR.
C    ALUM = POLYNOMIAL REPRESENTING ATTENUATION BY ALUMINUM.
C    DMUFCN IS THE FUNCTIONAL FORM OF THE DERIVATIVE OF ALUM.
C    AMUDFN IS THE FUNCTIONAL FORM OF THE DOSIMETER ABSORPTION.
C    THESE COEFFICIENTS HAVE UNITS OF CM**2/GM.
C    CAPF REPRESENTS THE OBSERVED SPECTRUM.
C    FLAMBA REPRESENTS THE CORRECTED  OR  TRUE  X-RAY SPECTRUM.
C    SEP = PLATE SEPARATION OF VARIABLE PLATE SEPARATION ION
C    CHAMBER AT WHICH ABSORPTION DATA WAS COLLECTED.
C    GAMFCN = THE GAMMA FUNTION-VALUE OF THE CONSTANT, GAMMA.
C    MUNOT = THE VALUE OF MU-ALUM( TOTAL ) AT 50 KV.
C    CONVRT = VALUE OF A UNIT CONVERSION CONSTANT.
C
      FUNCTION G(X)
      REAL MUNOT
      COMMON A1,A2,A3,A4,A5,A6,P1,P2,P3,P4,P5,P6,R1,R2,R3,
     1  R4,R5,R6,S1,S2,S3,S4,S5,B1,B2,B3,B4,B5,B6,AA,BB,CC,
     2   DD,EE,FF,A,B,C,ALPHA,GAMMA,SEP,PI,CONVRT,MUNOT,GAMFCN
      DMUFCN(X,A2,A3,A4,A5,A6)  =
     1         ((((5.*A6*X+(4.*A5))*X+(3.*A4))*X+(2.*A3))*X)+A2
      AMUDFN(X,B1,B2,B3,B4,B5,B6) =
     1         (((((B6*X+B5)*X+B4)*X+B3)*X+B2)*X)+B1
      BETOT(X,P1,P2,P3,P4,P5,P6) =
     1         (((((P6*X+P5)*X+P4)*X+P3)*X+P2)*X)+P1
      BEABS(X,R1,R2,R3,R4,R5,R6) =
     1         (((((R6*X+R5)*X+R4)*X+R3)*X+R2)*X)+R1
      ALUM(X,A1,A2,A3,A4,A5,A6) =
     1         (((((A6*X+A5)*X+A4)*X+A3)*X+A2)*X)+A1
      AIR(X,S1,S2,S3,S4 ,S5) =
     1      ((((S5*X+S4)*X+S3)*X+S2)*X)+S1
C
      BE1 = BETOT(X,P1,P2,P3,P4,P5,P6)
      BE2 = BEABS(X,R1,R2,R3,R4,R5,R6)
```

```
      AT = AIR(X,S1,S2,S3,S4,S5)
      ALU = ALUM(X,A1,A2,A3,A4,A5,A6)
      DER = DMUFCN(X,A2,A3,A4,A5,A6)
      DOS = AMUDFN(X,B1,B2,B3,B4,B5,B6)
      T = ALU - MUNOT
      EXPON1 = B* SQRT(C)-C*T-((B*B)/(4.*T))
      TERM1 = ((A*B)* EXP(EXPON1)/(2.* SQRT(PI)*T**1.5))
      CAPF1 = TERM1*DER
      SEPC = SEP*CONVRT
      BOT = SEPC*DOS*7817.4805
      FLAMB1 = CAPF1/BOT
      FA1 = FLAMB1*4.305
      Y1 = FA1* EXP(+CC*BE1+DD*BE2+EE*AT+FF*ALU)
      G = Y1
      RETURN
      END
C
C    FUNCTION SUBPROGRAM
C    SAME DEFINING STATEMENTS AS ABOVE HOLD HERE EXCEPT THE
C    RANGE OF LAMBDA IS 1.538 TO 1.728 ANGSTROMS.
C    THIS FUNCTION IS STILL THE CHARACTERISTIC RADIATION,
C    BUT NOW THE POLYNOMIALS ARE APPROXIMATE EXTRAPOLATIONS
C    OF THE CURVE-FITTED FUNCTIONS.
C
      FUNCTION H(X)
      REAL MUNOT
      COMMON A1,A2,A3,A4,A5,A6,P1,P2,P3,P4,P5,P6,R1,R2,R3,
     1  R4,R5,R6,S1,S2,S3,S4,S5,B1,B2,B3,B4,B5,B6,AA,BB,CC,
     2    DD,EE,FF,A,B,C,ALPHA,GAMMA,SEP,PI,CONVRT,MUNOT,GAMFCN
      UBET = 0.2943*X*X*X
      UBEA = 0.2020*X*X*X
      UAIR = 2.5230*X*X*X
      UALUM=12.6400*X*X*X
      DER =37.92*X*X
      UDOS = 0.9502*X*X*X
      ALU = UALUM
      DOS = UDOS
      BE1 = UBET
      BE2 = UBEA
      AT  = UAIR
C
      T = ALU - MUNOT
      EXPON1 = B* SQRT(C)-C*T-((B*B)/(4.*T))
      TERM1 = ((A*B)* EXP(EXPON1)/(2.* SQRT(PI)*T**1.5))
      CAPF1 = TERM1*DER
      SEPC = SEP*CONVRT
      BOT = SEPC*DOS*7817.4805
      FLAMB1 = CAPF1/BOT
      FA1 = FLAMB1*4.305
      Y1 = FA1* EXP(+CC*BE1+DD*BE2+EE*AT+FF*ALU)
      H = Y1
      RETURN
      END
C    FUNCTION SUBPROGRAM
```

```
C    THIS SUBPROGRAM DEFINES THE BREMSTRALUNG SPECTRUM FROM
C    LAMBDA = 0.248 TO 1.538 ANGSTROMS.
      FUNCTION BR1(X)
      REAL MUNOT
      COMMON A1,A2,A3,A4,A5,A6,P1,P2,P3,P4,P5,P6,R1,R2,R3,
     1  R4,R5,R6,S1,S2,S3,S4,S5,B1,B2,B3,B4,B5,B6,AA,BB,CC,
     2   DD,EE,FF,A,B,C,ALPHA,GAMMA,SEP,PI,CONVRT,MUNOT,GAMFCN
      DMUFCN(X,A2,A3,A4,A5,A6)  =
     1         ((((5.*A6*X+(4.*A5))*X+(3.*A4))*X+(2.*A3))*X)+A2
      AMUDFN(X,B1,B2,B3,B4,B5,B6) =
     1         (((((B6*X+B5)*X+B4)*X+B3)*X+B2)*X)+B1
      BETOT(X,P1,P2,P3,P4,P5,P6) =
     1         (((((P6*X+P5)*X+P4)*X+P3)*X+P2)*X)+P1
      BEABS(X,R1,R2,R3,R4,R5,R6) =
     1         (((((R6*X+R5)*X+R4)*X+R3)*X+R2)*X)+R1
      ALUM(X,A1,A2,A3,A4,A5,A6) =
     1         (((((A6*X+A5)*X+A4)*X+A3)*X+A2)*X)+A1
      AIR(X,S1,S2,S3,S4 ,S5) =
     1       ((((S5*X+S4)*X+S3)*X+S2)*X)+S1
      BE1 = BETOT(X,P1,P2,P3,P4,P5,P6)
      BE2 = BEABS(X,R1,R2,R3,R4,R5,R6)
      AT = AIR(X,S1,S2,S3,S4,S5)
      ALU = ALUM(X,A1,A2,A3,A4,A5,A6)
      DER = DMUFCN(X,A2,A3,A4,A5,A6)
      DOS = AMUDFN(X,B1,B2,B3,B4,B5,B6)
      T = ALU  - MUNOT
      EXPON2 = -ALPHA*T
      TERM2 =  ((1.-A)*(ALPHA**GAMMA)*T**(GAMMA-1.)
     1          * EXP(EXPON2))/GAMFCN
      CAPF2 = TERM2*DER
      SEPC = SEP*CONVRT
      BOT = SEPC*DOS*7817.4805
      FLAMB2 = CAPF2/BOT
      FA2 = FLAMB2*4.305
      Y2 = FA2* EXP(+CC*BE1+DD*BE2+EE*AT+FF*ALU)
      BR1 = Y2
      RETURN
      END
C
C    THIS SUBPROGRAM DEFINES THE BREMSTRALUNG RADIATION FROM
C    1.538 TO 1.728 ANGSTROMS AND USES THE EXTRAPOLATED
C    POLYNOMIALS.
C
      FUNCTION BR2(X)
      REAL MUNOT
      COMMON A1,A2,A3,A4,A5,A6,P1,P2,P3,P4,P5,P6,R1,R2,R3,
     1  R4,R5,R6,S1,S2,S3,S4,S5,B1,B2,B3,B4,B5,B6,AA,BB,CC,
     2   DD,EE,FF,A,B,C,ALPHA,GAMMA,SEP,PI,CONVRT,MUNOT,GAMFCN
      UBET = 0.2943*X*X*X
      UBEA = 0.2020*X*X*X
      UAIR = 2.5230*X*X*X
      UALUM=12.6400*X*X*X
      DER =37.92*X*X
      UDOS = 0.9502*X*X*X
```

```
      ALU = UALUM
      DOS = UDOS
      BE1 = UBET
      BE2 = UBEA
      AT  = UAIR
      T = ALU  - MUNOT
      EXPON2 = -ALPHA*T
      TERM2 =  ((1.-A)*(ALPHA**GAMMA)*T**(GAMMA-1.)
     1         * EXP(EXPON2))/GAMFCN
      CAPF2 = TERM2*DER
      SEPC = SEP*CONVRT
      BOT = SEPC*DOS*7817.4805
      FLAMB2 = CAPF2/BOT
      FA2 = FLAMB2*4.305
      Y2 = FA2* EXP(+CC*BE1+DD*BE2+EE*AT+FF*ALU)
      BR2 = Y2
      RETURN
      END
```

Program #9

```
C     SIMPSON INTEGRATION OF SPECTRAL DISTRIBUTION WEIGHTING
C     FUNCTION.
C
C     THIS PROGRAM IS LOOPING 3 TIMES TO COMPARE THE IMPORTANCE
C     OF THE UPPER BOUND OF INTEGRATION.
C     INTEGRATING VIA SIMPSON'S METHOD THE OBSERVED X-RAY SPECTRAL
C     DISTRIBUTION FUNCTION OVER THE  LAMBDA RANGE OF INTEREST.
C     THE INTEGRAL-FOR A PARTICULAR ABSORBER THICKNESS - WHEN
C     EVALUATED PREDICTS THE I(X). TO OBTAIN THE J(X),
C     MULTIPLY THE INTEGRAL BY EXP( MU-NOT*X ).
C
C     SEP  = ABSOLUTE PLATE SEPARATION OF DOSIMETER AT WHICH
C     ABSORPTION DATA WAS COLLECTED. HERE, SEP = 0.360 INCHES.
C     AO   = LOWER BOUND OF INTEGRATION; THE LAMBDA-NOT;
C     HERE LAMBDA-NOT = 50KV---0.2480
C     BO   = UPPER BOUND OF INTEGRATION = 1.540 ANGSTROMS.
C
C - - - - - - - - - - - - - - - - - - - - - - - - - - - - - -
C
      REAL MUNOT
      REAL MUNTMA
      COMMON XO(50),A,B,C,ALPHA,GAMMA,GAMFCN,A1,A2,A3,A4,A5,
     1  A6,B1,B2,B3,B4,B5,B6,SEP,PI,MUNOT,CONVRT,D1,D2,D3,
     2   D4,D5,D6,MUNTMA,JJ
  100 FORMAT( I10, 3E18.8)
  101 FORMAT( 5E12.8)
  102 FORMAT( 6E12.8)
  103 FORMAT( 4E18.8)
      READ(1,101)  A,B,C,ALPHA,GAMMA
      READ(1,102)  B1,B2,B3,B4,B5,B6
      READ(1,102)  A1,A2,A3,A4,A5,A6
      DO 717 JOE = 1,3
      READ(1,103) AO, BO,       GAMFCN
      DO 727 JACK = 1,2
      READ(1,100)  NXO, SEP, PI,CONVRT
      READ(1,102) D1,D2,D3,D4,D5,D6
      READ(1,102) (XO(J) , J=1,NXO )
      AT50KV = .2479288
      MUNTMA = AMUNTM( AT50KV )
      MUNOT = AMUNOT( AT50KV )
C
C  - - - - - - - - - - - - - - - - - - - - - - - - - - - - - -
C
      DO 3  J = 1, NXO
      JJ = J
      CALL SIMPSN( AO,BO,1.E-04,14,SIL,S,N,IER)
      WRITE(3,900)  J, XO(J), S, N,IER
  900 FORMAT(//,10X,I4,' ATTENUATION BY',F10.6,
     1  '  GM/CM**2 YIELDS I(X) = ',F16.6,/,7X,'  AFTER USING'
     2  ,I6,'  SUBINTERVALS TO INTEGRATE',' ERROR CODE = ',
     3   I3,///)
      PROD = S*EXP(MUNTMA*XO(J) )
      WRITE(3,800) PROD
```

```
  800 FORMAT(/,10X,' J(X) = I(X)*EXP( MU-NOT*XTHICK)    = ',
     1  F16.4,//)
    3 CONTINUE
  727 CONTINUE
  717 CONTINUE
      RETURN
      END
C
C  - - - - - - - - - - - - - - - - - - - - - - - - - - - - -
C
C   SUBROUTINE  SIMPSN
C
C   PURPOSE:
C     INTEGRATES THE GIVEN FUNCTION OVER THE PRESCRIBED RANGE
C
C   INSTRUCTIONS:
C   CALL SIMPSN(  A ,B ,DEL,IMAX,SIL,S,N,IER)
C
C   DESCRIPTION OF PARAMETERS:
C   F = NAME OF USER FUNCTION SUBPROGRAM WHICH CONTAINS THE
C   FUNCTION TO BE INTEGRATED.
C   AO= LOWER INTEGRATION LIMIT
C   BO= UPPER INTEGRATION LIMIT
C   DEL = REQUIRED ACCURACY OR TOLERANCE
C   IMAX= MAXIMUM NUMBER OF RECOMPUTATIONS OF THE INTEGRAL VALUE
C   SIL = RESULTANT VALUE OF INTEGRAL JUST PRIOR TO FINAL VALUE
C   S = RESULTANT FINAL VALUE OF INTEGRAL
C   N = RESULTANT NUMBER OF INTERVALS USED IN COMPUTING S
C   IER = RESULTANT ERROR CODE WHERE:
C         IER = 0  NO ERROR
C         IER = 1  A = B
C         IER = 2  DEL = ZERO
C         IER = 3  IMAX LESS THAN 2
C         IER = 4  REQUIRED ACCURACY NOT MET IN IMAX STEPS.
C
C   SUBROUTINES AND FUNCTION SUBPROGRAMS REQUIRED
C   F = FUNCTION SUBPROGRAM WHICH COMPUTES F(X) FOR X BETWEEN
C   A AND B.
C
C   METHOD:
C   SIMPSON'S RULE IS PERFORMED WITH INTERVAL HALVING UNTIL
C   DIFFERENCE BETWEEN SUCCESSIVE VALUES OF THE INTEGRAL IS
C   LESS THAN DEL. FAILURE TO REACH THE TOLERANCE AFTER IMAX
C   TRIES TERMINATES THE SUBROUTINE,
C   EXECUTION.
C
C   - - - - - - - - - - - - - - - - - - - - - - - - - - - -
C
      SUBROUTINE SIMPSN(  A ,B ,DEL,IMAX,SIL,S,N,IER)
C
C   ----- - - - - - - - - - - - - - - - - - - - - - - - - -
C
C   IF A DOUBLE PRECISION VERSION OF THIS ROUTINE IS DESIRED,
```

```
C    THE C IN COLUMN 1 SHOULD BE REMOVED FROM THE DOUBLE
C    PRECISION STATEMENT WHICH FOLLOWS:
C
C      DOUBLE PRECISION A,B,DEL,SIL,S,BA,X,SUMK,FRSTX,XK,FINC,F
C
C    THE C MUST ALSO BE REMOVED FROM DOUBLE PRECISION STATE-
C    MENTS APPEARING IN OTHER ROUTINES USED IN CONJUNCTION
C    WITH THIS ROUTINE.
C
C    THE DOUBLE PRECISION VERSION OF THIS SUBROUTINE MUST ALSO
C    CONTAIN DOUBLE PRECISION FORTRAN FUNCTIONS. THE ABS IN
C    STATEMENT 27 MUST BE CHANGED TO DABS.
C
C    USER FUNCTION SUBPROGRAM,F,MUST BE IN DOUBLE PRECISION.
C
C    - - - - - - - - - - - - - - - - - - - - - - - - - - - -
C
      SIL = 0.0
      S = 0.0
      N = 0
      BA =B-A
      IF(BA)20,19,20
   19 IER = 1
      RETURN
   20 IF(DEL)22,22,23
   22 IER = 2
      RETURN
   23 IF(IMAX-1) 24,24,25
   24 IER= 3
      RETURN
C
C    COMPUTE SIGMA(1)
C
   25 X =BA/2. + A
      NHALF = 1
      SUMK = F(X)*BA*2./3.
      S = SUMK+ (F(A)+F(B))*BA/6.
C
C    DIVIDE (A,B) INTO 2,4,6,.....,2**I INTERVALS,
C    COMPUTE SIGMA(2),SIGMA(4),....., SIGMA(I)
C
      DO 28 I = 2,IMAX
      SIL = S
      S = (S-SUMK/2.)/2.
      NHALF = NHALF*2
      ANHLF = NHALF
      FRSTX = A+(BA/ANHLF)/2.
      SUMK = F(FRSTX)
      XK = FRSTX
      KLAST = NHALF-1
      FINC = BA/ANHLF
      DO 26 K=1,KLAST
      XK =XK+FINC
```

```
   26 SUMK = SUMK +F(XK)
      SUMK = SUMK*2.*BA/(3.*ANHLF)
      S = S + SUMK
C
C   COMPARE THE I-TH AND (I-1)ST RESULTS.
C
   27 IF( ABS(S-SIL) - ABS(DEL*S) ) 29,28,28
   28 CONTINUE
      IER = 4
      GO TO 30
   29 IER = 0
   30 N = 2*NHALF
      RETURN
      END
C
C   FUNCTION SUBPROGRAM
C   EVALUATING OUR OBSERVED F; THE CAPF(LAMBDA)
C   ALITLF = FUNCTION REPRESENTING TRUE OR REBUILT SPECTRUM.
C   TOT = MU-TOTAL
C   DOS = MU-DOSIMETER(PHOTOELECTRIC)
C   DER = DERIVATIVE OF MU-TOTAL
C   AMATL = MUTOTAL FOR THE ABSORBING MATERIAL.
      FUNCTION  F(X)
      REAL MUNOT
      REAL MUNTMA
      COMMON XO(50),A,B,C,ALPHA,GAMMA,GAMFCN,A1,A2,A3,A4,A5,
     1  A6,B1,B2,B3,B4,B5,B6,SEP,PI,MUNOT,CONVRT,D1,D2,D3,
     2    D4,D5,D6,MUNTMA,JJ
      AMATL = (((((D6*X+D5)*X+D4)*X+D3)*X+D2)*X)+D1
      TOT = (((((A6*X+A5)*X+A4)*X+A3)*X+A2)*X)+A1
      DER =  ((((5.*A6*X+4.*A5)*X+3.*A4)*X+2.*A3)*X)+A2
      DOS = (((((B6*X+B5)*X+B4)*X+B3)*X+B2)*X)+B1
      T = TOT-MUNOT
      SEPC = SEP*CONVRT
      EXPON1 = B* SQRT(C)-C*T-((B*B)/(4.*T))
      EXPON2 = -ALPHA*T
      TERM1 = ((A*B)* EXP(EXPON1)/(2.* SQRT(PI)*T**1.5))
      TERM2 =  ((1.-A)*(ALPHA**GAMMA)*T**(GAMMA-1.)
     2         * EXP(EXPON2))/GAMFCN
      CAPF = (TERM1 + TERM2)*DER
      BOT = SEPC*DOS
      ALITLF = CAPF/BOT
      EXPON3 = -AMATL*XO(JJ)
      F = CAPF*EXP( EXPON3 )
      RETURN
      END
C
C   EVALUATE MU-NOT OF THE ALUMINUM FOR F VIA POLYNOMIAL.
      FUNCTION AMUNOT(X)
      REAL MUNOT
      REAL MUNTMA
      COMMON XO(50),A,B,C,ALPHA,GAMMA,GAMFCN,A1,A2,A3,A4,A5,
     1  A6,B1,B2,B3,B4,B5,B6,SEP,PI,MUNOT,CONVRT,D1,D2,D3,
```

```
     2    D4,D5,D6,MUNTMA,JJ
      AMUNOT = (((((A6*X+A5)*X+A4)*X+A3)*X+A2)*X)+A1
      WRITE(3,100) X,AMUNOT
  100 FORMAT(//,10X,' AT LAMBDA = ',F12.7,'   MU-NOT = ',
     1  F16.7,///)
      RETURN
      END
C
C   EVALUATE THE MU-NOT OF THE ABSORBER MATERIAL.
      FUNCTION AMUNTM(X)
      REAL MUNOT
      REAL MUNTMA
      COMMON XO(50),A,B,C,ALPHA,GAMMA,GAMFCN,A1,A2,A3,A4,A5,
     1  A6,B1,B2,B3,B4,B5,B6,SEP,PI,MUNOT,CONVRT,D1,D2,D3,
     2    D4,D5,D6,MUNTMA,JJ
      AMUNTM = (((((D6*X+D5)*X+D4)*X+D3)*X+D2)*X)+D1
      WRITE(3,100) X,AMUNTM
  100 FORMAT(/,15X,' AT LAMBDA = ',F12.7,
     1  ' MU-NOT OF MATERIAL = ',F12.7)
      RETURN
      END
```

BIBLIOGRAPHY

AITKEN, J.H. and W.R. Dixon (1958) X-ray Spectra from a 100 Kv Machine. NRC (Canada) Report 4864.

BELL, G.E. (1936) Spectral Distribution in the Continuous X-ray Spectrum and the Specification of X-ray Quality. *Brit. J. Rad.* 9, p. 680-692.

BERGER, R.T. (1961) X- or Gamma-Ray Energy Absorption or Transfer Coefficient: Tabulations and Discussion. *Rad. Res.* 15, p. 1-29.

BOAG, J.W. and T. Wilson (1952) The Saturation Curve at High Ionization Intensity. *Brit. J. Appl. Phys.* 3, p. 222-229.

BURKE, E.A. and R.M. Pettit (1960) Absorption Analysis of X-ray Spectra Produced by Beryllium Window Tubes Operated at 20 to 50 KvP. *Rad. Res.* 13, p. 271-285.

EHRLICH, M. (1955) Scintillation Spectrometry of Low-Energy Bremsstrahlung. *J. Research Natl. Bur. Standards* 54 #2, p. 107-118.

EMIGH, C.R. and L.W. Megill (1953) Semi-Empirical Equations for the Spectral Energy Distribution in X-ray Beams. *Non-destructive Testing* 11 #3, p. 30-33.

EPP, E.R. and H. Weiss (1966) Experimental Study of the Photon Energy Spectrum of Primary Diagnostic X-rays. *Physics in Medicine and Biology* 11 #2, p. 225-238.

GREENFIELD, M.A., R.D. Specht, P.M. Kratz and K. Hand (1952) Spectral Energy Distribution in X-ray Beam as a Function of Wavelength. *J. Opt. Soc. Am.* 42 #1, p. 6-11.

GREENING, J.R. (1947) The Determination of X-ray Energy Distribution by the Absorption Method. *Brit. J. Rad.* 20 #230, p. 71-78.

GREENING, J.R. (1950) The Determination of X-ray Wavelength Distributions from Absorption Data. *Proc. Phys. Soc.*, A. 63, p. 1227-1234.

GREENING, J.R. (1951) A Method of Determining the Wavelength Distribution of the X-Radiation at a Point in a Scattering Medium. *Brit. J. Rad.* 24 #280, p. 204-206.

GRODSTEIN, G.W. (1957) X-ray Attenuation Coefficients from 10 Kev to 100 Mev. National Bureau of Standards Circular 583 (U.S. Government Printing Office, Washington). Issued 30 April 1957.

HETTINGER, G. and N. Starfelt (1958a) Improved NaI Scintillation Spectrometer for the Study of Continuous X-ray Spectra. *Nucl. Instr.* 3, p. 25-26.

HETTINGER, G. and N. Starfelt (1958b) Bremsstrahlung Spectra from Roentgen Tubes. *Acta Radiol.* 50, p. 381-394.

HINE, G.J. and G. L. Brownell (1956) Radiation Dosimetry. Academic Press, New York. 932p.

ICRU (1964) Recommendations of the International Commission on Radiological Units and Measurements (I.C.R.U.), Report 10b, 1962: *Physical Aspects of Irradiation* (National Bureau of Standards Handbook 85, U.S. Government Printing Office, Washington). Issued 31 March 1964.

JAEGER, R. and W. Kolb (1956) Scintillationsspektrometrie weicher Röntgenstrahlung. *Sonderbände Strahlenther* 35, p. 285.

JENNINGS, W.A. (1953) A Theoretical Study of Radiation Outputs and Qualities from a Beryllium Window Tube Operated at Low Kilovoltages (10-50 KvP). *Brit. J. Rad.* 26 #304, p. 193-206.

JONES, D.E.A. (1947) The Determination from Absorption Data of the Distribution of X-ray Intensity in the Continuous X-ray Spectrum. *Brit. J. Rad.* 13 #147, p. 95-101.

JOYNER, H.S. (1967) Absolute Soft X-ray Dosimetry for Radiation Chemistry Studies. Thesis, University of Missouri - Rolla. 59p.

KOLB, W. (1955) Scintillationsspektrometrie weicher Röntgenstrahlung. *Naturwissenschaften* 43, p. 53.

KRAMERS, H.A. (1923) On the Theory of X-ray Absorption and of the Continuous X-ray Spectrum. *Phil. Mag.* 46, p. 836-871.

LOEVINGER, R. and S.S. Yaniv (1965) Absorbed Dose Determination in the Grenz-ray Region. *Physics in Medicine and Biology* 10 #2, P. 213-227.

McGINNIES, R.T. (1959) X-ray Attenuation Coefficients from 10 Kev to 100 Mev. National Bureau of Standards Supplement to Circular 583 (U.S. Government Printing Office, Washington). Issued 30 October 1959.

NORMAN, A. and M.A. Greenfield (1955) Spectral Dose-Rate Distribution in the X-ray Beam from a Beryllium Window Tube Operated at 50 KvP. *Rad. Res.* 3, p. 401-416.

RAY, S., C.G. Dodd, G.M. Muchow, G.F. Neilson and D.J. Kaup (1967) Derivation and Experimental Verification of an Equation for Exposure-Dose Rate due to X-ray Continua. *J. Appl. Phys.* 38 #8, p. 3122-2136.

SILBERSTEIN, L. (1933) Spectral Composition of an X-ray Radiation Determined from its Filtration Curve. *Phil. Mag.*, series 7, 15 #98, p. 375-394.

STORM, E. and H.I. Israel (1967) Photon Cross Sections from 0.001 to 100 Mev for Elements 1 through 100. Los Alamos Scientific Laboratory Publication LA-3753, UC-34 PHYSICS, TID-4500 (Clearinghouse for Federal Scientific and Technical Information, National Bureau of Standards, Springfield, Va.). Issued 15 November 1967.

ULREY, C.T. (1918) An Experimental Investigation of the Energy in the Continuous X-ray Spectra of Certain Elements. *Phys. Rev.* 11 #5, p. 401-410.

VICTOREEN, J.A. (1943) Probable X-ray Mass Absorption Coefficients for Wave-Lengths Shorter than the K Critical Absorption Wave-Length. *J. Appl. Phys.* 14, p. 95-102.

VILLFORTH, J.C., R.D. Birkhoff and H.H. Hubbell (1958) Comparison of Theoretical and Experimental Filtered Spectra. ORNL-2529.

WANG P.K.S., R.J. Raridon and R.C. Crawford (1957) X-ray Spectrum from a Beryllium Window Tube--II. Laplace Transformation. *Brit. J. Rad.* 30 #351, p. 153-157.

WHYTE, G.N. (1959) Principles of Radiation Dosimetry. Wiley, New York. 124p.

WHYTE, G.N. (1963) Energy Per Ion Pair for Charged Particles in Gases. *Rad. Res.* 18, p. 265-271.

WU, C.K. (1967-68) Personal Communication.

VITA

The author was born on 10 June 1943 in Abilene, Texas. He received his primary and secondary education in Franklin, Indiana. After graduating from Franklin High School, he entered Franklin College of Indiana; in June of 1965, he received the Bachelor of Arts degree in Physics (cum laude). While attending Franklin College, he received a four year scholarship from the Kappa Kappa Sigma Sorority and was employed during the junior and senior years as a laboratory assistant in the department of physics. During the summer of 1964, he was awarded an NSF Summer Traineeship at Wayne State University. In September of 1965, he entered the Graduate School of the University of Missouri - Rolla where he was appointed as a research assistant at the Graduate Center for Materials Research of the Space Sciences Research Center of the University of Missouri.

Permanent Address: R. R. 4 Box 24
Franklin, Indiana 46131